

11-13-2020

## Investigation of DNA Damage and Genomic Organization in the Cellular Response to Platinum Chemotherapy

Abdulhadi Abdulwahed  
aabdu049@fiu.edu

Follow this and additional works at: <https://digitalcommons.fiu.edu/etd>



Part of the [Public Health Commons](#)

---

### Recommended Citation

Abdulwahed, Abdulhadi, "Investigation of DNA Damage and Genomic Organization in the Cellular Response to Platinum Chemotherapy" (2020). *FIU Electronic Theses and Dissertations*. 4539.  
<https://digitalcommons.fiu.edu/etd/4539>

This work is brought to you for free and open access by the University Graduate School at FIU Digital Commons. It has been accepted for inclusion in FIU Electronic Theses and Dissertations by an authorized administrator of FIU Digital Commons. For more information, please contact [dcc@fiu.edu](mailto:dcc@fiu.edu).

□ □ □  
FLORIDA INTERNATIONAL UNIVERSITY

Miami, Florida

INVESTIGATION OF DNA DAMAGE AND GENOMIC ORGANIZATION IN THE  
CELLULAR RESPONSE TO PLATINUM CHEMOTHERAPY

A dissertation submitted in partial fulfillment of

the requirements for the degree of

DOCTOR OF PHILOSOPHY

in

PUBLIC HEALTH

by

Abdulhadi Mohammed S Abdulwahed

2020

□ □ □  
To: Dean Tomás R. Guilarte  
R.Stempel College of Public Health and Social Work

This dissertation, written by Abdulhadi Mohammed S Abdulwahed, and entitled Investigation of DNA Damage and Genomic Organization in the Cellular Response to Platinum Chemotherapy, having been approved in respect to style and intellectual content, is referred to you for judgment.

We have read this dissertation and recommend that it be approved.

\_\_\_\_\_  
Diana Azzam

\_\_\_\_\_  
Changwon Yoo

\_\_\_\_\_  
Helen Tempest

\_\_\_\_\_  
Deodutta Roy, Co-Major Professor

\_\_\_\_\_  
Marcus S. Cooke, Co- Major Professor

Date of Defense: November 13, 2020

The dissertation of Abdulhadi Mohammed S Abdulwahed is approved.

\_\_\_\_\_  
Dean Tomás R. Guilarte  
R.Stempel College of Public Health and Social Work

\_\_\_\_\_  
Andrés G. Gil  
Vice President for Research and Economic Development  
and Dean of the University Graduate School

Florida International University, 2020

## DEDICATION

I dedicate my dissertation work to my father, Mohammed S Abdulwahed, who believed in me and to whom I promised to obtain the doctoral degree before he left us in February 2017. My lovely mother, Hussah Al Ahmed, who first taught me the value of education and critical thought. My brothers and sisters who never stop supporting me throughout my dissertation.

## ACKNOWLEDGMENTS

I would like to express my appreciation to my committee members who were more than generous with their helpful advice and valuable time. I would acknowledge my supervisor, Dr. Marcus S. Cooke, to guide me through this exciting research project. I am so pleased that I had the chance to be your student in the past five years; I have improved with you, personally and professionally. A special thanks to Dr. Helen Tempest for her countless hours of helping me all the time and for her valuable advice during our weekly lab meetings.

I wish to thank Dr. Deodutta Roy, Dr. Changwon Yoo, Dr. Alok Deoraj, and Dr. Diana Azzam for agreeing to serve on my committee and for all their support and guidance during my Ph.D. journey.

I would also acknowledge all members of the Oxidative Stress Group that I have worked with; They are my family in Miami, and I have learned a lot from everyone.

My appreciation also goes to my Saudi Arabian Government for their generous support.

□ □ □

ABSTRACT OF THE DISSERTATION

INVESTIGATION OF DNA DAMAGE AND GENOMIC ORGANIZATION IN THE  
CELLULAR RESPONSE TO PLATINUM CHEMOTHERAPY

by

Abdulhadi Mohammed S Abdulwahed

Florida International University, 2020

Miami, Florida

Professor Marcus S. Cooke, Co-Major Professor

Professor Deodutta Roy, Co-Major Professor

Ovarian cancer (OC) is the primary reason for gynecological cancer-related deaths among women. This cancer rarely has specific symptoms making early detection challenging. Platinum compounds have been used as the first-line treatment for OC. However, OC patients often develop chemoresistance to current platinum/taxane chemotherapy regimens upon recurrence, leaving patients with no alternative treatment options. The purpose of this thesis was to investigate the molecular basis of chemoresistance in OC by analyzing the damage of DNA response and gene positioning after treatment exposure. A modified comet assay was used to measure interstrand cross-link (ICL) formation and repair in chemoresistant (CR) (SKOV-3) and chemosensitive (CS) (A2780/OCIP5X) ovarian cancer cell lines. Although the peak of ICL formation for the three cell lines was at 12 h, a significant attenuation of ICL formation in SKOV-3 was observed, compared to the chemosensitive lines. Furthermore, ICL levels in SKOV-3 did not return baseline, in contrast to the chemosensitive cell lines. We further investigated the basis of this differential DNA damage response by examining the potential role of nuclear organization,

via the comparison of damage induction in nucleoid bodies versus intact cells. The results demonstrated the same rank order of dose-response in nucleoid bodies as observed in intact cells, with chemoresistant cells being considerably more resistant to damage formation, at all doses of cisplatin. When studying gene positioning, we hypothesized that there is a difference in the organization of chromatin in CS and CR ovarian cancer cell lines. The organization of seventeen genes was tested in CR and CS cells. Non-random organization was observed for the majority of genes (47.06%). *BRAF* and *AKT3* were randomly organized in CS and non-randomly organized in CR. A significantly increased copy number was observed in the CR cell line compared to the CS in the majority of the studied genes. The overall data provide the basis for further investigation to improve our understanding of the differential DNA damage response and gene positioning associated with chemosensitive and chemoresistant ovarian cells. Elucidating the mechanisms of chemoresistance may ultimately lead to novel therapeutic interventions that may resensitize or prevent the development of chemoresistance.

## TABLE OF CONTENTS

CHAPTER	PAGE
CHAPTER 1	1
INTRODUCTION	1
1. Introduction	2
1.0 Ovarian cancer and chemotherapy.....	2
1.1 Symptoms and treatments of ovarian cancer .....	2
1.1.1 Treatment options .....	3
1.2 Platinum compounds .....	4
1.2.1 Cisplatin .....	6
1.2.2 Carboplatin.....	8
1.2.3 Oxaliplatin.....	8
1.3 The Molecular mechanism of chemoresistance in ovarian cancer .....	8
1.3.1 Decreased of intracellular drug accumulation .....	9
1.3.2 Deactivation of intracellular cisplatin .....	9
1.4 DNA Repair systems .....	10
1.4.1 Nucleotide excision repair .....	10
1.4.2 Mismatch repair .....	11
1.4.3 Homologous recombination.....	14
1.4.4 Nonhomologous end-joining .....	17
1.4.5 Fanconi anemia pathway.....	20
1.4.6 Base excision repair .....	20
1.5 Role of epigenetic changes in cisplatin resistance.....	23
1.5.1 Chromatin remodelling .....	23
1.5.2 Histone acetylation.....	28
1.5.3 Histone methylation .....	32
1.6 Methods to detect DNA damage and repair induced by cisplatin .....	34
1.6.1 Polymerase chain reaction (PCR) .....	34
1.6.2 The comet assay .....	34
1.6.3 Comet-FISH.....	35
1.6.4 Terminal deoxynucleotidyl transferase dUTP nick end labelling (TUNEL) assay .....	35
1.6.5 Enzyme-linked immunosorbent assay (ELISA) .....	35
1.6.6 Immunohistochemistry .....	36
1.6.7 Immunological assay .....	36
1.6.8 High-performance liquid chromatography-mass spectrometry (HPLC-MS).....	37
1.6.9 Gas chromatography–mass spectrometry (GC-MS).....	37
1.7 Hypothesis and specific aims.....	38
 CHAPTER 2	 40
MATERIALS AND METHODS	40
2. Materials and Methods	41

2.1.1 Ovarian cell lines .....	41
2.1.2 Materials for cell culture.....	41
2.1.3 Materials for the alkaline comet assay.....	42
2.1.4 Materials for FISH.....	42
2.1.5 Materials for ELISA .....	43
2.2 Methods .....	43
2.2.1 Cell culture.....	43
2.2.2 Cell freezing.....	44
2.2.3 Cell thawing.....	44
2.2.4 Cell counting.....	45
2.2.5 Cisplatin treatment.....	45
2.2.6 Ultraviolet Irradiation of Cells.....	45
2.2.7 Nuclear DNA Damage and Repair Measured by the Alkaline Comet Assay ...	46
2.2.7.1 Cell treatment for comet assay.....	48
2.2.7.2 The alkaline comet assay procedure .....	48
2.2.7.3 Comet image scoring .....	52
2.2.7.4 Analysis of base excision repair .....	54
2.2.7.4.1 hOGG1-modified comet assay.....	54
2.2.7.5 Analysis of nucleotide excision repair .....	55
2.2.8 Optimization of comet assay analysis parameters .....	56
2.2.8.1 Optimization of hOGG1 concentration.....	56
2.2.8.2 Optimization of T4endoV concentration .....	56
2.2.8.3 Optimization of PI concentration.....	57
2.2.8.4 Optimization of microscope magnification for scoring comet images.....	57
2.2.9 Detection and quantification of cisplatin induced DNA Interstrand Cross-Links (ICL) .....	58
2.2.9.1 ICL-modified alkaline comet assay .....	58
2.2.9.2 Cell treatment for ICL-modified alkaline comet assay.....	58
2.2.10 Cell survival.....	62
2.2.10.1 Clonogenic assay .....	62
2.2.11 DNA extraction.....	62
2.2.12 Cytotoxicity .....	63
2.2.12.1 Cell Counting Kit-8.....	63
2.2.12.2 Measuring cell toxicity of triazole-modified nucleosides and/or their enhancement with cisplatin efficiency in ovarian cell line.....	64
2.2.13 Quantification of platinum in DNA using Inductively Coupled Plasma Mass Spectrometry (ICP-MS).....	65
2.2.13.1 Cell treatment for ICP-MS.....	65
2.2.13.2 General procedure of ICP-MS .....	65
2.2.14 Detection and quantification of cisplatin induced DNA adducts .....	66
2.2.14.1 Cell treatment for ELISA) .....	66
2.2.14.2 ELISA .....	66
2.2.14.3 Optimization of ELISA conditions .....	67
2.2.15 Evaluation of gene positioning in chemosensitive and chemoresistant ovarian cancer cells .....	68
2.2.15.1 Cell treatment for Fluorescence In-Situ Hybridization.....	69

2.2.15.2 FISH.....	70
2.2.15.3 Image capture.....	73
2.2.16 Statistical analyses.....	75
CHAPTER 3.....	76
EXAMINATION OF THE DIFFERENCE IN THE DNA DAMAGE RESPONSE IN CHEMORESISTANT AND CHEMOSENSITIVE OVARIAN CELL LINES.....	76
3.1 Introduction.....	77
3.2 Methods.....	78
3.2.1 Ovarian cancer cell lines.....	78
3.2.2 Cisplatin treatment.....	78
3.2.4 The alkaline comet assay procedure.....	79
3.2.4.1 Time course of DNA crosslink formation and repair in ovarian cancer cells.....	79
3.2.4.2 DNA Crosslink formation in intact cells and nucleoid bodies from chemosensitive and resistant ovarian cell lines.....	79
3.2.4.3 Optimization of hOGG1 concentration for ovarian cell lines.....	79
3.2.4.4 Analysis of base excision repair.....	80
3.2.4.5 UVB dose response.....	80
3.2.4.6 UVC dose response.....	80
3.2.4.7 Optimization of T4endoV concentration for ovarian cell lines.....	80
3.2.4.8 Analysis of nucleotide excision repair.....	81
3.2.4.9 Crosslink formation on ovarian cell with environmental and chemical agents.....	81
3.2.5 ELISA.....	81
3.2.6 Quantification of platinum in DNA using Inductively Coupled Plasma Mass Spectrometry (ICP-MS).....	82
3.2.7 Measuring cell toxicity of triazole-modified nucleosides and/or their enhancement with cisplatin efficiency in ovarian cell line.....	82
3.3 Results.....	83
3.3.1 Treatment with cisplatin cause a decrease in ovarian cancer cell survival.....	83
3.3.2 Chemoresistant tumor cells are refractory to the formation of cisplatin-induced DNA crosslinks.....	85
3.3.4 Both cells and nucleoid bodies from chemoresistant cells are refractory to crosslinks formation.....	90
3.3.5 Optimization of PI concentration.....	92
3.3.7 Optimization of hOGG1 concentration for ovarian cell lines.....	95
3.3.8 Equivalent BER ability occurs in chemosensitive and chemoresistant ovarian tumor cells.....	97
3.3.10 UVC dose response.....	103
3.3.11 Optimization of T4endoV concentration for ovarian cell lines.....	105
3.3.12 NER repair of UV radiation-induced CPD in ovarian cells.....	108
3.3.13 Examination of ovarian cancer cells response to environmental and chemical agents.....	111
3.4 Discussion.....	114

CHAPTER 4	117
EVALUATION OF GENE POSITIONING AND COPY NUMBER CHANGES IN CHEMOSENSITIVE AND CHEMORESISTANT OVARIAN CANCER CELL LINES	117
4.1 Introduction	118
4.2 Methods	121
4.2.1 Ovarian cancer cell lines.....	121
4.2.2 Cisplatin treatment.....	121
4.2.3 Dual color FISH.....	122
4.2.4 FISH image capture .....	127
4.2.5 Assessment of gene copy number.....	127
4.2.6 Radial assessment of gene positioning in interphase nuclei.....	127
4.2.7 Assessment of nonrandom gene positioning in interphase nuclei and statistical analysis.....	128
4.3 Results	129
4.3.1 Nonrandom gene positioning in ovarian cancer cell lines.....	129
4.3.2 Differences in the nuclear localization of genes in chemosensitive and chemoresistant cell lines .....	137
4.3.3 Copy number changes in chemoresistant and chemosensitive cell lines.....	141
CHAPTER 5	150
CONCLUSION AND DIRECTIONS FOR FUTURE RESEARCH	150
5.1 Conclusion	151
5.2.1 Isolation and characterization of nuclear associated proteins in the chemosensitive and chemoresistant cells. ....	152
5.2.2 Measuring cell toxicity of triazole-modified nucleosides and/or their enhancement with cisplatin efficiency in ovarian cell line .....	158
5.2.3 Examination changes in the DNA damage response with acquired chemoresistance .....	162
5.2.4 Optimization of sonication procedure and number of cycles .....	163
REFERENCES	167
VITA	188

□ □ □

## LIST OF TABLES

TABLE	PAGE
Table 1.1.1 Chemical structures of the platinum family of chemotherapeutic agents	5
Table 1.1.2 Classification of HDAC family	29
Table 2.2.1 Putative genes involved in ovarian cancer formation and selected to study gene positioning in chemosensitive and chemoresistant ovarian cancer.	72
Table 4.4.1 Descriptive table of all genes used in the study (Gene Cards Human Gene Database)	124
Table 4.4.2 Nonrandom gene positioning in control and cisplatin treated A2780, OCI-P5X, and SKOV3 ovarian cancer cell lines	131
Table 5.5.1 Proteins shared between A2780 and SKOV3 nucleoids	155
Table 5.5.2 Proteins were found only in A2780.	156
Table 5.5.3 Proteins were found only in SKOV3.	157

□ □ □

## LIST OF FIGURES

FIGURE		PAGE
Figure 1.1.1	Different kinds of cisplatin DNA adducts	7
Figure 1.1.2	Overview of the NER pathway	13
Figure 1.1.3	Schematic representation of MMR pathway	16
Figure 1.1.4	Overview of the HR and NHEJ pathway	19
Figure 1.1.5	Overview of the BER repair pathway	22
Figure 1.1.6	 Schematic of histone methylation and acetylation in the chromatin	27
Figure 1.1.7	Schematic of Histone acetylation and deacetylation	31
Figure 2.2.1	Schematic representation of the alkaline comet assay demonstrating how comets are formed during the assay	47
Figure 2.2.2 (A)	Principle of the alkaline comet assay procedure	50
Figure 2.2.2 (B)	Demonstration of the slide chilling tray (Cleaver Scientific Ltd., UK).	51
Figure 2.2.3	Example of comet images and DNA damage analysis using comet assay IV software	53

Figure 2.2.4	A schematic representation of the principle of cross-link formation induced by cisplatin	60
Figure 2.2.5	Representative comet images illustrating ICL detection following cisplatin treatment	61
Figure 2.2.6	Representation figure illustrating the radial analysis of OCI-5Px stained for KRAS (green) and BRCA1 (red) genes and counterstained DAPI (blue) using FISH technique	74
Figure 3.3.1	Chemoresistant cells have a significantly cellular cell survival in response to cisplatin compared to chemosensitive cell lines	84
Figure 3.3.2	Chemoresistant tumor cells are refractory to the formation of cisplatin-induced DNA crosslinks	87
Figure 3.3.3A	A Quantification of platinum in DNA using ICP-MS in chemoresistant and chemosensitive ovarian cancer cells	88
Figure 3.3.3B	Formation of DNA crosslinks and repair in ovarian tumor cells measured by ELISA	89
Figure 3.3.4	The differential response to cisplatin treatment derives from proportion associated with the nucleoid body	91
Figure 3.3.5	Levels of DNA damage in HaCaTs irradiated with UVB determined by alkaline comet assay	93
Figure 3.3.6	Potential limitation of using high concentrations of P.I	94
Figure 3.3.7	Induction of DNA breaks and the amount of 8-oxodG in A2780 and SKOV-3 following treatment with H <sub>2</sub> O <sub>2</sub> (50 μM) determined by hOGG1-modified comet assay	96

Figure 3.3.8	Kinetics of base excision repair of oxidized purines (A) (+ hOGG1) and repair of strand breaks (B) (- hOGG1) does not differ between chemosensitive and chemoresistant ovarian cells	98
Figure 3.3.9	Significant levels of oxidized purines + SB/ALS were induced by H <sub>2</sub> O <sub>2</sub> in ovarian cancer cells	99
Figure 3.3.10	Induction of DNA breaks in ovarian cancer cells following the exposure to UVB	101
Figure 3.3.11	Representation of comet pictures of DNA damage following the exposure to UVB in ovarian cancer cells	102
Figure 3.3.12	Induction of DNA damage in ovarian cancer cells following exposure to UVC	104
Figure 3.3.13	Damaged comet images from SKOV-3 and A2780 cells following the treatment with different concentrations of T4endoV enzyme.	106
Figure 3.3.14	Typical comet images from SKOV-3 cells following the treatment with the optimum concentration of T4endoV for removal of CPD from ovarian cells	107
Figure 3.3.15	kinetics of nucleotide repair of CPD (+ T4endoV) and strand breaks (- T4endoV) in ovarian cancer cells	109
Figure 3.3.16	Significant levels of CPD + SB/ALS were induced by UVB in ovarian cancer cells	110
Figure 3.3.17	Chemoresistant cells are more resistant to ICL formation from cisplatin + formaldehyde, a representation environmental crosslinks agent	113
Figure 4.4.1	Differences in gene positioning (BRAF/AKT3) between CS and CR ovarian cell lines.	132

Figure 4.4.2	KRAS and SOX17 were randomly organized only in A2780)	133
Figure 4.4.3	RB1 was randomly organized only in A2780	134
Figure 4.4.4	PAX3 was randomly organized in A2780	135
Figure 4.4.5	Differences in gene positioning (MECOM/PTEN) between CS and CR ovarian cell lines)	136
Figure 4.4.6	Differences in gene positioning (CCNE1) between CS and CR ovarian cell lines	138
Figure 4.4.7	Differences in gene positioning (FOLR1) between CS and CR ovarian cell lines	139
Figure 4.4.8	Differences in gene positioning (NF1) between CS and CR ovarian cell lines)	140
Figure 4.4.9	The highest increase in ploidy was observed in CR cell line SKOV-3	142
Figure 4.4.10	There was a significantly increased copy number observed in CR cell line (SKOV3) compared to the CS (A2780 and OCIP5X)	143
Figure 4.4.11	There was a significantly increased copy number observed in CR cell line (SKOV3) compared to the CS (A2780 and OCIP5X)	144
Figure 4.4.12	There was a significantly increased copy number observed in CR cell line (SKOV3) compared to the CS (A2780 and OCIP5X)	145
Figure 5.5.1	Number of top proteins identified after mass spectrometry analysis in the chemosensitive and chemoresistant cells	154

Figure 5.5.2	Cell viability as measured by WST-8 assay using A2780 cells after 24 h of incubation with 8-TrzdG of different concentrations	160
Figure 5.5.3	Gel electrophoresis of A2780 cell line after the treatment of 8-TrzdG	161
Figure 5.5.4	DNA sonication of SKOV-3 using a sonicator (Probes)	165
Figure 5.5.5	DNA sonication of SKOV-3 using a sonicator (Probes)	166



□ □ □

## LIST OF NON-STANDARD ABBREVIATIONS

% TD	The percentage of tail DNA
8-oxodG	8-oxo-7,8-dihydro-2'-deoxyguanosine
ALS	Alkali labile sites
BER	Base excision repair
BSA	bovine serum Albumin
CCD	Charge-coupled device camera
CPD	Cyclobutane pyrimidine dimer
DMSO	Dimethyl sulfoxide
EDTA	Ethylenediaminetetraacetic acid
ELISA	Enzyme-linked Immunosorbent Assay
ERB	Enzyme reaction buffer
FA	Fanconi anemia
μM	Micromolar
mm	Millimeter

•  
MMR

•  
Mismatch repair

•  
NER

•  
Nucleotide excision repair

•  
NHEJ

•  
Non-homologous end joining

PBS

Phosphate buffered saline

rpm

Revolutions per minute

SB

Strand breaks

T4endoV

T4 endonuclease V enzyme

U

•  
Unit

•  
UVB

•  
Ultraviolet B

•  
UVC

•  
Ultraviolet C

•  
UVR

•  
Ultraviolet radiation

•

•



**CHAPTER 1**

**INTRODUCTION**

## **1. Introduction**

### **1.0 Ovarian cancer and chemotherapy**

The leading cause of women's mortality due to a malignancy of the female reproductive system is caused by ovarian cancer. Ovarian cancer is ranked fifth in terms of deaths amongst women, compared to the other types of cancer [1]. Most women who have ovarian cancer usually experience severe symptoms during the last stages of ovarian cancer. It is during the late stages of the disease that most women are diagnosed. This is because many women are usually asymptomatic or have non-specific symptoms during the early stages of ovarian cancer, where the disease can be cured more effectively [2]. When it comes to managing early and advanced phases of ovarian cancer, the most commonly used treatment techniques include cytoreductive surgery to remove the tumor, followed by chemotherapy. The chemotherapy involves a taxane doublet and a platinum compound [3, 4, 5]. Following surgery and chemotherapy, the initial response rate ranges from 70% to 80%; however, disease relapse occurs in less than two years in many patients. Unfortunately, some patients' chemoresistance makes it challenging to manage the condition when it recurs [6,7]. Therefore, this chapter will focus on reviewing ovarian cancer in general and the factors involved in the chemoresistance.

### **1.1 Symptoms and treatments of ovarian cancer**

Ovarian cancer, in its early stage, is generally asymptomatic and is often incidentally diagnosed. It shows nonspecific symptoms, which are generally noticeable only when the cancer advances and spreads throughout the abdominal cavity. Symptoms associated with malignancy include abdominal fullness, vague pain in the abdomen, early satiety, bowel habit changes, bloating, and dyspepsia. If identified in the early stages, the

□ □ □

five-year survival rate of ovarian cancer is up to 90 %, whereas, in the case of late-stage, the five-year survival rate is less than 30 % [8]. Currently, ultrasound and CA-125 (Cancer Antigen 125) are used as detection strategies. However, these techniques have shortcomings, which results in a lack of a robust and sensitive screening test for the disease

### **1.1.1 Treatment options**

At present, the first-line treatment option for most ovarian cancers is surgery. The decision to which surgery should be carried out depends on the spread of cancer and the patient's general health. If the patient is diagnosed at early stages, it is possible to treat cancer without removing women's uterus and ovaries for certain types of tumors.

Another option is chemotherapy, in which cytotoxic drugs are used to treat cancer. The chemotherapy acts at a systemic level where the drugs enter into the bloodstream and reach more or less all the body regions. This method can help eliminate malignant cells that may have been left after surgery, for metastasized cancers, or for shrinking oversized cancer to facilitate surgery. In most cases of chemotherapy, drugs are injected into a vein (IV) or given orally. In other cases, the intraperitoneal (IP) chemotherapy method is used. In this method, drugs are injected directly into the abdominal cavity through a catheter.

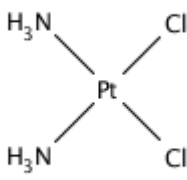
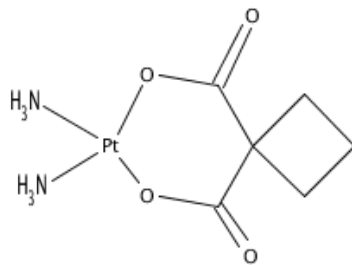
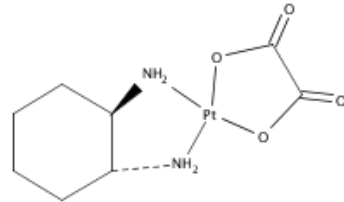
Usually, two different types of drugs are used together in the chemotherapy treatment of ovarian cancer. The combination drug approach used to treat ovarian cancer is more efficacious than utilizing a single-drug approach. Generally, the combination approach includes two kinds of chemotherapy drugs involving a platinum compound and taxane (a chemotherapeutic agent that blocks cell growth by stopping cell division). Common platinum compounds used for treatment include cisplatin or carboplatin, whereas paclitaxel (Taxol) or docetaxel (Taxotere) are generally used as the taxane. These

treatments are generally given every three to four weeks into a vein. Depending on the type and stage of ovarian cancer, a typical chemotherapy course involves the treatment of 3 to 6 cycles [8-9].

## **1.2 Platinum compounds**

In the oncology field, there has been an increased focus on platinum compounds such as cisplatin, carboplatin, and oxaliplatin for the past forty years (Table 1.1.1). They play a vital role in treating cervical cancer, lung cancer, colorectal cancer, head and neck cancer, and bladder cancer [10]. They are most effective against germ cell tumors and epithelial ovarian cancer. Cisplatin is often used as a first-line treatment option when it comes to managing cancerous cells. However, in the matter of the treatment of colorectal cancer, oxaliplatin is more effective than cisplatin. The key mechanism to their activity is the formation of DNA crosslinks, which interrupts the proper functioning of cellular DNA, which subsequently induces apoptosis [11].

**Table 1.1.1 Chemical structures of the platinum family of chemotherapeutic agents**

Platinum compound	Formula	Structure
<b>Cisplatin</b>	$\text{Pt}(\text{NH}_3)_2\text{Cl}_2$	
<b>Carboplatin</b>	$\text{C}_6\text{H}_{12}\text{N}_2\text{O}_4\text{Pt}$	
<b>Oxaliplatin</b>	$\text{C}_8\text{H}_{14}\text{N}_2\text{O}_4\text{Pt}$	

### 1.2.1 Cisplatin

Cisplatin is considered as a chemotherapeutic agent for a variety of different types of tumors. It is the oldest member of the platinum family whose toxicity profile is well-recognized, including renal dysfunction, emesis, neurotoxicity, and ototoxicity [12]. DNA is the primary cellular target for cisplatin, however it can also react with protein. Cisplatin can bind with the N7 position in purine bases in DNA once cisplatin molecules enter a cell and become active by displacing the chloride ligands with water molecules; different adducts then will be formed (Figure 1.1.1) [13]. The formation of these bulky DNA adducts alters DNA's conformation, which disturbs replication and inhibits DNA synthesis. If the DNA damage were not sufficient to cause cells to undergo apoptosis, the cisplatin lesions would arrest cells in the G2 and S phases of the cell cycle. This phenomenon exerts a cytoprotective effect by either preventing potentially abnormal or abortive mitoses or allowing the DNA repair mechanisms to re-establish the integrity of the DNA [14]. However, if the DNA repair systems fail to repair the damage induced, cells will typically undergo apoptosis.

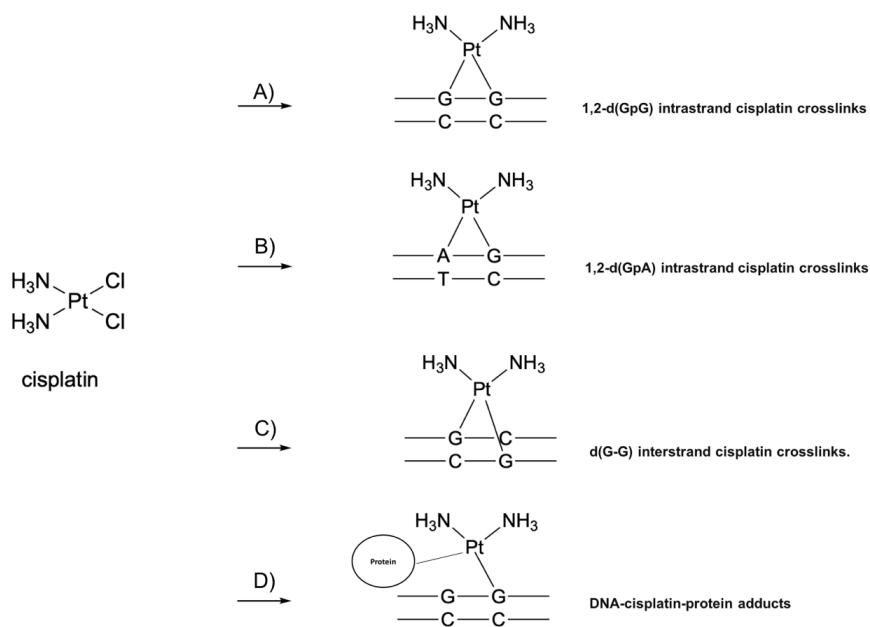


**Figure 1.1.1 Different kinds of cisplatin DNA adducts.** A) 1,2-d(GpG) intrastrand cisplatin. B) 1,2-d(GpA) intrastrand cisplatin crosslinks. C) d(G-G) interstrand cisplatin crosslinks. D) DNA-cisplatin-protein adducts, which known as a monoadduct.

### **1.2.2 Carboplatin**

Carboplatin is typically used for chemotherapy of neck, lung, and ovaries. The drug has a structure that is composed of a ligand of bidentate dicarboxylate, unlike cisplatin which has ligands of two chlorides in the same position. The carboplatin structure can reduce reactivity and minimize binding mechanisms to DNA even though the crosslinks are the same as those formed while using cisplatin at a similar dose [15].

### **1.2.3 Oxaliplatin**

The mode of action of oxaliplatin is the same as that seen in cisplatin and carboplatin. However, the oxaliplatin–DNA complex cannot be recognized by the enzymes involved in the repair of DNA mismatch. This is because the complex has a larger size compared to cisplatin (Table 1.1). This drug is frequently used in the management of gastric, pancreatic, and colorectal cancers.

Platinum-based chemotherapeutic agents are used to treat many types of cancer. However, in most malignancies, the efficacy of a platinum chemotherapeutic agent is limited by resistance development. Although various factors are known to contribute to platinum resistance, alterations of DNA repair processes are known to be significant in mediating the resistance. Recent studies have provided an in-depth understanding of the molecular mechanisms of pathways involved in DNA repair and their influence on chemotherapy [16].

## **1.3 The Molecular mechanism of chemoresistance in ovarian cancer**

Mutations that occur in an individual's genes lead to drug resistance in many cases, which has resulted in a multifactorial challenge. The abnormal balance between numerous pathways in the cells and the undermining of tumor suppressors, which participate in

□ □ □  
regulating apoptosis, enhance drug detoxification and clearance, and decrease the drug's efficacy due to increased DNA repair, are some of the problems caused by mutations [17].

Here are the key factors that may play roles in chemoresistance in ovarian cancer.

### **1.3.1 Decreased of intracellular drug accumulation**

Platinum-resistant cells, in an invitro study , showed a reduction in cellular uptake with cisplatin chemotherapy [18]. The decreased accumulation of cisplatin is attributed to either drug efflux increases or drug uptake inhibition. At times, both factors may contribute to decreased accumulation of cisplatin in chemoresistant cells [18].

Through the processes of facilitated transport and passive diffusion, accumulation of cisplatin and other compounds related to it occur in the cells. The influx of cisplatin and its analogs are controlled by the copper transporter-1 (CTR1). A study showed that the deletion of the *CTR1* gene resulted in increased resistance to cisplatin and decreased accumulation of the drug in different cell lines (cisplatin-sensitive and cisplatin-resistant mammalian cells) that comprised ovarian cancer [19].

### **1.3.2 Deactivation of intracellular cisplatin**

Glutathione is an intracellular thiol found in large amounts in cells and plays a vital role in the detoxification of cisplatin and its related compounds and removing many other toxins found in cells. The compound performs this function together with other elements such as proteins rich in cysteine, metallothionein, and methionine. However, an enzyme known as GSH-S-transferase  $\pi$  can effectively transform intracellular cisplatin into inactive conjugates of cisplatin-thiol. The enzymes  $\gamma$ -glutamylcysteine synthetase and GST $\pi$  play a role in making some cell lines resistant such as those in the lung, cervical, and ovarian cancer [20, 21, 22].

### **1.3.3 Increased DNA repair**

The presence of cisplatin-DNA adducts is responsible for cisplatin cytotoxicity. A balance between the repair of DNA and DNA damage determines the survival or death of cancerous cells after using the cisplatin drug during the management period. Many defects in the DNA can be successfully repaired by the DNA repair mechanisms, including eliminating platinum-DNA adducts [23].

Cisplatin is a chemotherapeutic agent that induces DNA damage, however, it is less effective with the involvement of the DNA repair systems. Section 1.4 explores details regarding the types of DNA repair systems involved in repairing the damaged DNA following cisplatin treatment.

### **1.4 DNA Repair systems**

Several repair systems are involved in the repair process following the cisplatin-induced DNA damage. The major repair systems involved in the repair of the cisplatin-DNA adducts are nucleotide excision repair (NER), mismatch repair (MMR), homologous recombination (HR), nonhomologous end joining (NHEJ), and base excision repair (BER) [24]. From several studies, the association of the cisplatin chemoresistance and the mentioned DNA repair pathways are reviewed in this section.

Moreover, recent studies indicated that Fanconi anemia pathway (FA) plays a role in increasing the sensitivity to interstrand cross-links (ICLs) [25]. Section 1.4.5 describes some recent evidence indicating the relationship between the FA pathway (to repair ICLs) and the chemoresistance.

### 1.4.1 Nucleotide excision repair

NER has a role in the repair of cisplatin-DNA adducts. There are two pathways in this repair system, transcription-coupled repair (TC-NER) and global genome repair (GG-NER), which are involved in recognizing and repairing DNA damage. Different repair proteins are involved in each pathway, explained in detail elsewhere [26].

There are several steps in the NER pathway; upon detecting bulky adducts in DNA, a patch consisting of approximately 30 nucleobases is removed by two distinct complexes (one 5' to the damage and one 3' to the damage). A polymerase then fills the gap using the undamaged strand as a template, thereby relegating the DNA backbone by DNA ligase IV [26]. Figure 1.1.2 illustrates the main steps of the NER pathway, repairing bulky DNA lesions.

ICLs are one of the lesions created by cisplatin. Processing and removing ICLs by DNA repair proteins include NER, HR, and FA pathways. NER has been reported to be the primary repair pathway for removing the cisplatin lesions [27, 28]. Cisplatin can activate NER proteins because it can bind to the DNA helix and make adducts that damage the DNA [29].

Numerous studies showed the association of the NER pathway and cisplatin resistance. The XPF and ERCC1 are associated with cisplatin chemoresistance for several types of cancer [26-30]. Moreover, evidence showed that ERCC1-XPF is involved in repairing ICL and decrease the DNA backbone in the region 5' in the NER pathway [31, 32]. However, it also plays an imperative role in regulating sensitivity to severity of cisplatin [31, 32]

□ □ □

Another primary lesion caused by DNA damage induced by cisplatin is the intrastrand crosslink, which is often repaired by NER. Mutations in NER can result in the rare autosomal recessive condition xeroderma pigmentosum. This condition causes affected individuals to be highly sensitive to UV light and have a significantly increased risk of developing skin cancer. Cells from these patients have also been shown to exhibit sensitivity to cisplatin [33].

Moreover, the reduction of ERCC1 and XPA protein production in testis tumor cells resulted in increased sensitivity in these cells to cisplatin-induced DNA adducts [34, 35]. In many studies, the overexpression of XPA and ERCC1 was linked to cisplatin resistance [34-36]. For instance, in a study of ovarian cancer cell lines, alternative splicing occurred, which was influenced by the presence of ERCC1 exon VIII [36, 37]. Even though the excision never interfered with the amount of ERCC1, the repair function that occurs after excision was significantly reduced.

Moreover, epigenetic factors such as ERCC1 hypermethylation increase cisplatin's sensitivity because this is inversely correlated with the amount of ERCC1 mRNA [37]. In addition, this study has also explained that the binding factor of ERCC1 is needed to repair DNA damage induced by cisplatin [38]. The sensitivity of cisplatin was further enhanced through a double knockdown of a complex formed between ERCC1 and XPF of lung cancer cells [38].

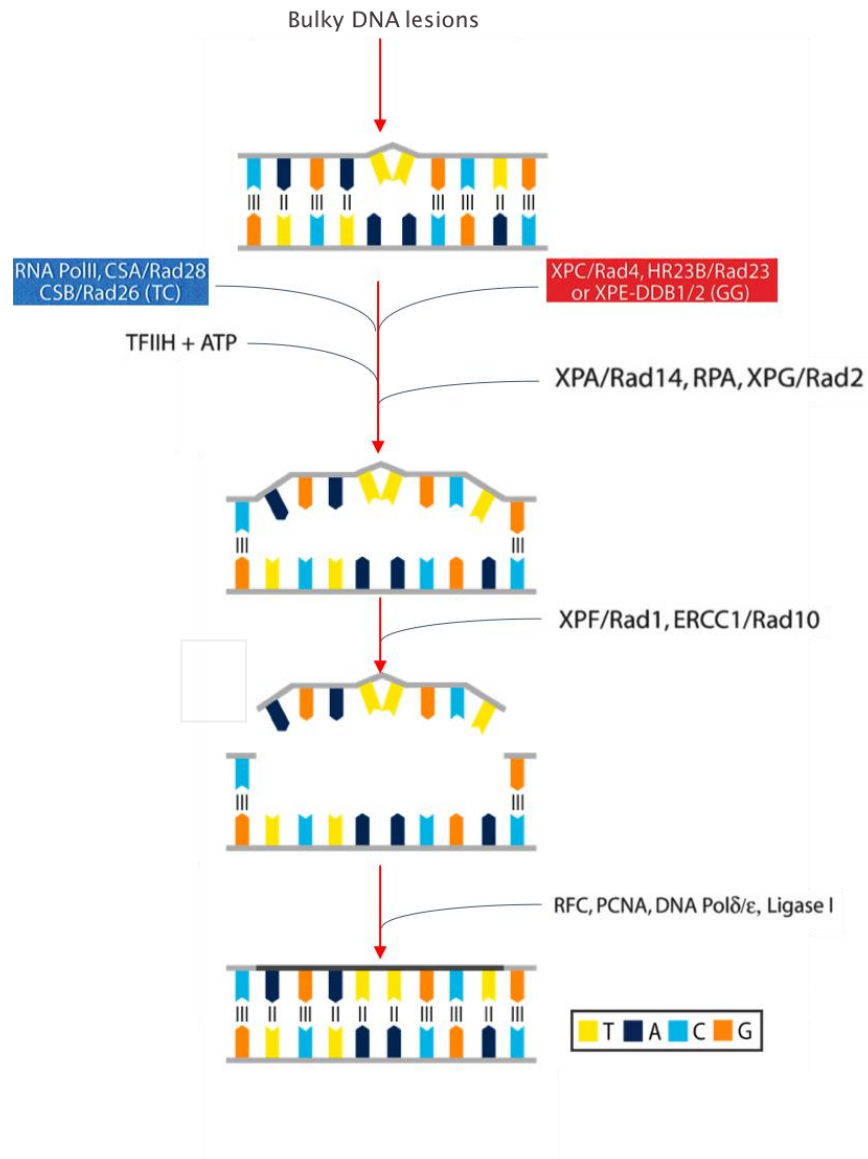


**Figure 1.1.2 Overview of the NER pathway.** Bulky DNA lesions like cyclobutane pyrimidine dimers (CPDs), 6-4 photoproducts (6-4 PPs) or ICLs are removed by NER. Subsequent steps are shared and include local duplex unwinding, DNA strand dual incision, DNA synthesis, and ligation.

### 1.4.2 Mismatch repair

MMR is a strand-specific, highly conserved repair pathway that is initiated with the recognition of DNA damage and follows a stepwise process [39, 40]. Unmatched or mismatched DNA base pairs or insertion-deletion loops are recognized by MMR proteins called as Mut proteins, which initiate the assembly of proteins that excise the affected region. Afterward, the excised region is resynthesized by DNA polymerase using the unaffected template strand by DNA polymerase. Figure 1.1.3 shows a schematic illustration of the MMR pathway; proteins involved in MMR and main steps were reviewed in detail elsewhere [41]

Deficiencies in the MMR process can result in the accumulation of unrepaired regions of DNA, which can result in microsatellite instability [42]. The accumulation happens due to the replication of unrepaired base pair mismatches during DNA replication, and repeats are formed due to the slippage of the replication machinery in these areas.

Defects in MMR may occur through epigenetic silencing of an essential MMR gene [42, 43, 44] or be inherited [45]. It has been indicated that in several types of cancer, such as ovarian, gastric, and colorectal carcinoma, the epigenetic silencing of MMR has been shown to happen by hypermethylation of hMLH1 promoter [46, 47, 48]. Moreover, a study investigated the Mut proteins involved in the MMR pathway showed an increase in cisplatin effectivity in MSH2/MSH6-dependent manner, which lead to apoptosis [49]. In comparison, MLH1-deficient cells showed less response to cisplatin than MLH1-proficient cells. Moreover, cisplatin induces cell death was associated with proteolysis of MLH1 [50]. These facts were associated with the destabilization of XIAP, which prompts caspase activation [51]. Unlike the NER pathway, there is an association with faulty MMR and

chemoresistance of carboplatin and cisplatin resistance [51, 52, 53] as a result of apoptosis activation through MMR proteins [54, 55].



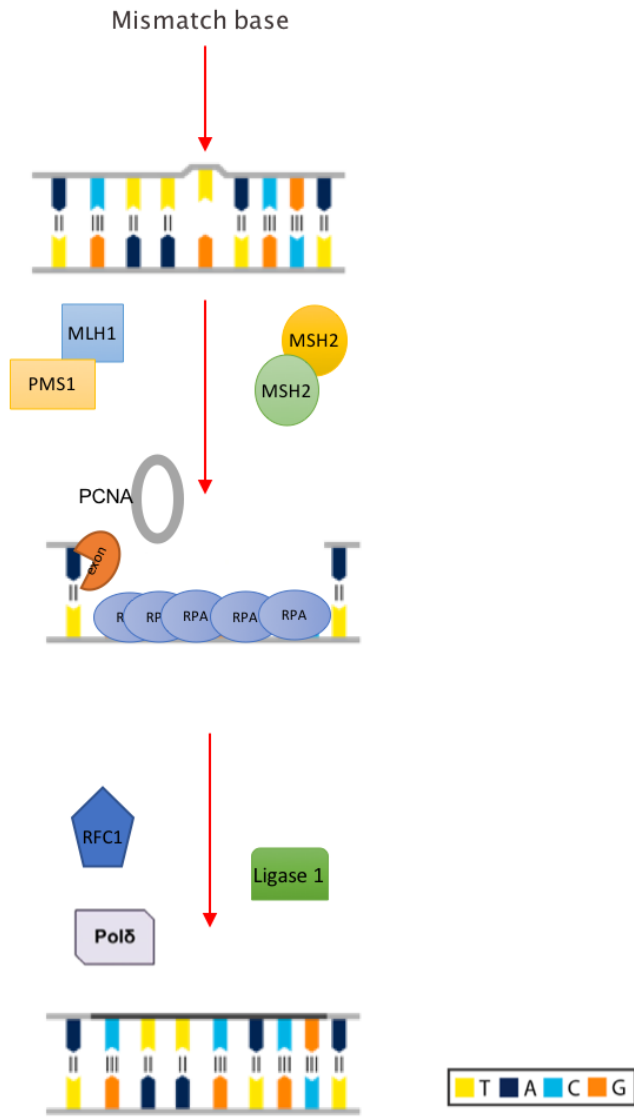


**Figure 1.1.3 Schematic representation of MMR pathway.** Mismatched nucleobase is recognised in the new strand and removed. In the next step the mismatch base replaced with the correct nucleotides. The DNA ligase will be used to seal the gap in the DNA as a final step.

### 1.4.3 Homologous recombination

HR pathway is involved in the repair process of double-strand breaks (DSBs) and ICLs. Different proteins are involved in the HR process, which starts with recognizing the strand breaks. Afterward, BRCA1 mediates the MRN complex, which was activated by ATM kinase through phosphorylation. Eventually, resection of the complex takes place at the 3' ends of the DSB, unzipping the DNA single-strand to facilitate the invasion of the sister chromosome by the destroyed 3' end where RAD51 and BRCA2 are involved. The extension of the destroyed 3' is then achieved by DNA polymerase, which utilizes the complementary strand (Figure 1.1.4) [56, 57]. The process and the involved proteins in the HR pathway were reviewed in detail elsewhere [58]

HR pathway plays a role in repairing ICLs induced by cisplatin; different studies indicated the relationship between the HR pathway and cisplatin. For instance, the deflection in *BRCA2* in cancer cells enhances the chemosensitivity to cisplatin [59]. *BRCA2* is an essential factor in the HR pathway during the conjunction step with Rad51 [60]. Therefore, ovarian carcinoma patients with *BRCA1/2*-mutation respond to platinum chemotherapy, which improves their survival [61]. However, different trials have also shown that mutation in these two genes leads to cisplatin resistance [62,63]

### 1.4.4 Nonhomologous end-joining

NHEJ is another pathway to repair DSBs, which can be induced by different genotoxic agents such as anthracyclines, topoisomerase toxins, and bleomycin. The NHEJ pathway process includes different types of proteins, which been described in detail elsewhere [64]. Following the DSB occurred, the catalytic component and regulatory

□ □ □

component make up the regulatory subunit (the Ku70/Ku80 heterodimer) and the DNA-dependent protein kinase (DNA-PKcs) enzyme.

DNA PKcs is composed of threonine or serine kinase from the category of phosphatidyl inositol-3 kinase. The complex's regulatory subunit shows no dependence on the sequence when it binds to the DNA strand and double-stranded ends. These ends are essential in activating and promoting the subunit made of the catalytic component. Also, during the NHEJ pathway, extra proteins such as DNA ligase IV and Artemis are used. Considering that there is usually no dependence on the complementary strand, insertion, and deletion of nucleotides occur during DNA duplexes fusion [65, 66].

Several investigations showed the relationship between the NHEJ pathway and cisplatin. It was demonstrated that cisplatin leads to increased cancer cells' sensitivity to ionizing radiation via inhibition of NHEJ [67]. Moreover, cancer cells become sensitive to cisplatin inducing ICL following DNA-PK inhibition, which is a factor involved in DSBs repairing via its Ku subunits. [68]

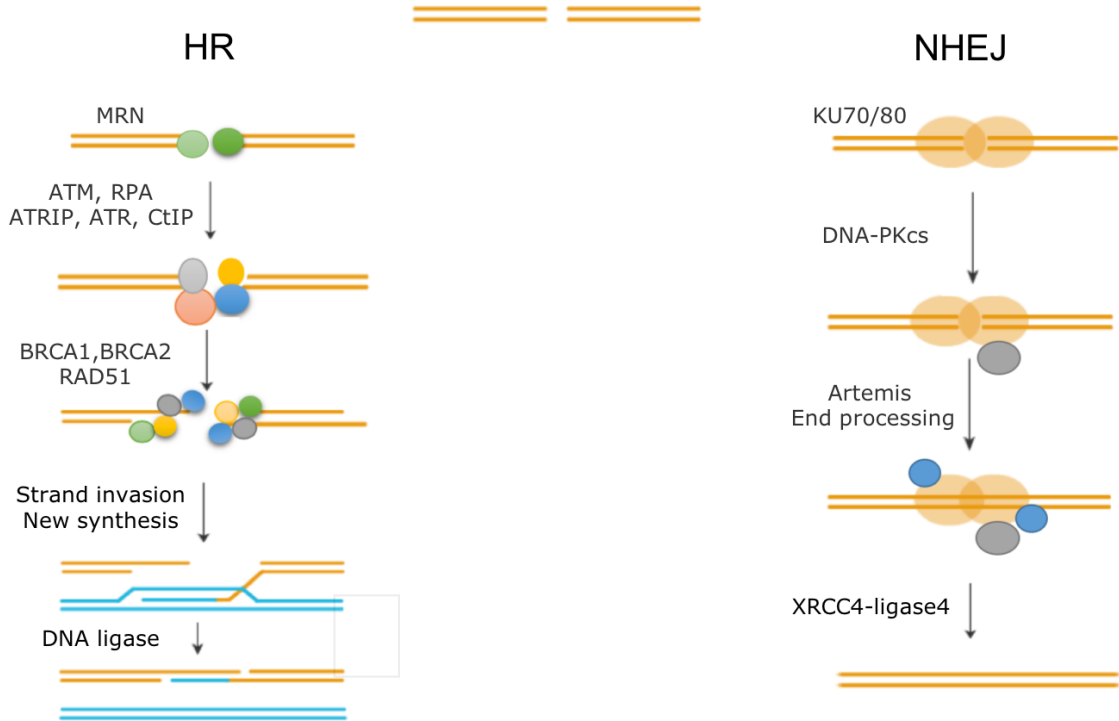


**Figure 1.1.4 Overview of the HR and NHEJ pathway.** After detection of the DSB, the 5' strands are resected, producing long 3' single-stranded DNA tails that then serve as a substrate for assembly of a Rad51 nucleoprotein filament. Branch migration of this joint DNA molecule, DNA synthesis, ligation, and resolution of Holliday junctions restores the DNA templates. An alternative pathway for DSB repair is nonhomologous end-joining (NHEJ). In this case, the two broken ends are processed and ligated directly. NHEJ generally leads to small DNA sequence deletions.

#### 1.4.5 Fanconi anemia pathway

FA is a human disorder caused by the mutation of different genes. The function of these genes (at least 14) has not been entirely understood. However, strong indications show that these genes, including the *BRCA2* (known as *FANCD1*), engage in a standard repair pathway of ICLs. The HR repair pathway is promoted via the FA pathway when the FA cells are treated with crosslinks inducing agents. [69]. There is an intersect between the FA pathway elements and other DNA damage repair pathways, including HR and NER. The FA proteins and the steps involved in the pathway have been reviewed in detail elsewhere [69, 70]

FA pathway plays a crucial role in eliminating ICLs, and recent studies using FA cells as a model to understand the chemoresistance. The process starts when ICLs are identified at approaching a replication fork. Followed by the monoubiquitination of FANCD2/FANCI heterodimers, which allow the activation of damage response of DNA. Despite ensuring sufficient repair process, the FA pathway also helps in the coordination of the transcription process, which is achieved through HR and using corrective mechanisms that prevent the occurrence of errors during chromosome segregation. Mutations within FA genes increases cancer cells' sensitivity to cisplatin chemotherapy [70, 71].

#### 1.4.6 Base excision repair

BER is a DNA repair pathway that helps to fix damaged base. Different enzymes, like glycosylases, are involved in this pathway. This cellular mechanism starts with identifying the damaged base first. The AP site will then be formed after the hydrolysis of

□ □ □

the N-glycosidic bond [72]. Figure 1.1.5 shows the BER pathway's main steps in the presence of a damaged base in DNA.

The involvement of the BER pathway in repairing the ICLs was indicated [73]. More evidence suggests the involvement BER pathway following inducing DNA adducts with different crosslink agents such as psoralen, mitomycin C, and cisplatin [74-76]. Clinical relevance has confirmed the involvement of deregulated proteins associated with the BER pathway from different cancer types [74, 75, 76].

Several studies indicated that the sensitivity of cisplatin is significantly influenced by BER [76, 77, 78]. Some factors, such as Apurinic or apyrimidinic endonuclease (APE1), contribute to resistance during cisplatin chemotherapy. For instance, a study showed that overexpression of APE1 was linked to the chemoresistance. While the inhibition of APE1 in a lung cancer cell line, A549, leads to increased cisplatin sensitivity [76]. On the other hand, there was no substantial proof that shows the association of platinum drug and the repair mechanism found in some studies [79, 80, 81].

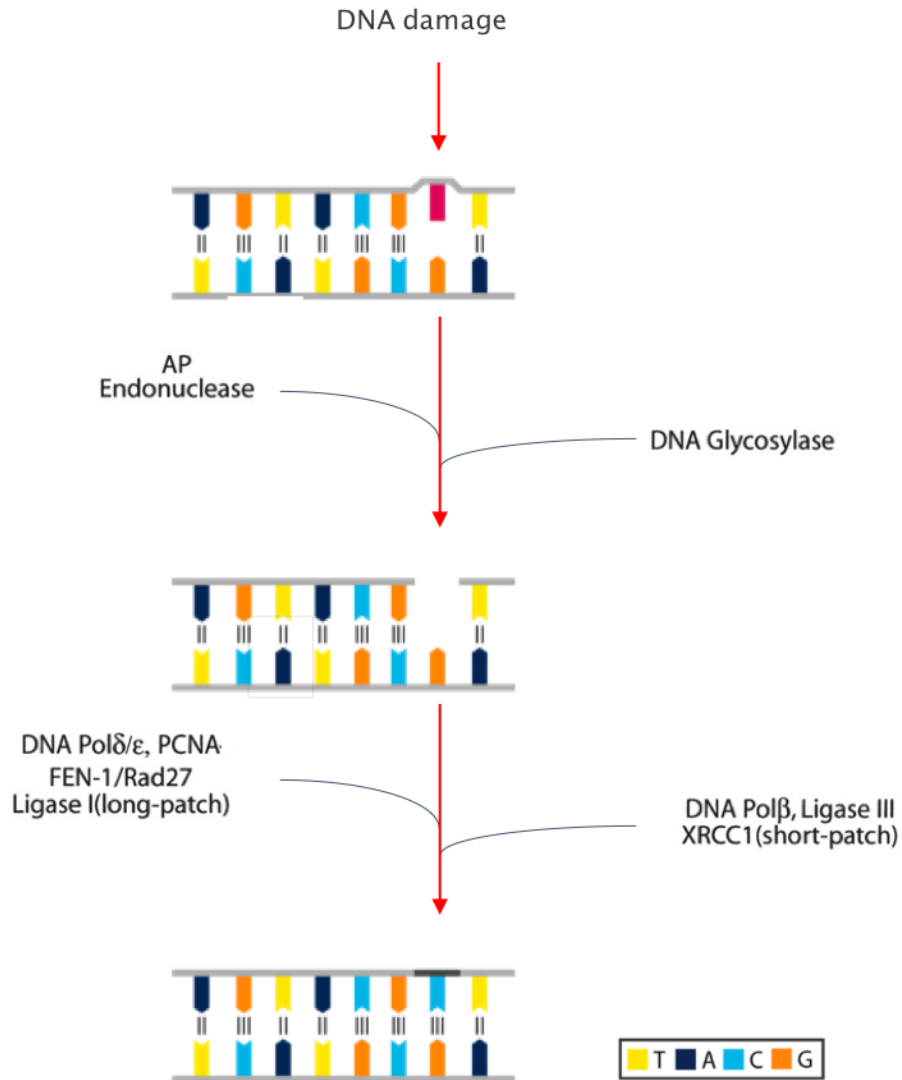


**Figure 1.1.5 Overview of the BER repair pathway.** Glycosylase action creates an apyrimidinic/apurinic (AP) or abasic site, which is processed by an AP endonuclease. a single or multiple nucleotide are added, followed by ligation.

□ □ □

By gaining more knowledge and insight regarding DNA repair pathways' involvement in platinum chemotherapy, it becomes clear that different factors are involved in the repair system that reduces the chemotherapy's effectivity, as previously mentioned in section 1.5. Therefore, further investigations must also focus on different biological key factors (e.g., epigenetic) may improve our understanding of the cytotoxicity of cisplatin. Therefore, the role of epigenetic changes in cisplatin resistance should be investigated (section 1.6). For instance, essential insights from different studies indicated that repositioning of genes in the interphase nucleus may play a role in cancer and chemotherapy (more information in chapter 4).

### **1.5 Role of epigenetic changes in cisplatin resistance**

In this section, the key factors of epigenetic contributions to cancer and chemotherapy were reviewed, in particular, the role of chromatin remodeling, histone acetylation and methylation.

#### **1.5.1 Chromatin remodelling**

The arrangements of nucleosomes in three-dimensional structure results in the formation of chromatin. Recent studies have emphasized that chromatin structure plays a vital role in gene expression. A nucleosome consists of histone octamer with a 146 base pair length of DNA chain wrapped around it. Two copies each of H2A, H2B, H3 and H4 histone proteins comprises the central core of histone. [82]. At the centre of the core, two copies each of H3 and H4 histone form a tetramer. A stable complex is formed by the H3/H4 tetramer, and H2A/H2B dimers [83]. H1 is a linker Histone that is located between each octamer.

□ □ □

Depending on its function, there are two categories of chromatin: euchromatin and heterochromatin. The majority of the genes are transcribed when euchromatin is decondensed, which occur during the interphase; however, throughout the cell cycle, heterochromatin remains condensed and contains mostly inactive genes (Figure 1.1.6) [84]. Chromatin structure plays roles in regulates all processes that occur in DNA, including replication, transcription, recombination, and repair [85]. There are two ways to modify and regulate the structure of chromatin; which known as post-translational modifications (PTMs) and ATP-dependent chromatin remodelling activities. These two types of chromatin modifications may result in modifications of the nucleosome in a particular area in the chromatin structure; or generally [86, 87, 88, 89].

In PTMs, the N-terminal tail histone is modified by enzymes through different modifications like methylation and acetylation. Many DNA metabolism processes are regulated by the histone PTMs, including DNA repair and transcription; not only this, but also PTMs was linked to DNA damage response [90, 91, 92]. For instance, histone H3, at lysine 9 and lysine 14, acetylation is correlated with the NER [85]. This modification is also found in the euchromatin on H3K4 trimethylation [93, 94, 95]. Moreover, histone methylation is a key factor implicated in chromatin stability and cell cycle progression; not only this but also an essential part in cell signalling following DNA damage occurred.

In the enzymes-based ATP-dependent chromatin remodelling, energy from ATP hydrolysis is used for the modification of DNA-histone complex, which results in an alteration in nucleosome structure [96]. This facilitates greater access of nucleosome DNA to interacting proteins [97, 85]. There are four families of complexes which are involved in the chromatin modellers, including ISWI, the switching defective/sucrose non-

□ □ □

fermentable (SWI/SNF) INO80/SWR1 and CHD complexes. Chromatin structure is modified by these complexes by moving/sliding, unwrapping, ejecting or restructuring nucleosomes [98]. A subunit of the Snf2 family is contained by all of the ATP remodeller complexes. This family comprises certain DNA repair proteins, such as RAD54 [99, 100].

Furthermore, the ATP-dependent chromatin remodelling factors are involved in DNA repair. For instance, the SWI/SNF complex is needed for the excision of CPDs. Also, the INO80 remodeller enhances XPC and XPA enrolments in the NER repair system [101]. There is considerable evidence indicates the involvement of the ATP-dependent chromatin remodelling in DNA repair following induces the damage by genotoxic agents [85, 102, 103]. Therefore, it will be beneficial to understand the role of chromatin remodelling involvement in repair of DNA damage induced by cisplatin.

For instance, the SWI/SNF complex modifies the appearance of chromatin in the event that DNA damage has occurred. For the repair process to be effective, the chromatin is unwound. The ICLs and the intrastrand adducts of cisplatin incomplete repairs were seen in cells that lacked Brm and Brg1 (catalytic subunits of SWI/SNF) [104].

According to a study that examined the impact of cisplatin management on changes that occur after the modification of histones in cancerous cells, it was found the histone H3 phosphorylation occurred at Ser-10, mediated by MAPK p38 pathway, which happened after treatment with cisplatin. Additionally, histone H4 hyperacetylation occurred after the utilization of the drug. Altogether, these results demonstrate the association between modifications in the structure of chromatin could be changed following the cisplatin chemotherapy [105]. Notably, histone deacetylase inhibitors (HDAC) are important in the management of cancer as they effectively control regulatory genes in the cell-cycle. In

guinea pigs, sodium butyrate which is an HDAC offered protection against ototoxicity of cisplatin by single-dose administration. This makes HDAC plausible for possible clinical use when patients undergo chemotherapy using cisplatin considering that the HDACs have minimal side effects [106]. Therefore, it is essential to investigate other epigenetic key factors such as histone acetylation and methylation to understand cancer and chemotherapy better.



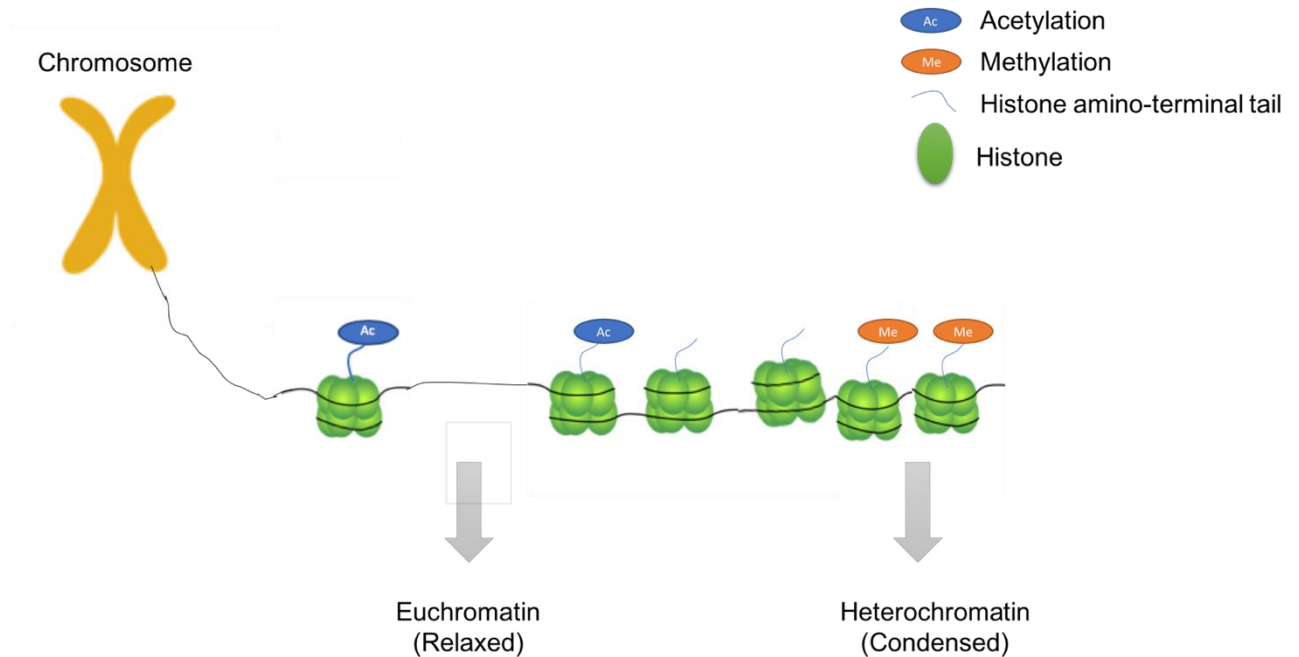


**Figure 1.1.6 Schematic of histone methylation and acetylation in the chromatin.**

Adding methyl groups to the tails of histone core cause histone methylation, which produce condensed state of chromatin known as heterochromatin, which lead eventually to transcriptional repression. Adding acetyl groups to lysine residues in the N-terminal tails of histones lead to histone acetylation, which produce a relaxed state of chromatin known as euchromatin, which lead eventually to active transcription status.

### 1.5.2 Histone acetylation

Chromatin structure is very dynamic, and changes occur in response to environmental and extracellular signals [107]. One important chromatin modification is the histone tail acetylation, which alters accessibility of DNA to regulating enzymes by transforming the structure of chromatin from compact to relaxed which is permissive of gene expression [108, 109]. The acetylation status is ultimately determined by the balance between histone acetyltransferase (HAT) and histone deacetylase (HDAC) activities (Figure 1.1.7) [110]. Histone acetylation is involved in mitosis and meiosis, cellular differentiation, DNA damage, DNA transcriptional regulation, DNA replication, and circadian rhythms [111, 112, 113, 114].

Based on structural homology, enzymatic activity, and cellular localization, mammalian HDACs are divided into four classes [115, 116, 117, 118]. Class I HDACs interact with histones and other proteins (HDAC 1, 2, 3, and 8) and are mainly nuclear [119, 120], whereas class II HDACs (HDAC 4, 5, 6, 7, 9, and 10) are tissue-specific and can be both cytoplasmic and nuclear [121]; Both class I and class II enzymes are inhibited by most of the HDAC inhibitors [119, 121]. Sirtuins (SIRT1 – 7; silent information regulators) is considered as a class III HDACs. They are not responsive to majority of HDAC inhibitors but require the cofactor NAD<sup>+</sup>. Lastly, HDAC11, which is a class IV HDAC, is expressed in the nucleus. It is homologous to class I and class II HDACs (Table 1.1.2) [121, 122].

**Table 1.1.2 Classification of HDAC family**

Class	Members	Subcellular localization
I	HDAC1	Nucleus
	HDAC2	Nucleus
	HDAC3	Nucleus
	HDAC8	Nucleus/cytoplasm
II	HDAC4	Nucleus/cytoplasm
	HDAC5	Nucleus/cytoplasm
	HDAC7	Nucleus / cytoplasm / mitochondria
	HDAC9	Nucleus/cytoplasm
	HDAC6	Mostly cytoplasm
	HDAC10	Mostly cytoplasm
III	sirtuins in mammals (SIRT1, SIRT2, SIRT3, SIRT4, SIRT5, SIRT6, SIRT7)	-----
IV	HDAC11	Nucleus

□ □ □

In the transcriptional activation HATs are involved, and in humans, five families of HATs are present. GNAT, p300/CBP, MYST, TF-related HATs, and NR co-activators are the nuclear HAT families. The first recognized family of HATs are Gcn5 (GNAT) related N-acetyltransferases. In eukaryotes, Gcn5 homologs are highly conserved proteins and are noted in numerous organisms [123].

Mutation, overexpression, or translocation can alter the HAT and HDAC activity, therefore disrupting the balance between acetylation and deacetylation. Consequently, they contribute to cancer hallmarks; these epigenetic alterations have been observed in different types of malignancies including different types of cancer (breast, prostate, colorectal, and ovarian cancers) [119, 124]. Alterations in acetylation participate in carcinogenesis by silencing the promoters of tumor suppressor gene (such as *p21*) [123, 125], abnormal recruitment of HATs or HDACs or activation of repressed genes [119].

Once DNA binds to cisplatin agents, adducts of platinum-DNA components are produced. The intact structure of chromatin dramatically reduces the access of DNA by cisplatin, while using HDAC inhibitors makes DNA easily accessible to the agents due to the fact that they relax the chromatin structure [126].

The modification of histone enables the optimal function of chromatin as well as determining its structure. Currently, it has been discovered that histone acetylation is important in DNA repair and the transcription process, and several reports indicate a link between cisplatin resistance and HAT gene expression [127].

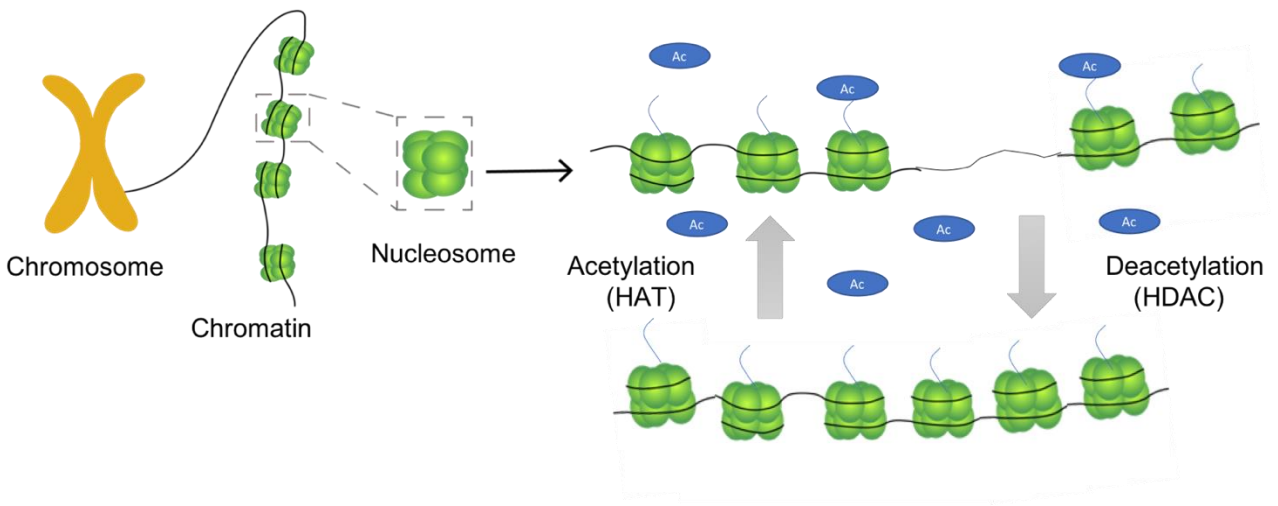


**Figure 1.1.7 Schematic of Histone acetylation and deacetylation.** Histone acetyltransferase (HATs) adds acetyl groups (Ac) onto histone tails, which cause nucleosome opening thus help transcription factors to be in contact with DNA and initiate gene transcription. Histone deacetylases (HDACs) eliminate the Ac from the histone tails, which cause a closed chromatin structure

### 1.5.3 Histone methylation

Methyl groups are transferred from S-adenosylmethionine to lysine or arginine residues of histone H3 and H4 by histone methyltransferases (HMT) [128]. Lysine 20 of amino terminal end of H4 and lysine 4, 9 and 27 of amino terminal ends of H3 are methylated frequently [129]. HMTs are classified into three different groups based on the structure and sequence of their catalytic domains: 1) SET domain containing methyltransferases 2) Arginine methyltransferases and 3) Dot 1 like lysine methyltransferases [130]. Four subfamilies of SET domains have been identified namely, the SET1 family, the SUV39 family, the SET 2 family and RIZ family [131]. Arginine 3 on histone H4 is methylated by protein arginine methyltransferase (PRMT1) which is a histone methyltransferase [132]. This methylation by PRMT1 seems to be vital in vivo for the maintenance or establishment of a broad range of "active" chromatin modifications. Co-activator-associated arginine methyltransferase 1 (CARM1) is involved in enhanced deposition of arginine 17 methylation [133].

Epigenetic factors such as DNA methylation and histone modification help in suppressing tumor suppressor genes. The modification which takes place at H4 and H3 is achieved through lysine methylation and H3-K9 methylation promotes the suppression of cancerous cells [134]. The pharmacodynamic effects of drugs in DNA methylation are significant in the histone methylation process. In this case, the onset of drug resistance in regard to cisplatin in the case of neuroblastoma cells showed that DNA methylation is dramatically relevant in the process [135].

In regard to ovarian cancer and epigenetics, many experts have studied and reviewed many factors such as PAR-4, modified regulation TMS1/ASC, DAPK, LOT1,

□ □ □

BRCA1 hypermethylation, [136,137,138,139,140]. Moreover, in ovarian cancer, some enzymes such as H3K9 methyltransferase G9a are found in large amounts in correlation with negative health outcomes and reduced rate of survival [141]. Considering the benefits of DNA methylation in the case of ovarian cancer, many drugs that specifically target the methylation process have been manufactured. Some examples of manufactured drugs include decitabine and 5-azacytidine which are both inhibitors of DNA methylation. Unfortunately, the immunosuppressive impacts associated with the use of these drugs have made their use limited [142]. Nonetheless, ovarian cells that are platinum-resistant 2008/C13 were shown to become sensitive to carboplatin when combined together with azacytidine through preheating [143].

Collectively, these facts provide additional evidence regarding the role of epigenetic changes in cancer and chemotherapy. Moreover, the DNA repair systems have a substantial effect on decreasing the chemotherapy's effectivity, as reviewed in section 1.4. However, despite all these findings, the chemoresistance of cisplatin is not well understood. Therefore, further investigation should be conducted in other relevant biological aspects. It is essential to identify approaches that indicate the mechanism of cisplatin-induced DNA damage and demonstrate the DNA repair systems' involvement, which will help us to understand the mechanism(s) of chemoresistance better. Identification of ways to measure the damage will help to improve our knowledge about the chemoresistance, thereby refining current disease treatment. Therefore, section 1.6 will briefly described standard approaches to measure the DNA damage induced by cisplatin and the repair systems' involvement.

## **1.6 Methods to detect DNA damage and repair induced by cisplatin**

Several factors dramatically target DNA, including chemotherapeutic drugs, oxidative stress, certain environmental carcinogens, DNA alkylators, and UV radiation exposure, which interfere with DNA structure. Exposure to these agents results in strand breaks and may lead to mutation [144,145]. Cisplatin is a chemotherapeutic drug that induces DNA damage via crosslink formation [146,147]. However, following cisplatin induced DNA adducts, DNA repair mechanisms are activated to repair the damaged DNA (section 1.4), making the treatment less effective [148]. To find a way to understand the mechanism(s) of chemoresistance better, section 1.6 explores the standard approaches that are commonly used to measure the DNA damage and the repair systems' involvement.

### **1.6.1 Polymerase chain reaction (PCR)**

The PCR is beneficial in detecting DNA damage as the amplification process often comes to a halt after encountering a damaged site. During the use of this technique, specific regions of DNA are replicated, observed with the help of agarose gels that analyze DNA fragments depending on the percentage of the gel [149].

### **1.6.2 The comet assay**

In this method, the breaks that occur in DNA, induced by cisplatin, could be measured using single-cell gel electrophoresis. This technique involves putting cells in an agarose gel placed on a microscope slide, which is then lysed with salt and detergent to produce nucleoids composed of supercoiled loops connected to the nuclear matrix. At high pH, the electrophoresis forms a structure whose appearance is more like comets when observed using fluorescence microscopy. The total DNA breaks are represented by the intensity of the relative relationship between the head and the tail of the comet [150]. Also,

□ □ □

in this assay, it is possible to monitor the repair process of DNA through treating cells with cisplatin that induces DNA damage and then incubating them at 37 °C to allow the cells to repair the damage [150].

### **1.6.3 Comet-FISH**

This technique works by detecting repair and DNA damage in certain regions on the genome [151]. The method has been successful in several studies where specific probes for gene and chromosomes are utilized in regard to DNA damage in the comets (reviewed in [152]).

In a single cell, specific gene localization domains can be determined by combining Fluorescence In-Situ Hybridization (FISH) and comet assay. Fluorescent signals identify the extent of damage and repair in DNA at particular sites and their total number.

### **1.6.4 Terminal deoxynucleotidyl transferase dUTP nick end labelling (TUNEL) assay**

TUNEL is a beneficial method to detect DNA fragments whereby the free terminals of DNA are fluorescent so that apoptosis can be observed using a fluorescence microscope [153]. The TUNEL assay can also be used to detect breaks that occur in double stranded DNA [154, 155].

### **1.6.5 Enzyme-linked immunosorbent assay (ELISA)**

Different substances, such as hormones, antibodies, proteins, and peptides, can be quantified and detected in this assay. When it comes to the quantification of DNA damage, competitive ELISA is a frequently used immunological approach for the process. Different kinds of ELISA use enzymes such as peroxidase and phosphatase to detect major

□ □ □  
antibodies. ELISA can be classified into four major types: direct, indirect, competitive, and sandwich.

There is an antigen on a surface during ELISA, which is then combined with the enzyme-linked antibody. Detection can be achieved by evaluating the conjugated enzyme activity together with a substrate where a product that can be measured is formed. The interaction between the antigen and the antibody dramatically influences the assay's success rate [156]. Therefore, ELISA is an excellent approach to detect and semi-quantify cisplatin-induced DNA adducts in ovarian cancer cell lines, especially with an antibody that recognizes cisplatin DNA adducts (including interstrand crosslinks, intrastrand crosslinks, and monoadducts). In section 2.2.14, measuring the cisplatin-induced DNA adducts was explained in detail by using ELISA.

#### **1.6.6 Immunohistochemistry**

This immunohistochemical assay is usually performed on tissue and also different samples (cells) that are fixed. During fixation, samples are treated with RNase and proteases to remove RNA and protein. Afterward, propidium iodide is used to counterstain cells so that visualization of nuclei in cells that are adduct-negative can be achieved in immunofluorescence. It is a powerful technique that can be useful even with small amounts of samples and can also recognize adducts in individual cells in the tissue [157].

#### **1.6.7 Immunological assay**

The immunological assay is very specific and sensitive. In this assay, a small amount of DNA is considered so that when detecting small adduct levels. The immunodot-blot assay was utilized to detect 6-4PPs and CPDs and the Dewar valence isomers of the components under ultraviolet-irradiated mammalian cells [158].

### **1.6.8 High-performance liquid chromatography-mass spectrometry (HPLC-MS)**

The HPLC-MS is also specific and sensitive but has a significant shortcoming. The assay is not useful when it comes to the detection of oxidative base damages, particularly guanine. This is attributed to premature elution in liquid chromatography. Electrospray soft ionizing characteristic enables the assessment of DNA adducts induced by chemicals [159, 160], CPDs, and 6-4PPs induced by UV exposure.

### **1.6.9 Gas chromatography–mass spectrometry (GC-MS)**

The GC-MS uses the principles of mass spectrometry and gas chromatography to detect several components in a sample [161]. This technique is widely used when it comes to the evaluation of oxidative DNA damage, given its characteristic of identifying many products of base modification [161].

As previously explained in section 1.6, several approaches are currently utilized to detect different types of DNA damage and repair. However, there exist some benefits and shortcomings in these approaches (reviewed in detail in [162]). Therefore, it is essential to consider improving these approaches and using different detection techniques that reveal the severity of the damage and quantify DNA damage and repair from different aspects. Altogether, these strategies will help to understand the mechanism(s) of chemoresistance better and improve cancer treatment.

Conclusively, ovarian cancer is one of the highest diagnosed reproductive cancers in women. The main routes to treat ovarian cancer are invasive surgery and chemotherapy (including cisplatin in combination with other chemotherapeutic drugs). The chemotherapy has proven to be effective in some patients; however, a high percentage of patients relapse after the initial treatment due to abnormally high activity of their repair systems or

□ □ □

mutations occurring in genes sensitive to chemotherapy. Therefore, this thesis investigates DNA damage and genomic organization in the cellular response to platinum chemotherapy in ovarian cancer cells.

### **1.7 Hypothesis and specific aims**

Several platinum compounds, including cisplatin, are currently used as anticancer drugs to treat ovarian cancer. However, ovarian cancer patients often develop chemoresistance to current platinum/taxane chemotherapy regimens either during initial treatment or upon recurrence, which leaves patients with no alternative treatment options. The mechanisms responsible for acquired tumor chemoresistance remain unclear. It is hypothesized that differences in the formation and repair of platinum-derived DNA adducts will exist between chemoresistant and chemosensitive ovarian tumor cells. Therefore, the purpose of this thesis was to investigate the basis of chemoresistance in ovarian cancers. Also, to gain knowledge in knowing the modifications that exist in sensitive cell lines compared to the resistant cell lines. This can be achieved by understanding their response to DNA damage and repair capacity (chapter 3). Furthermore, it is hypothesized that there is a difference in the organization of chromatin in chemosensitive and chemoresistant ovarian cancer cell lines, and gene repositioning and copy number changes are associated with resistance to chemotherapy in ovarian cancer cell lines (chapter 4).

In order to achieve the goal of this thesis, the following aims have been identified:

**Aim 1.** To examine the difference in the DNA damage response in chemoresistant and chemosensitive ovarian cell lines.

**Aim 1A.** To examine changes in the DNA damage response with acquired chemoresistance cell line.

**Aim 2.** To investigate the potential role of gene positioning and copy number changes in chemosensitive vs chemoresistant ovarian tumor cell lines





**CHAPTER 2**

**MATERIALS AND METHODS**

## **2. Materials and Methods**

### **2.1.1 Ovarian cell lines**

This study utilized cells that were derived from ovarian cancers, the chemosensitive cell lines were (A2780 and OCI-P5x), and the chemoresistant cell line was (SKOV-3). A2780, human ovarian cancer cell line, is an established cell line that has been used in toxicity testing and cancer genetic studies [163]. The A2780 ovarian cancer cell line, chemosensitive, was taken from a patient with ovarian carcinoma (ECACC Ref No: 93112519). SKOV-3 is an ovarian cancer cell line that taken from the ascites of a Caucasian female with an ovarian serous cystadenocarcinoma (ECACC Ref No: 91091004). SKOV-3 cells are resistant to several cytotoxic drugs including diphtheria toxin, cisplatin and adriamycin. The A2780 and SKVO-3 cells, were purchased from the European Collection of Cell Cultures, ECACC (Louis, MO, USA). OCI-P5x is a primary ovarian cell line, established from a human high-grade serous ovarian carcinoma [164]. OCI-P5x cells were purchased from the Live Tumor Culture Core facility at the University of Miami (Miami, FL, USA).

### **2.1.2 Materials for cell culture**

RPMI 1640 culture medium, McCoy's 5A culture medium, fetal bovine serum (FBS), GlutaMax, 10X trypsin-EDTA, crystal violet, and phosphate-buffered saline (PBS) were obtained from Fisher (Waltham, MA, USA). Cis-diamineplatinum (II) dichloride (cisplatin) was purchased from Sigma-Aldrich (St. Louis, MO, USA). Ovarian Carcinoma Modified Ince medium (OCMI ) is a specific medium and was used to culture the ovarian cancer cell line OCI-P5x. OCMI was obtained from the Live Tumor Culture Core at the Sylvester Comprehensive Cancer Center, Miller School of Medicine, University of Miami.

□ □ □  
Dimethyl Sulfoxide (DMSO) was obtained from Corning (Corning, NY, USA). The cell culture flasks, petri dishes, and six well plates were obtained from Fisher (Waltham, MA, USA).

### **2.1.3 Materials for the alkaline comet assay**

Potassium hydroxide, sodium chloride, sodium hydroxide, ethylenediaminetetraacetic acid, disodium salt dihydrate, Tris base, hydrochloric acid, agarose, low melting point agarose (LMA), and frosted microscope slides were purchased from Fisher (Waltham, MA, USA). Human 8-oxoguanine DNA glycosylase 1 (hOGG1) and T4 endonuclease V (T4endoV) were obtained from New England Biolabs (Beverly, MA, USA). Hydrogen peroxide solution and pH-indicator strips were obtained from Millipore (Bedford, MD, USA), while the propidium iodide solution was purchased from Sigma-Aldrich (St. Louis, MO, USA). 4-(2-hydroxyethyl)-1-piperazineethanesulfonic acid (HEPES), Fisher (Waltham, MA, USA).

### **2.1.4 Materials for FISH**

FISH is a molecular cytogenetic method that utilizes fluorescent probes that bind only to complementarity sequence of the genes of interest. The FISH experiments utilized the following items: glass slides, 1 % pepsin solution, 1 % paraformaldehyde/PBS, and a solution of 0.7 X saline sodium citrate (SSC)/0.3 % Tween 20 which were all purchased from Fisher (Waltham, MA, USA). Dual color [fluorescein isothiocyanate (FITC), and tetramethyl rhodamine isothiocyanate (TRITC)] labelled FISH probes, were used in this study. BAC FISH probes labelled, with FITC or TRITC, were obtained from Empire genomics (Buffalo, NY, USA). 4',6-diamidino-2-phenylindole (DAPI) stain was purchased from Vector Laboratories (Burlingame, CA, USA).

### **2.1.5 Materials for ELISA**

Acetic acid, ethanol, Tween 20, 1-Step™ Ultra TMB-ELISA substrate solution and the stop solution for TMB substrates were purchased from Fisher (Waltham, MA, USA). The QIAamp DNA mini kit was obtained from Qiagen (Valencia, CA, USA). DNA-bind clear 96-well polystyrene plates was obtained from Corning (Corning, NY, USA). Non-fat milk was purchased from American Bio-Science Laboratories (Van Nuys, CA, USA). The primary monoclonal antibody, which recognizes cisplatin DNA adducts (including interstran, intrastrand crosslinks, and monoadducts), was purchased from Abcam (Cambridge, MA, USA). The peroxidase-labelled anti-rat IgG, secondary antibody, was obtained from Millipore Sigma (Temecula, CA, USA).

## **2.2 Methods**

### **2.2.1 Cell culture**

Cells were cultured using the supplier's recommended media for all cell lines. Cells were incubated at 37 °C in a 5% CO<sub>2</sub> and humidified atmosphere. The A2780 ovarian cancer cell line was cultured using RPMI 1640 medium supplemented with 10% (v/v) fetal calf. The SKOV-3 ovarian cancer cell line was maintained in McCoy's 5A medium supplemented with 10% (v/v) FBS . The OCI-P5x ovarian cancer cell line was cultured in OCMI medium. This medium was supplemented with epidermal growth factor (EGF), cholera toxin and serum as described previously [164]. Cells were regularly tested for Mycoplasma infection using a PCR-based assay developed in-house within the Florida International University, cell culture core facility.

□ □ □

Briefly, cells were cultured on the T75 flask and allowed to grow with the proper cell culture media at 37 °C in a 5% CO<sub>2</sub> and humidified atmosphere. Cells were split when they were about 80% confluent. In detail, cells were washed with PBS, and 1X trypsin-EDTA were added to flasks and were then placed in the incubator for 4 mins. Proper cell culture medium was added, and cells were then centrifuged for 5 min. The pellets, in the tube, were then resuspended in the proper medium (1 mL), and according to the proper split ratio, cells were seeded to a new T75 flask with the cell culture medium then placed to the incubator.

### **2.2.2 Cell freezing**

Ovarian cells were washed with PBS and then trypsinized using 1X trypsin-EDTA. Proper cell culture medium were then added, and cells were centrifuged for 5 min, and the pellets were then resuspended in RPMI, McCoy's 5A or OCMI medium containing 10 % DMSO. Cells ( $1 \times 10^6$  cells/mL) were then aliquoted into cryopreservation tubes (1.8 mL, Thermo Scientific), which were placed in liquid nitrogen later on.

### **2.2.3 Cell thawing**

Cryopreservation tubes were thawed in a 37 °C water bath. The cells were transported to a 50 mL tube with 9 mL of specific culture medium. The tubes were then centrifuged at 1600 rpm for 5 min. After centrifugation, the supernatant was removed, and cells were mixed with cell culture medium and subsequently transported to cell culture flasks and placed in the incubator.

#### **2.2.4 Cell counting**

After splitting cells, cells were resuspended in 1 mL of PBS and 50  $\mu$ L of this cell suspension was diluted immediately with 50  $\mu$ L of trypan blue. A hemocytometer was used to count the cells (Horsham, PA, USA); cells diluted with trypan blue were loaded onto slides and cells were counted in all areas (four areas).

#### **2.2.5 Cisplatin treatment**

All cells were treated with cisplatin under sterile conditions with specific concentrations of the chemotherapeutic agent, depending on the type of the experiment (0 - 300  $\mu$ M). Cisplatin powder, from Sigma-Aldrich (St. Louis, MO, USA), was dissolved in PBS to prepare the stock solution (2 mM). The desired final concentrations were then prepared in media and cell lines were treated with cisplatin for 1 h. Subsequently, the cell culture media containing the cisplatin was removed and replaced with drug-free media for differing periods of time (0 - 48 h) depending on the type of the experiment.

#### **2.2.6 Ultraviolet Irradiation of Cells**

UVB and UVC irradiation were achieved using Blak-Ray Lamps (model XX- 15M and XX- 15S) (San Gabriel, California, USA). The UV intensity was determined with a UVX radiometer to estimate the exposure time to accomplish the needed dose to induce the DNA damage.

Briefly, ovarian cells were seeded in Petri dishes; the next day, cells were washed twice with PBS and then irradiated in 1 mL PBS. The petri dish lid was removed prior to irradiation. Subsequently, fresh media was added to the petri dish, and the cells were

□ □ □  
incubated in a 5 % CO<sub>2</sub> incubator at 37 °C for different times (0 – 30 h) to assess DNA repair in ovarian cancer cells.

### **2.2.7 Nuclear DNA Damage and Repair Measured by the Alkaline Comet Assay**

The alkaline comet assay was used to measure the levels of DNA damage and repair in chemoresistant and chemosensitive ovarian tumor cells. The comet assay is an accessible assay popularly used to assess DNA damage. This assay typically recognizes DSB and SSB; and it is based on electrophoresis of fixed cells in an alkaline buffer after lysing step. The electric current helps the damaged DNA migrate far from the nucleus, creating the comet shape; the comet tail's percentage is related to damage induced [165]. The comets were visualized by fluorescence microscopy, which will be described in section 2.2.7.3. The principle of the assay is illustrated in Figure 2.2.1. The comet assay is a beneficial method to assess the ability of DNA repair [166]. That can be assessed by inducing damage using a DNA-damaging agent and then incubate the cells in a 5 % CO<sub>2</sub> incubator at 37 °C for different times (0 – 30 h) to assess DNA repair in the cells by comparing all time points to 0 h, which did not allow to repair.

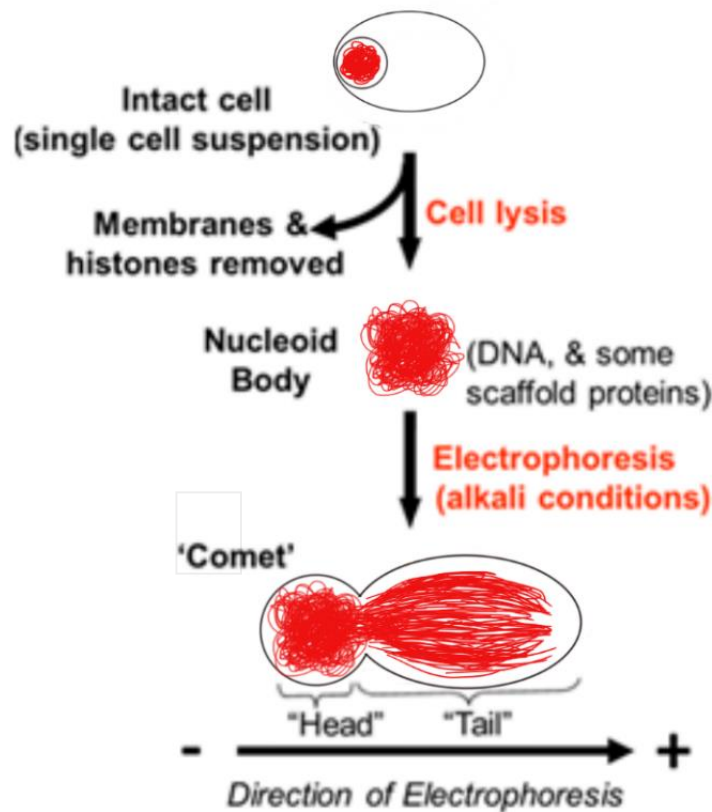


**Figure 2.2.1 Schematic representation of the alkaline comet assay demonstrating how comets are formed during the assay.** Following the cell treatment with DNA-damaging agent, cell, on glass microscope slides, will be lysed under high pH, which lead to remove the cell membranes. Electrophoresis will pull the DNA out of the nucleoid body making a tail, which has a comet shape. Slides will be then neutralized and washed with cold water before drying overnight.

### **2.2.7.1 Cell treatment for comet assay**

Ovarian cancer cells were trypsinized and pelleted by centrifugation at 9000 rpm for 5 min. The cells were then counted and  $3 \times 10^4$  cells in 500  $\mu$ L of PBS were placed in petri dishes for UV irradiation (for the crosslinking experiments, cells were treated with cisplatin first then were trypsinized as will be described in section 2.2.9.2).

### **2.2.7.2 The alkaline comet assay procedure**

The alkaline comet assay was completed as described by Karbaschi et al. [167-169] (Figure 2.2.2.A). Following treatment, the cells were centrifuged at 9000 rpm for 5 min, and the cell pellets were resuspended in 200  $\mu$ L of 0.6 % LMA. The slides were previously pre-coated with 1 % normal melting point agarose (NMA). The mixture of LMA was made by adding 120 mg LMA in 20 mL PBS. After that, 80  $\mu$ L of the cells mixed with LMA was placed onto pre-coated microscope slides with 1 % NMA and covered with coverslip. The pre-coated slides with cells were then placed upon a slide chilling tray (Cleaver Scientific Ltd., UK) (Figure 2.2.2B), to let the agarose to solidify. The coverslips were then removed from all slides and transferred to a lysis buffer tank (100 mM EDTA, 2.5 M NaCl, 10 mM Tris-base, 1 % of Triton 100, set pH 10) for the next day in the dark at 4 °C.

Following 12-16 h of lysis, the slides were placed in the washing box with cold water for 30 min. The electrophoresis step was then performed (25 V and 700 mA for 20 min) in the dark. The slides were then neutralized with 0.4 M Tris-base (pH 7.0) for 20 min. Slides were subsequently placed in washing box and incubated for the next day at 37 °C to dry. For the staining step, slides were first rehydrated by placing them in water for 30 min; and then stained with 2.5  $\mu$ g/mL of propidium iodide solution and incubated for 20 min in the dark. The slides were then washed, in the dark, with water for 20 min. The slides were kept

in the dark until they were scored and analyzed. It was essential to carry out all the steps in the dark to minimize additional DNA damage (Figure 2.2.2A). The comets were visualized by fluorescence microscopy, and the tail intensity of the comets was measured using Comet Assay IV Software (Perceptive Instruments, Haverhill, UK).



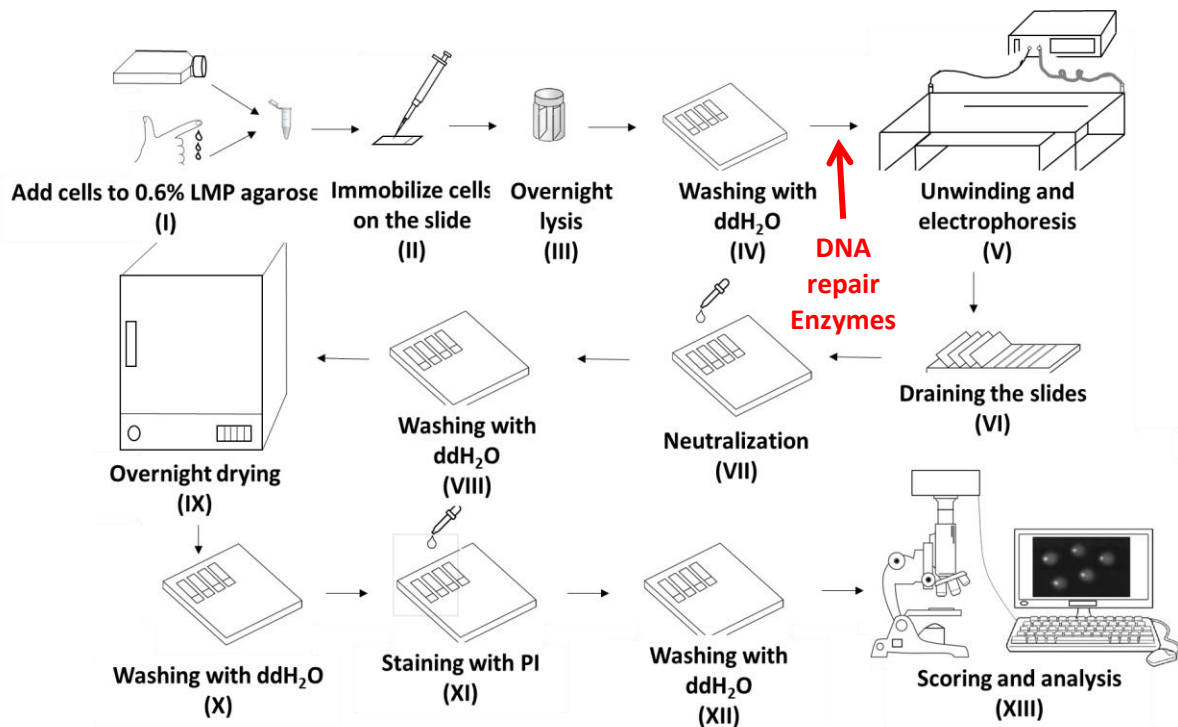


**Figure 2.2.2 (A) Principle of the alkaline comet assay procedure.**

(i) Cells ( $3 \times 10^4$ ) were mixed with low melting point agarose. (ii) Then mixture was layered onto microscope slides, pre-coated with agarose (1%), and the agarose allowed to solidify (iii) The cells were lysed with high pH (pH 10) before (iv) washing with cold water. The existence of strand breaks and high pH facilitate the DNA to unwind. (iv\*) Only in the enzyme-modified comet assay, repair enzymes (diluted with enzyme reaction buffer) were added on slides in this step. (v) Electrophoresis carried the DNA out of the nucleoid body creating a tail. The % Tail DNA (the quantity of DNA in the tail contrasted with the head) is relative to the initial quantity of DNA damage. The slides were then (vi) allowed to dry, (vii) neutralized and (viii) washed with cold water before (ix) drying overnight in the incubator 37 °C. Next, further (x) slides being rinsed in cold water, the slides were then (xi) PI stained, (xii) washed and finally (xiii) the comets were visualized by fluorescence microscopy, and the tail intensity of the comets was measured using Comet Assay IV Software (Perceptive Instruments, Haverhill, UK). This figure reproduced from (Karbaschi and Cooke, 2014).



**Figure 2.2.2 (B) Demonstration of the slide chilling tray (Clever Scientific Ltd., UK).** The tray can carry up to 26 slides on both sides, while the ice pack can be placed underneath of the tray to keep the slides cold and allow the LMA, on the slides, to solidified after seeding the cells.

### **2.2.7.3 Comet image scoring**

Images of comets were at 40 x using an on-line charge-coupled device camera. The tail intensity of the comets was measured using comet assay IV software (Perceptive Instruments, Haverhill, UK). Fifty cells per gel (100 cells in duplicate slides) were scored, and the percentage of tail DNA was measured for each comet in an individual replicate out of three replicates (Figure 2.2.3). During the scoring, the comets located in the edges of the gels were excluded from scoring to avoid any misrepresented comet to the damage.



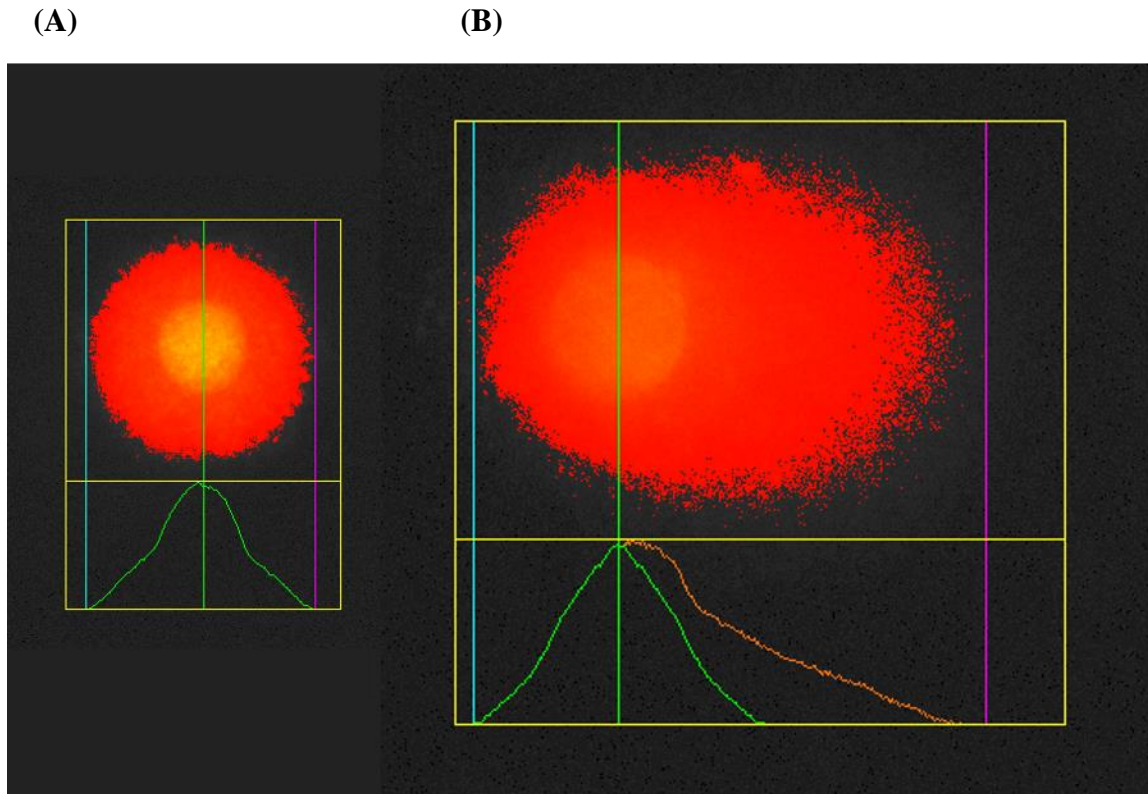


**Figure 2.2.3 Example of comet images and DNA damage analysis using comet assay IV software.** (A) control has minimal levels of DNA strand breaks, so the DNA remains complexed with the nucleoid body, whereas in (B) DNA strand breaks allow the migration of the DNA (under electrophoresis) away from the nucleoid body something along these lines. Electrophoresis carried the DNA out of the nucleoid body creating a tail. The relative size of the tail is an indicator of DNA damage. Percentage tail DNA and tail moment are the two most often parameters to analyze comet assay results. The comet assay IV software (Perceptive Instruments, Haverhill, UK) helps to characterize and quantify the degree of DNA. The software draws a box around the comet, which indicate the beginning of the comet head (blue line), the middle of the head (green line), and the end of the comet tail (purple line). These lines provide the software with the amount of DNA damage in each comet.

#### **2.2.7.4 Analysis of base excision repair**

BER was measured in all ovarian cancer cell lines, using the hOGG1-modified comet assay as described previously [170, 171]. The hOGG1 repair enzyme was used to recognize and remove oxidized purines (such as 8-oxodG) in the DNA of the ovarian cell lines. Inducing oxidized purines, e.g. by H<sub>2</sub>O<sub>2</sub> exposure, and then studying their removal, using the hOGG1-modified comet assay provides an indication of the BER ability for the cell lines studied. hOGG1 acts both as a N-glycosylase and an AP-lyase. The N-glycosylase activity removes damaged purines from double stranded DNA, producing an apurinic (AP) site. The AP-lyase action cleaves 3' to the AP site leaving a 5' phosphate and a 3'-phospho- $\alpha$ ,  $\beta$ -unsaturated aldehyde, which, under the alkaline conditions of the comet assay, becomes a detectable single strand break.

##### **2.2.7.4.1 hOGG1-modified comet assay**

The comet assay was performed as described in 2.2.7.2 with the following changes; cells were treated with 50  $\mu$ M H<sub>2</sub>O<sub>2</sub> and allowed to repair in an incubator for different periods of time (0, 1, 2, 6, 12, and 24 h). The time points were selected with the consideration of ability of the cells to be fully repaired. DNA damage was then measured using hOGG1-modified comet assay, with some modifications [167, 168]. After finishing the lysis step (Figure 2.2.2), 1X enzyme reaction buffer (ERB) was made as 20 mL of 10X ERB (9.532 g of HEPES, 7.46 g of KCl, 186.2 mg of Na<sub>2</sub>EDTA, and 200 mg of BSA dissolved in 100 mL of ddH<sub>2</sub>O, pH 8.0) diluted in 180 mL of cold water. Afterward, the slides were placed in the box for washing with 1X ERB for 10 min. All slides were placed in the incubator for 1 h, and 3.2 U/ $\mu$ L of hOGG1 enzyme, which was diluted in the enzyme reaction buffer (1X ERB) (60  $\mu$ L per gel), was added to all the gels and covered with a coverslip. The

□ □ □  
concentration of the enzyme was optimized as will be described in section 2.2.8.1. After incubation, all coverslips were removed, and the alkaline comet assay was performed, as described in section 2.2.7.2 (Figure 2.2.2 with using step iv\*)

### **2.2.7.5 Analysis of nucleotide excision repair**

Using a similar principle as described for BER, DNA damage that repaired by NER can be induced into the cells of interest, and then the removal of that damage is studied as an indicator of NER. Cyclobutane thymine dimers are DNA damage that can be detected using the T4 endonuclease V (T4endoV)-modified comet assay. T4endoV cleaves the glycosyl bond of the 5' end of the pyrimidine dimer and the 3'-phosphodiester bond, resulting in breakage of the DNA strand, which is detectable by the alkaline comet assay (ACA).

#### **2.2.7.5.1 T4endoV-modified comet assay**

The T4endoV modified comet assay was performed following the same procedure described previously in section 2.2.7.2 with some modifications as described previously [170, 173, 174]. Cells were exposed to UVB (0.5 J/cm<sup>2</sup>) and allowed to repair in an incubator for different periods of time (0, 1, 2, 6, 12, and 24 h). The UVB dose response was previously optimized and 0.5 J/cm<sup>2</sup> is the optimum dose for all tested cell lines. The time points (0 – 30 h) were selected with the consideration of ability of the cells to be fully repaired; therefore, the period between the time points were short. Every gel was incubated with 0.0001 U/μL of T4endoV enzyme diluted in enzyme reaction buffer (1X ERB) for 1 h at 37 °C in a humid atmosphere. The concentration of the enzyme was optimized and mentioned in following section 2.2.8.2

## **2.2.8 Optimization of comet assay analysis parameters**

### **2.2.8.1 Optimization of hOGG1 concentration**

Optimizing the concentration of hOGG1 enzyme was essential for studying the repair ability in ovarian cancer cells. If the concentration of hOGG1 is too high, non-specific nicking may occur, if it is too low, not all the oxidized purines will be discovered. Cells were treated with 50  $\mu\text{M}$  of  $\text{H}_2\text{O}_2$  and slides were then placed in lysis buffer. Cells were treated with increasing concentration of hOGG1 (0.16, 0.32, 1.6, 4.0, 8.0 U/mL), and then DNA damage was assessed using hOGG1-modified alkaline comet assay (as described in section 2.2.7.4.1). A linear increase in the DNA damage with increase of hOGG1 concentration was observed in all ovarian cell lines. Between concentrations 4.0 U/mL and 8.0 U/mL, the activity level of the enzyme come to a plateau. For this reason, 4.0 U/mL of hOGG1 was selected as the optimum concentration of this enzyme for detection of 8-oxodG induced on the DNA of ovarian cell line

### **2.2.8.2 Optimization of T4endoV concentration**

Optimizing the concentration of T4endoV enzyme was also important for studying the NER ability in all ovarian cancer cell lines. If the concentration of T4endoV is too high, non-specific nicking may occur, if it is too low, not all the thymine dimers will be revealed. Cells were exposed to UVB ( $0.5 \text{ J/cm}^2$ ) and slides were then placed in lysis buffer. Cells were then treated with increasing concentrations of T4endoV (0.16, 0.32, 1.6, 4.0, 8.0 U/mL). The assay was then continued according to the T4endoV-modified comet assay, based on the ACA method described in section 2.2.7.5.1. The concentration of the stock provided by the company was high which lead to rapture the whole DNA and show no comets after using serial dilution of the enzyme. The CPD were demonstrate at low

□ □ □  
concentration with all cell line at 0.0001 U/ $\mu$ L, where the increase of the tail in the comet clear comparing to the other concentrations. The optimum concentration of T4endoV for removal of CPD from ovarian cells was selected as 0.0001 U/ $\mu$ L.

### **2.2.8.3 Optimization of PI concentration**

The concentration of PI plays important role for comet scoring; the optimum concentration of PI will help the software to detect the comet easily. Therefore, it was important to optimize the concentration of PI using the same supplier described previously in section 2.2.7.2 with some modifications. Cells were exposed to UVB (0.5 and 1.0 J/cm<sup>2</sup>) and slides were carried out using the same procedure of comet assay in section 2.2.7.2. During the staining step, slides were washed with cold water and stained with different concentrations of PI (2.5, 3.0, 3.5, and 4.0  $\mu$ g/mL) for 20 min. The comets were visualized by fluorescence microscopy, to measure the tail intensity of the comets using comet assay IV software (Perceptive Instruments, Haverhill, UK). The optimum concentration of PI was 2.5  $\mu$ g/mL. There was no significant different among all the concentrations following the exposure with different doses of UVB; however, using higher concentrations showed some issues of detecting the comets.

### **2.2.8.4 Optimization of microscope magnification for scoring comet images**

Comet Assay IV Software was used to detect the DNA damage. The software is well established and can detect the comet easily; however, it was important to optimize the magnification used to have an accurate detection of the DNA damage for every single comet. Two magnifications (20x and 40x) were investigated to determine the best detection of the comets. The optimum magnification that show better detection of the comets was 40x.

## **2.2.9 Detection and quantification of cisplatin induced DNA Interstrand Cross-Links (ICL)**

### **2.2.9.1 ICL-modified alkaline comet assay**

Cisplatin-induced DNA crosslink formation was examined using a modification of the ACA. The principle of the assay is that the presence of ICL in DNA will retard the migration of damaged DNA, formed following an oxidizing insult, in the comet assay. In this instance, the shorter the comet tail, the greater the number of ICL (Figure 2.2.4 and 2.2.5) [172-174].

### **2.2.9.2 Cell treatment for ICL-modified alkaline comet assay**

In time course experiments, the cells were treated with cisplatin (100  $\mu$ M) for 1 h at 37 °C, 5% CO<sub>2</sub>, then cells were placed at 37 °C for different time points (0, 3, 6, 12, 24, 30, 48 h) to measure the peak of the crosslink and repair ability. Cells were then treated with 0 (control) or 50  $\mu$ M H<sub>2</sub>O<sub>2</sub> (to induce a requisite number of strand break to create a DNA tail). After treatment, the cells were pelleted (9000 rpm for 5 min), washed three times with 1 ml PBS and processed for the ICL-modified ACA. In the dose response experiments, following the treatment with a DNA crosslinking agent for 1 h, cells were then placed in agent-free media for 3 h. Cisplatin and formaldehyde were used as a crosslinking agent at different concentrations (50, 150, 300  $\mu$ M). Cells were then exposed to 0 (control) or 0.5 J/cm<sup>2</sup> of UVB (to induce a requisite number of strand break to create a DNA tail). After the exposure, the cells were pelleted (9000 rpm for 5 min) and processed for the ICL-modified alkaline comet assay. To study the effectiveness of the crosslinking agent in different cell-DNA substrates, cells were treated with cisplatin (50, 100, and 200  $\mu$ M) for 1 h at 37 °C, 5% CO<sub>2</sub>, then cells were placed at 37 °C for 3 h. Cells were then exposed to

□ □ □  
0 (control) or 0.05 J/cm<sup>2</sup> of UVC (to induce a requisite number of strand break to create a DNA tail). After the exposure, the cells were pelleted (9000 rpm for 5 min) and processed for the ICL-modified alkaline comet assay.

Comet images were captured using fluorescence microscopy and analyzed by the Comet Assay IV software. The tail moment for comets were evaluated, and the level of DNA interstrand cross-linking was expressed as percentage decrease in tail moment compared to H<sub>2</sub>O<sub>2</sub> treated controls (2.2.7.9 and 2.2.7.10) and calculated according to the following formula:

$$\% \text{ decrease in tail moment} = [1 - ((TM_{di} - TM_{cu}) / (TM_{ci} - TM_{cu}))] \times 100$$

Where  $TM_{di}$  = tail moment of cisplatin-treated and H<sub>2</sub>O<sub>2</sub> treated sample;  $TM_{cu}$  = tail moment of untreated with cisplatin, untreated with H<sub>2</sub>O<sub>2</sub> (control);  $TM_{ci}$  = tail moment of untreated with cisplatin, treated with H<sub>2</sub>O<sub>2</sub>.

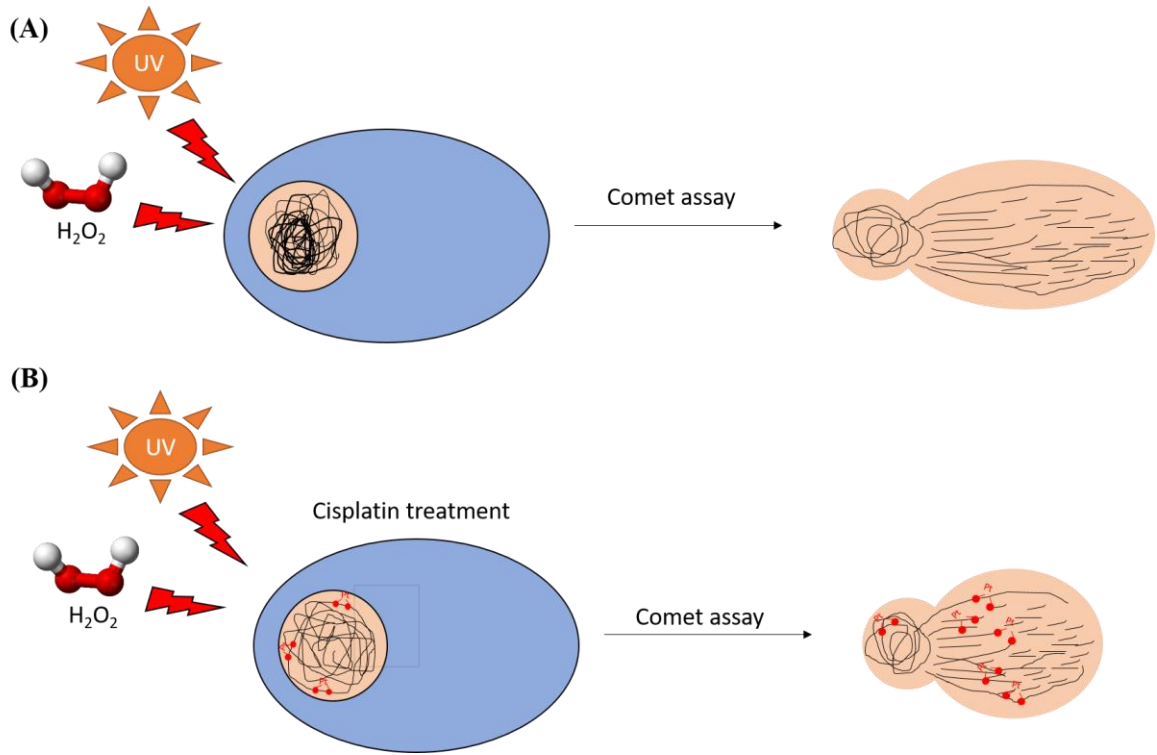


**Figure 2.2.4 A schematic representation of the principle of cross-link formation induced by cisplatin.** The comet assay is a sensitive technique that can detect DNA damage induced by UV or H<sub>2</sub>O<sub>2</sub>. The longer the tail the comet has, the more DNA damage present in the cell. (A) In the absence of cisplatin treatment, the DNA breaks migrate with the current forming the comet shape. However, in the presence of the cisplatin, (B), and with using the same dose of DNA damage agent, the tail become shorter as a result of the formation of crosslinks.

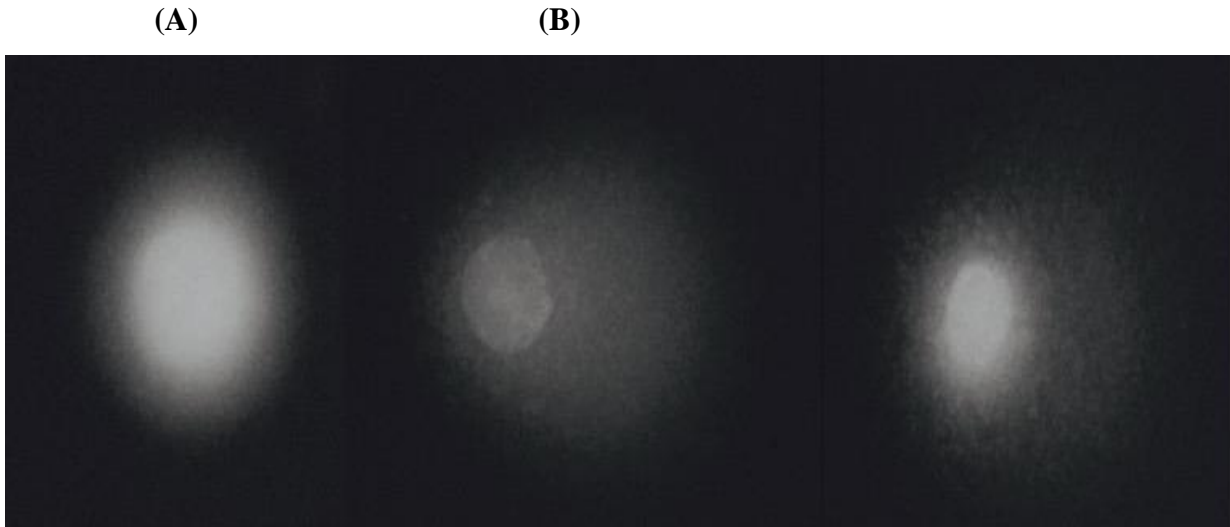


**Figure 2.2.5 Representative comet images illustrating ICL detection following cisplatin treatment.** Comet images with and without cisplatin treatment after inducing strands breaks with hydrogen peroxide in an ovarian cell line (SKOV-3). The comets showed a decrease in tail moment in response to cisplatin treatment (200  $\mu\text{M}$ ) in SKOV-3 cell line. Cisplatin was able to form crosslinks, resulting in a decrease in tail moment after DNA damage induced by  $\text{H}_2\text{O}_2$  (50  $\mu\text{M}$ ). (A) Control cells without any treatment, (B) Cells were treated with  $\text{H}_2\text{O}_2$  (50  $\mu\text{M}$ ) only, (C) Cells were treated with  $\text{H}_2\text{O}_2$  (50  $\mu\text{M}$ ) and cisplatin (200  $\mu\text{M}$ ).

## **2.2.10 Cell survival**

The cell survival of the ovarian cancer cell lines used in this thesis was measured by the clonogenic assay. The clonogenic assay is based on the capability of a single cell to grow, or not, into a colony after being treated with a toxic agent (e.g., cisplatin).

### **2.2.10.1 Clonogenic assay**

Ovarian cancer cells were harvested from cell culture flasks by trypsinization (section 2.2.1), counted (section 2.2.4) and seeded (100 cells/well) in six-well plates. Cells were treated with different doses of cisplatin (10-100  $\mu\text{M}$ ) at 37 °C for 1 h and then incubated in drug-free media for 7 days to measure the ability of cells to produce colonies. During this time, the plates were incubated without replacing media for a period long enough to form colonies of at least 50 cells. For all three cell lines, 7 days of incubation after treating with cisplatin was required to form colonies of at least 50 cells (The incubation time was optimized as described in the following section 2.2.10.2). After incubation, cell culture media was removed, and cells were washed with PBS. Cells were then fixed using 3:1 ethanol:acetic acid and clones were stained with 0.05 % crystal violet and counted under a microscope. Clones containing more than 50 cells were counted and considered as colonies.

### **2.2.11 DNA extraction**

DNA extraction is an essential procedure that required by different assays that conducted in this study like ELISA and inductively coupled plasma mass spectrometry. Following cell treatment with DNA-damaging agent, DNA of treated and untreated cell were extracted using a QIAamp DNA Mini Kit which was obtained from Qiagen (Valencia, CA, USA) as described in the manufacturer's protocol. Briefly, cells were trypsinized and

□ □ □

pelleted by centrifugation at 9000 rpm for 5 min. The cells ( $5 \times 10^6$ ) were then resuspended in 200  $\mu$ L of PBS in a 1.5 mL tube. A protease solution (20  $\mu$ L) was added to the cells and vortexed for 15 sec. cells were then incubated at 56 °C for 10 min and centrifuged for 15 sec. Ethanol (96-100%) (200  $\mu$ L) was then added and the tubes vortexed for 15 s and centrifuged for 15 sec. Samples were then transferred to QIAamp mini spin columns (provided with the kit) and centrifuged for 1 min at 8000 rpm. AW1 buffer (500  $\mu$ L) was then added to all the columns and centrifuged for 1 min at 8000 rpm. After that, 500  $\mu$ L of AW2 buffer was added to samples and centrifuged for 3 min at 14000 rpm followed with another centrifugation at the 15000 rpm for 1 min. AE buffer (200  $\mu$ L) was then added to samples and incubated for 5 min at room temperature, then the concentrations of the eluted DNA were measured. The concentration and purity of the extracted DNA were measured utilizing a Nanodrop (Thermo Scientific, Madison, WI, USA).

## **2.2.12 Cytotoxicity**

### **2.2.12.1 Cell Counting Kit-8**

Cytotoxicity, induced by DNA-damaging agents, was measured using the Cell Counting Kit-8 (CCK-8) (Dojindo Molecular Technologies, Gaithersburg, MD, USA). CCK8 is a sensitive colorimetric assay for measuring cell viability. CCK8 contains a highly water-soluble tetrazolium salt, WST-8, which reduced by dehydrogenase activities in cells to generate a yellow-color formazan dye, that is soluble in the cell culture media. The amount of the formazan dye, produced by the activities of dehydrogenases in cells, is relative to the number of living cells. Cells were seeded in a 96 well plate (5000 cells/well) and incubated overnight at 37 °C, 5% CO<sub>2</sub>. Cells were then treated with increasing concentrations of cisplatin (0, 1.56, 3.13, 6.25, 12.5, 25, 50, 100, and 200  $\mu$ M). After

incubation for 24 h, CCK-8 mixture (10  $\mu$ L) was added to every well and the plates were placed for 4 h at 37 °C, 5% CO<sub>2</sub>. The plate was read at 450 nm in a Biotech plate reader (Winooski, VT, USA).

### **2.2.12.2 Measuring cell toxicity of triazole-modified nucleosides and/or their enhancement with cisplatin efficiency in ovarian cell line**

Triazole-modified nucleosides (8-(1-H-1,2,3-triazol-4-yl)-2'-deoxyadenosine (8-TrzdA) and 8-(1-H-1,2,3-triazol-4-yl)-2'-deoxyguanosine (8-TrzdG)) are chemical compounds that have a fluorescent property. These compounds were obtained from Dr. Stanislaw F. Wnuk (Florida International University, Miami, FL, USA). Using these chemical compounds in the presence of cisplatin is reported to enhance the effectiveness of the chemotherapy treatment [175, 176]. Cell toxicity of triazole-modified nucleosides was measured and their enhancement with cisplatin efficacy in ovarian cell line was measured using CCK-8. Briefly, cell viability was measured by the CCK-8 assay using the in a chemosensitive cell line (A2780) after 24 h of incubation with 8-TrzdG of different concentrations. Five thousand cells were treated with both cisplatin (100  $\mu$ M) and triazole-modified nucleosides to establish if these compounds enhanced the efficacy of the cisplatin treatment in ovarian cell line. Moreover, these compounds were examined to see if they could be incorporated into DNA using the A2780 chemosensitive cell line. Briefly, cells were treated with 8-TrzdG (204.8  $\mu$ g/mL) for 24 h, DNA was then isolated, and samples were fragmented using a sonicator for 30 cycles (30 sec ON/Off). DNA samples were then loaded in a 1 % agarose gel to observe if there was any fluorescence in the bands using UV transilluminator source, or if the size of the DNA bands were larger compared to the control.

## **2.2.13 Quantification of platinum in DNA using Inductively Coupled Plasma Mass Spectrometry (ICP-MS)**

### **2.2.13.1 Cell treatment for ICP-MS**

The chemosensitive cell lines and the chemoresistant cell line were treated with cisplatin (100  $\mu$ M) for 1 h at 37 °C, 5% CO<sub>2</sub>, and incubated in drug free media for 12 h. DNA was extracted as described in section 2.2.11. Samples were then sent to measure the platinum concentration in the DNA using ICP-MS. On different occasions, cells were also treated with cisplatin for 1 h and incubated in drug free media for different time points (0, 12, and 24 h).

### **2.2.13.2 General procedure of ICP-MS**

ICP-MS is an elemental analysis method which quantifies metals such as platinum in samples at milligram to nanogram levels per liter. Ovarian cancer cell lines were treated, as described in section 2.2.13.1, and the DNA extracted, as described in section 2.2.11. The platinum concentration in the DNA samples was measured using ICP-MS by Dr. Natalia Quinete (Florida International University, Southeast Environmental Research Center, Miami, FL, USA).

Briefly, DNA samples (200  $\mu$ L of DNA/platinum) were transferred to pre-cleaned 15 mL tubes. 1 mL of concentrated nitric acid was added to samples and then heated for 2 h at 90 °C in the heating block. After cooling at room temperature, 100  $\mu$ L of the internal standard mix was added (to a final concentration of 10  $\mu$ g/L) and the volume was made up to 10 mL with HNO<sub>3</sub> 3%. Bismuth was used as internal standard. A laboratory procedure blank, a spiked blank and a duplicate of the spiked blank were prepared and followed the same procedure as the DNA samples extracted from the cisplatin treated ovarian cancer cell

lines. Samples were directly analyzed by ICP-MS, SQ-KED (Single Quadrupole with Kinetic Energy Discrimination) mode. A calibration curve was made for platinum from 0.05 to 20  $\mu\text{g/L}$  ( $R_2=0.999$ ). After every 10 samples, the calibration curve verification (CCV) and a blank were run to check the consistency of the calibration curve and any contamination. All values were within the acceptable criteria and recoveries were 96-115%. The method detection limit for platinum was 0.016  $\mu\text{g/L}$ .

## **2.2.14 Detection and quantification of cisplatin induced DNA adducts**

### **2.2.14.1 Cell treatment for ELISA**

Ovarian cancer cell lines were treated with cisplatin (100  $\mu\text{M}$ ) for 1 h at 37  $^\circ\text{C}$ , 5%  $\text{CO}_2$ , then the media was changed to drug-free media and incubated for different time points (0, 6, 12, and 24). DNA of all cells were extracted as described in section 2.2.11.

### **2.2.14.2 ELISA**

ELISA was used to detect and semi-quantify cisplatin induced DNA adducts in ovarian cancer cell lines following cisplatin treatment. The ELISA was optimized as described in section 2.2.14.3, below. Following the cell treatment with 100  $\mu\text{M}$  of cisplatin (section 2.2.5), DNA was extracted as described in section 2.2.11. Following DNA denaturation, the 96 well plate was coated with 50  $\mu\text{L/well}$  DNA solution (50  $\mu\text{g/mL}$ ), diluted in PBS, and placed in the incubator for 1 h at 37  $^\circ\text{C}$  in a 5%  $\text{CO}_2$  and humidified atmosphere. After the plate was washed 3X with PBS, open sites were blocked by 150  $\mu\text{L/well}$  of a 4 % (w/v in PBS) dried skimmed milk (Canton, MA, USA) and incubated for one hour at the incubator; then the plate was washed 3X with PBS. The monoclonal anti-cisplatin DNA adduct antibody (Abcam, Cambridge, MA) was diluted in the blocking solution (0.004  $\text{mg/mL}$ ) added to the plate (50  $\mu\text{L/well}$ ), and incubated for one hour at 37  $^\circ\text{C}$ . This antibody

□ □ □

binds to cisplatin-induced adducts in DNA. The plate was washed three times (300  $\mu\text{L}/\text{well}$ ) with PBS containing 0.05 % (v/v) Tween. The peroxidase-labelled anti-rat IgG secondary antibody (Chemicon, Temecula, CA) was diluted in the blocking solution (0.16  $\mu\text{g}/\text{mL}$ ), and 50  $\mu\text{L}/\text{well}$  was added to the plate and incubated for one hour at 37 °C. The plate was washed three times (300  $\mu\text{L}/\text{well}$ ) with PBS containing 0.05 % (v/v) Tween. The 1-step slow TMB ELISA substrate solution was added (100  $\mu\text{L}/\text{well}$ ) in the dark for 15-30 min to allow the color to develop. Then the reaction was stopped using 0.16 M sulfuric acid (50  $\mu\text{L}/\text{well}$ ). The plate was read at 450 nm in an ELISA plate reader (Winooski, VT, USA). The human keratinocyte line (HaCaT) was exposed to UV and DNA was extracted and used as a positive control using thymine dimers as a positive control in the assay.

#### **2.2.14.3 Optimization of ELISA conditions**

It was important to test a range of parameters for the ELISA procedure to have reliable results, maximizing antibody binding to the DNA adducts, while eliminating non-specific binding. This was performed by optimizing different assay parameters, and then running the ELISA as follows: coating the plate with Poly-L-lysine (Sigma), denaturation of the DNA, concentration of bound DNA, choice of blocking solution (BSA and dry milk), and concentration of primary and secondary antibodies.

Every condition of the assay was tested individually. Briefly, cells were treated, and DNA isolated as described in section 2.2.11. and loaded on to the 96 well plate with or without a boiling step (DNA was boiled for 10 min then cooled rapidly on ice). This step was included to determine if the denatured DNA will have better binding to the ELISA plate. The concentration of the DNA was also optimized using a serial dilution to determine the optimum concentration of DNA (25, 50, 100, and 200  $\mu\text{g}/\text{mL}$ ). Moreover, the choice of

□ □ □

blocking solution was based on preventing the nonspecific binding. Rat monoclonal primary antibody (anti-cisplatin DNA adducts) was used in this study; and goat-anti rat conjugated with Horseradish Peroxidase (HRP) was used as a secondary antibody. The primary antibody was optimized using a serial dilution to determine the optimum concentration to use in this study (1:250 to 1:4000), stock concentration was 1 mg/mL. The plate was read at 450 nm in an ELISA plate reader (Biotech Instruments Inc, USA). After optimizing all conditions separately, Corning 96-well polystyrene plate was used for all experiments.

#### **2.2.15 Evaluation of gene positioning in chemosensitive and chemoresistant ovarian cancer cells**

FISH is a molecular cytogenetic method that utilizes fluorescent probes that have sequence complementarity to specific regions of the genome. FISH facilitates the enumeration of genomic regions of interest and visualization of regions of interest in both metaphase chromosome spreads and interphase nuclei. These labeled DNA probes hybridize with the cytological targets in the sample and can be imaged by fluorescence microscopy (Figure 2.2.6). FISH has a wide range of applications to assess chromosomal abnormalities (e.g., deletions, duplications, and structural rearrangements). However, FISH is also utilized to assess localization of genomic regions (e.g., chromosomes or genes) within the interphase. It has been established that the genome is highly organized within the interphase nucleus, this organization is evolutionarily conserved and cell-type specific and is believed to be another level of epigenetic regulation of the genome. For example, nuclear position may, in part, determine gene expression, DNA damage and repair amongst others.

□ □ □

It uses fluorescently labeled DNA probes complementary to the DNA sequence of specific genes (Table 2.2.1). The main goal of this aspect of the study was to determine if genes involved in ovarian cancer and tumorigenesis were randomly or non-randomly organized in the nucleus of the ovarian cancer cell lines in in this study (A2780, OCI-P5x, and SKOV-3) and to assess the copy number of these genes in the different cell lines. Furthermore, a secondary aim was to establish whether the nuclear localization of the investigated genes differed between chemosensitive (A2780 and OCI-P5x) and chemoresistant cell lines (SKOV-3).

#### **2.2.15.1 Cell treatment for Fluorescence In-Situ Hybridization**

Ovarian cancer cell lines were treated with cisplatin (100  $\mu$ M) in T25 flask for 1 h at 37 °C, 5% CO<sub>2</sub>, then media was replaced with drug-free media and incubated for 12 h to ensure to have a high percentage of DNA crosslinks. Cells were trypsinized and transferred to a 15 mL centrifuge tube, which were centrifuged at 9000 rpm for 5 minutes. The supernatant was removed, and the cell pellet was resuspended drop wise with 5 mL of 3:1 methanol: acetic acid. The sample was then centrifuged as described previously and the dropwise fixation followed by centrifugation steps were repeated a further 2-3 times. The dropwise fixation and resuspension of cells is a critical step to avoid cell clumping, as assessment of gene positioning requires individual cells. Following cell treatment and fixation, cell density was checked under a light microscope (40x phase contrast) by adding a 2  $\mu$ L drop onto a microscope slide, if samples had sufficient cell density and limited cell clumping samples were subsequently stored at - 20° C until required for experiments.

### 2.2.15.2 FISH

In preparation for FISH, fixed samples were removed from - 20° C, and 2-10 µL of the cell suspension was placed onto a slide, amount of cell suspension added was determined to achieve optimal cell density. Slides then were washed with PBS and dehydrated in an ethanol series (70%, 80%, and 100%) for five min each and air dried. Slides were then washed in ddH<sub>2</sub>O followed by rinsing in PBS before incubation in 4% paraformaldehyde/PBS at 4 °C for 10 min; slides were then rinsed with PBS followed by ddH<sub>2</sub>O at room temperature and another ethanol series was carried out at room temperature for 2 min each and the slides air dried. FISH probes complementary to specific genes used in this study are provided in Table 2.2.1. FISH probes were BAC probes spanning the gene of interest and were obtained from Empire genomics (Buffalo, NY, USA). Each probe was labeled with either a red or green fluorophore which facilitated a dual FISH approach and allowed the detection of two different genes simultaneously in cell nuclei. FISH probes were prepared as per the manufacturer's guidelines, the probes: hybridization mix ratio was 1:1:3 (red FISH probe: green FISH probe: hybridization mix). The FISH probe mix was then vortexed and pulse microfuged and subsequently pre-denatured at 73 °C, for 10 min in a water bath. Following denaturation of the FISH probes in hybridization mix 10 µL of probe was added to the slide and a 12x12 mm coverslip were placed on the slide (note, amount of probe was increased or decreased depending on the size of the coverslip utilized). Coverslips were sealed to the slide using parafilm to minimize probe evaporation. After adding the denatured FISH probes and coverslips to slides, the slides were placed in a hybrite (vysis) at 75 °C, for 90 sec and followed by hybridization overnight (16 h) at 37 °C in a humidified chamber. The hybridization was performed using a Thermobrite®

Statspin Thermobrite® Statspin (Illinois, IL, USA). Once the hybridization period was completed, the slides were washed in 0.4X SSC-0.3% tween to remove the coverslips at room temperature. Then, the slides were placed in a pre-warmed solution of 0.4 X SSC-0.3% Tween-20 at 73 °C and washed for 90 seconds to remove excess probe. Slides were then placed in 2X SSC-0.1% tween for a 1 min wash at room temperature followed by an ethanol series (2 min each). Finally, slides were air-dried and counterstained with DAPI and were ready for capturing.



**Table 2.2.1 Putative genes involved in ovarian cancer formation and selected to study gene positioning in chemosensitive and chemoresistant ovarian cancer.**

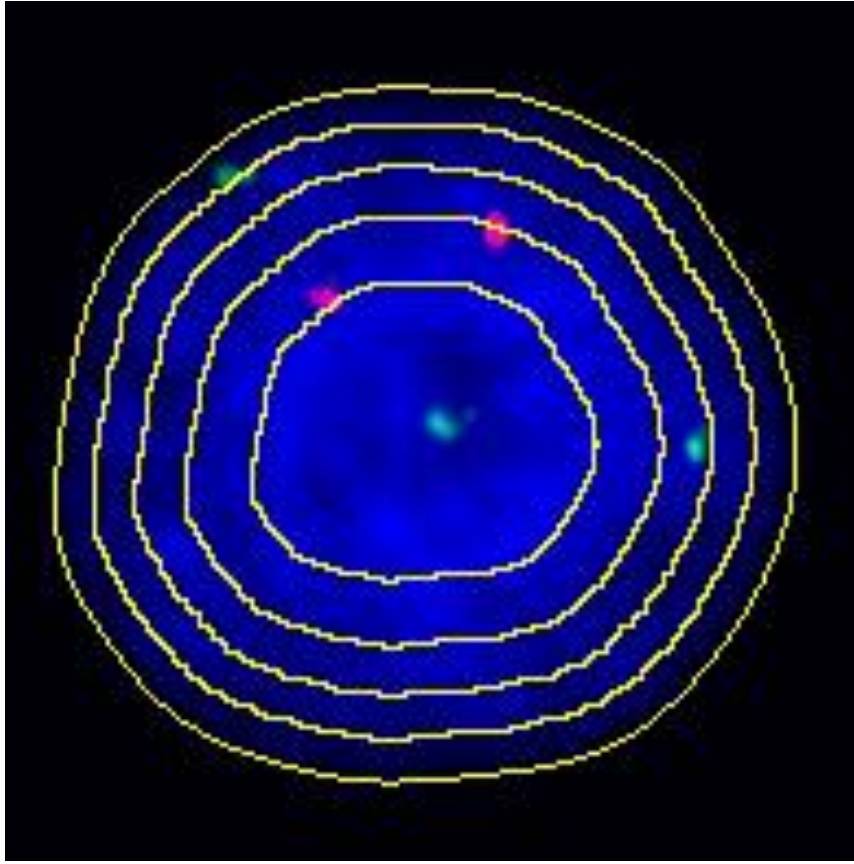
<b>Function</b>	<b>Genes</b>
Tumor suppressor	<i>BRCA1, BRCA2, NF1, PTEN, RB1, TP53</i>
Intracellular signalling/Transcription regulator/Regulator of cell signalling/Regulator of cell division	<i>BRAF, KRAS, MECOM, PAX3, CNNE1, AKT3, CTNNB1, PAX3, FOLR1, NACCI, ALG8</i>

Table 2.2.1 Putative genes involved in ovarian cancer formation and selected to study gene positioning in chemosensitive and chemoresistant ovarian cancer. As the fact that ovarian cancer-associated genes are various, this study focuses on numerous upregulated genes as examples to determine their roles in understanding the molecular etiology of ovarian cancer and their possible role as analytical indicators. FISH technique helps to examine if these genes are random or nonrandomly organized and if that changes between chemosensitive and chemoresistant cells, and if treating the ovarian cells with cisplatin will make some alteration on the ploidy or the organization.

### **2.2.15.3 Image capture**

Slides were examined on an Olympus BX-61 epifluorescence microscope supplied with a cooled CCD camera and appropriate filters. Three single band pass filters for FITC, TRITC, and DAPI were used in this study (Chroma Technology, Bellows Falls, VT, USA). Images were captured using SmartCapture 3 (Digital Scientific UK). A minimum of 100 cells were analyzed per FISH probe, per cell line, per condition (cisplatin treated and untreated).





**Figure 2.2.6** Representation figure illustrating the radial analysis of OCI-5Px stained for *KRAS* (green) and *BRCA1* (red) genes and counterstained DAPI (blue) using FISH technique. The radial analysis software measures the DAPI intensity and divides the nucleus into five shells of equal area. Shell 1 is innermost and shell 5 is outermost. These shells help to identify the location of the gene of interest. In the normal situation, two FISH signals would be expected reflecting the expected diploid content of the cell. In the ovarian cancer cell lines, some genes varied from the expected diploid content. For example, the *KRAS* gene has three copies, which indicates a copy number mutation or amplification of the *KRAS* gene in this cell.

### 2.2.16 Statistical analyses

Statistical analysis was performed using GraphPad Prism (GraphPad, CA, USA). The data, generated using comet assay, were analyzed using non-parametric t-tests (Mann Whitney) to compare the values between the groups. Three independent experiments were performed, and the data were represented as mean  $\pm$  SEM. For the FISH experiments, The Chi-squared goodness of fit ( $\chi^2$ ) was utilized to evaluate if the organization of each gene differed from being random ( $p < 0.05$ ) and to compare differences between conditions (cisplatin treated and untreated) in chemosensitive and chemoresistant cells. For the other experiments, the statistical analysis was mentioned in the experiment section. Significance limits were set at \* $p < 0.05$ , \*\* $p < 0.01$ , \*\*\* $p < 0.001$  and \*\*\*\* $p < 0.0001$ . I would like to thank Dr. Marcus Cooke, Dr. Helen Tempest, and Dr. Changwon Yoo for giving me guidance and help with data analysis.

### CHAPTER 3

#### EXAMINATION OF THE DIFFERENCE IN THE DNA DAMAGE RESPONSE IN CHEMORESISTANT AND CHEMOSENSITIVE OVARIAN CELL LINES

Work from this chapter has been partially published:



Karbaschi, Mahsa, Yunhee Ji, Abdulhadi Mohammed S. Abdulwahed, Alhanoof Alohal, Juan F. Bedoya, Shanna L. Burke, Thomas M. Boulos, Helen G. Tempest, and Marcus S. Cooke.

Evaluation of the Major Steps in the Conventional Protocol for the Alkaline Comet Assay

*International Journal of Molecular Sciences*

20, no. 23 (2019): 6072.

<https://doi.org/10.3390/ijms20236072>

### 3.1 Introduction

Ovarian cancer is the ranked fifth in terms of leading cause of cancer related mortality in women. Amongst the primary predisposing factors to the high rates of deaths is the tumors, which develop resistance to current treatment modalities. Researchers have not identified the strategies and treatments for reducing its vulnerability or possible regulatory mechanisms of the tumor. Currently, the tumor debulking surgeries followed by chemotherapy are considered the optimal treatment for patients with advanced ovarian cancer. Although there are various chemotherapeutic approaches for the treatment of advanced ovarian cancer, the combined therapy of cisplatin and paclitaxel is the most common. The mechanisms responsible for acquired tumor chemoresistance remain unclear. Cisplatin is clinically proven to be used for the treatment of numerous human cancers. However, many women with this disease may undergo relapse or even succumb to the disease as a result of resistance to chemotherapy. Cancer cells resistance to the antitumor drugs remains a significant impediment to effective treatment. Several research studies have been conducted to investigate the molecular mechanism of such chemical resistance to the cisplatin, but the mechanism has not yet been fully elucidated. The goal of this study was to investigate the basis of chemoresistance in ovarian cancers. The Comet assay can help in the measurement of ICLs repair and formation as well as their base excision repair in chemosensitive (OCI-P5x and A2780) and chemoresistant (SKOV-3). The idea is useful in the analysis of the potential DNA damages during formation or repair at the initial stages of single cells. This chapter provides a basis to further improve our understanding of the differential DNA damage response associated with chemosensitive and chemoresistant ovarian cell lines. Elucidating the mechanisms of chemoresistance may

□ □ □  
ultimately lead to novel therapeutic interventions that may resensitize or prevent the development of chemoresistance.

## **3.2 Methods**

### **3.2.1 Ovarian cancer cell lines**

Two chemosensitive ovarian cancer cells (A2780 and OCI-P5X) and one chemoresistant ovarian cancer cell (SKOV-3) were used in this study. All the ovarian cells were cultured according to the supplier's recommended media and condition for each cell line (section 2.2.1 to section 2.2.4). Ovarian cancer cells were cultured in T75 cell culture flask and allowed to grow with the appropriate cell culture media at 37 °C in a 5% CO<sub>2</sub> and humidified atmosphere. For all cell lines, two groups were prepared, one as a control group, and the other is treated with cisplatin.

### **3.2.2 Cisplatin treatment**

Treated groups were treated with cisplatin (100 μM) for 1 h at 37 °C in a 5% CO<sub>2</sub> and humidified atmosphere (section 2.2.5). Subsequently, the cell culture media containing the cisplatin was removed and replaced with drug-free media for differing periods of time (0 - 48 h) depending on the type of the experiment and placed at 37 °C in a 5% CO<sub>2</sub> and humidified atmosphere.

### **3.2.3 Clonogenic assay**

Cells were treated with different doses of cisplatin (10-100 μM) at 37 °C for 1 h and then incubated in drug-free media for seven days to measure the ability of cells to produce colonies. During this time, the plates were incubated without replacing media for a period long enough to form colonies of at least 50 cells (section 2.2.10 and 2.2.10.1).

### **3.2.4 The alkaline comet assay procedure**

The alkaline comet assay was carried out as described by Karbaschi et al. [170-171] for more detail review section 2.2.7 to 2.2.9.2.

#### **3.2.4.1 Time course of DNA crosslink formation and repair in ovarian cancer cells**

The comet assay was carried out to measure the level of DNA damage, and repair, induced by chemotherapeutic agent. Ovarian cancer cells (A2780, OCI-P5x, and SKOV3) were treated with 100  $\mu\text{M}$  for 1 h and incubated with drug free media for different time points. Cells were then treated with 0 (control) or 50  $\mu\text{M}$   $\text{H}_2\text{O}_2$  to induce a requisite number of strand break to create a DNA tail. The crosslink formation was assessed by comet assay.

#### **3.2.4.2 DNA Crosslink formation in intact cells and nucleoid bodies from chemosensitive and resistant ovarian cell lines.**

The comet assay was carried out to measure the level of DNA damage induced by different doses of cisplatin in different cell-DNA substrates. Ovarian cancer cells (A2780, OCI-P5x, and SKOV3) were treated with cisplatin (50, 100, and 200  $\mu\text{M}$ ) for 1 h at 37 °C, 5%  $\text{CO}_2$ . Cells were then expose to 0 (control) or 0.05  $\text{J}/\text{cm}^2$  of UVC to induce a requisite number of strand break to create a DNA tail

#### **3.2.4.3 Optimization of hOGG1 concentration for ovarian cell lines**

The optimum conditions for hOGG1 required to be determined for the ovarian cancer cell lines. To optimize the concentration of hOGG1 for deduction of 8-oxodG in ovarian cells, these cells were treated with 50  $\mu\text{M}$  of  $\text{H}_2\text{O}_2$ . A series of dilutions of the hOGG1 enzyme was set up from the stocks (1,600 U/mL) in enzyme reaction buffer. The hOGG1 modified comet assay was performed using different concentrations of hOGG1 for 60 min incubation. Optimization of PI were also preformed, it was reviewed in section 2.2.8.3.

#### **3.2.4.4 Analysis of base excision repair**

The hOGG1-modified comet assay was carried out to measure the repair of 8-oxodG after hydrogen peroxide treatment. The remaining percentage of tail DNA was detected at different time points immediately after the treatment, 1, 2, 6, 12, or 24 h. Ovarian cells were treated with 50  $\mu\text{M}$  of  $\text{H}_2\text{O}_2$  and allowed to repair for different time points assessed by hOGG1 modified comet assay.

#### **3.2.4.5 UVB dose response**

To measure the extent and linearity of CPDs and ALS induction in ovarian cells, a dose–response following UVB was determined. The comet assay was carried out to measure the level of DNA damage induced by several doses of UVB. Ovarian cells were exposed to 0, 0.25, or 0.5  $\text{J}/\text{cm}^2$  UVB and then measured by T4endoV modified comet assay. T4endoV modified comet assay was used to measure the induction of CPDs following UVB irradiation.

#### **3.2.4.6 UVC dose response**

The comet assay was carried out to measure the level of DNA damage induced by several doses of UVC. Ovarian cells were exposed to 0.025, 0.05, or 0.1  $\text{J}/\text{cm}^2$  UVC and then measured by comet assay.

#### **3.2.4.7 Optimization of T4endoV concentration for ovarian cell lines**

The T4endoV-modified comet assay was carried out to measure the repair in ovarian cancer cells after irradiated them with UVB. Ovarian cells were irradiated with 0.5  $\text{J}/\text{cm}^2$  of UVB, and then then measured by T4endoV modified comet assay. T4endoV modified comet assay was carried out to measure the CPDs. The stock enzyme which purchased from NEB (biolab tech) was concentrated and it was important to optimize the concentration that will

□ □ □

be used in the experiment. To optimize the concentration of T4endoV for removal of CPDs on ovarian cell lines, cells were exposed to 0.5 J/cm<sup>2</sup> of UVB. Different dilutions of the enzymes were made from the stocks [10,000 U/mL] in enzyme reaction buffer. Following the cell lysis step, ovarian cells were incubated with different concentrations of T4endoV for 1 h before electrophoresis in alkaline buffer. Control samples were not irradiated but incubated with different concentrations of T4endoV.

#### **3.2.4.8 Analysis of nucleotide excision repair**

The T4endoV-modified comet assay was carried out to measure the repair in ovarian cancer cells after irradiated them with UVB. Ovarian cells were irradiated with 0.5 J/cm<sup>2</sup> of UVB, and then the cells were allowed to repair at the incubator for different time points (0, 1, 2, 6, 12, 24, or 30 h). In addition, group of cells were not irritated and used as a control to measure the background level of DNA damage. Repair of the CPD in ovarian cells were determined by the T4endoV-modified comet assay

#### **3.2.4.9 Crosslink formation on ovarian cell with environmental and chemical agents**

The comet assay was carried out to measure the level of DNA damage induced by different doses of cisplatin and formaldehyde. Ovarian cells were treated with 0, 50, 150, or 300 of formaldehyde/cisplatin and cells were then expose to 0 (control) or 0.5 J/cm<sup>2</sup> of UVB to induce a requisite number of strand break to create a DNA tail. The crosslink formation was then assessed by comet assay.

#### **3.2.5 ELISA**

Ovarian cancer cell lines were treated with cisplatin (100 μM) for 1 h at 37 °C, 5% CO<sub>2</sub>, then the media was changed to drug-free media and incubated for different time points (0, 6, 12, and 24).

□ □ □

DNA was loaded to the coated plate with/without boiling step (10 min then cooled rapidly on ice). Anti-cisplatin DNA adducts were used as a primary Ab (1:1000, 1 mg/mL), and goat- anti rat were used as a secondary Ab (1:5000, 0.8 mg/mL). As a positive control, thymine dimer primary Ab were used (1:1000, 2 mg/mL) after exposing the cell to UVB (1 J/cm<sup>2</sup>), and goat- anti mouse were used as secondary Ab (1:2000, 2 mg/mL).

### **3.2.6 Quantification of platinum in DNA using Inductively Coupled Plasma Mass Spectrometry (ICP-MS)**

ICP-MS is an elemental analysis method which quantifies metals such as platinum in samples at milligram to nanogram levels per liter. Ovarian cancer cell lines were treated, as described in section 2.2.13.1, and the DNA extracted, as described in section 2.2.11. The platinum concentration in the DNA samples was measured using ICP-MS by Dr. Natalia Quinete (Florida International University, Southeast Environmental Research Center, Miami, FL, USA) as described in section 2.2.13.

### **3.2.7 Measuring cell toxicity of triazole-modified nucleosides and/or their enhancement with cisplatin efficiency in ovarian cell line**

Cell viability of A2780 cells was assessed by CCK-8 following the 24 h incubation with 8-TrzdG of different concentrations. Using this chemical compound was reported to enhance the effectiveness of cisplatin as a chemotherapeutic agent. The aim of using this approach was to demonstrate if the chemical compound was able to enter the cells and integrate with the DNA using the cell culture model. The chemical compound, 8-TrzdA, was reported previously to work effectively by other lab group who designed the nucleosides. They demonstrated that 8-TrzdA 5'-triphosphate was incorporated into duplex DNA [177]. Therefore, two group of cells were used, and treated with increased

□ □ □  
concentration of 8-TrzdG. After 24 h, and only one group the cells were treated with cisplatin (100  $\mu$ M) to demonstrate if that will increase the effectiveness of cisplatin with the chemosensitive cell line in the presence of the chemical compound.

### **3.3 Results**

#### **3.3.1 Treatment with cisplatin cause a decrease in ovarian cancer cell survival**

Clonogenic assay was carried out to measure the survival of the ovarian cancer cell lines. Clonogenic assay is based on the capability of a single cell to grow, or not, into a colony after being treated with a certain agent (e.g., cisplatin). In Figure 3.3.1, the chemosensitive cells showed low survival rates after seven days, in response to increasing doses of cisplatin, in both A2780 and OCI-P5x cell lines This indicated the sensitivity of these cell lines compared to the chemoresistant cells, (SKOV-3) ( $P < 0.05$ ). There was a rapid reduction in survival rate observed in the chemosensitive cell line (A2780) with the increasing concentrations of cisplatin.

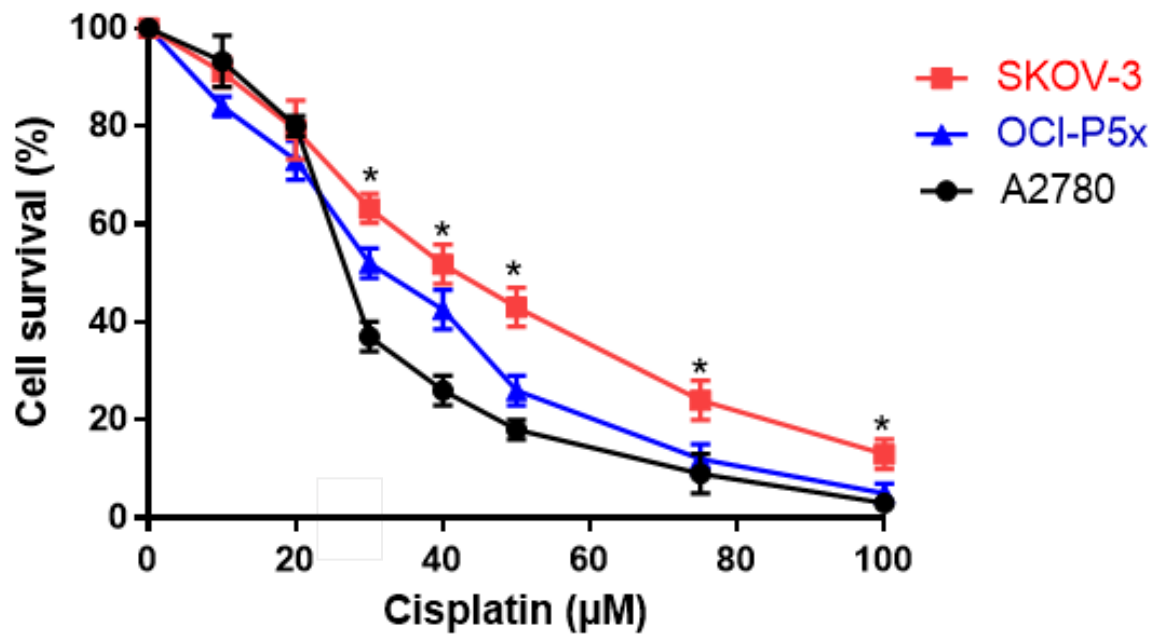


**Figure 3.3.1 Chemoresistant cells have a significantly cellular cell survival in response to cisplatin compared to chemosensitive cell lines.** SKOV showed lower survival rates compared to the chemoresistant cell (SKOV-3). Cells were exposed to cisplatin (0-100 µM) and stained 7 days after seeding for A2780, SKOV-3, and OCI-P5x. Data represent the mean +/- SEM from three experiments. \* P < 0.05

### **3.3.2 Chemoresistant tumor cells are refractory to the formation of cisplatin-induced DNA crosslinks**

As shown in Figure 3.3.2, the data revealed considerable differences among the ovarian cancer cell lines in response to cisplatin treatment. It was observed that the peak of cisplatin-induced crosslink formation for all three cell lines was at 12 h, which was confirmed by ICP-MS (Figure 3.3.3), we noted a significant attenuation ( $P < 0.0001$ ) of ICL formation in the chemoresistant cell line SKOV3, compared to the chemosensitive lines. In the first 12 h, there were no significant difference between both chemosensitive cell lines however, after 12 h, there was a slight reduction of DNA crosslinks in A2780 compared to the OCIP5x cell line. At 48 h the A2780 cells reached the baseline levels while the SKOV3 cell line still had around 20 % of DNA crosslinks remaining.

Moreover, the platinum concentration in DNA samples was quantified using ICP-MS in all ovarian cells after cisplatin treatment. As Figure 3.3.3 shows, there was a positive correlation observed between DNA crosslinks and platinum concentration in the chemosensitive cell line, OCIP5X, at 12 h post cisplatin treatment. The chemosensitive cell line had a significant increase in DNA crosslinks, and the final platinum concentration was higher than the chemoresistant cell line, SKOV3. As Figure 3.3.3 shows, the incubation with drug-free media for different time points following the treatment with cisplatin led to a significant increase of platinum concentration in the chemosensitive cell compared to the chemoresistant cell. As shown in Figure 3.3.3A, the chemosensitive cell, OCIP5X, had a significant increase in platinum concentration than the chemoresistant cells, SKOV3, at all time points ( $p < 0.0001$ ). OCIP5X had the highest platinum amount at 0 h post-treatment with 65 ug/g, while A2780 39 ug/g and SKOV3 had 35 ug/g. At 24 h post-treatment,

OCIP5X had a significant increase of platinum concentration comparing to the chemoresistant cell line, SKOV3.

Moreover, a slightly decreased platinum concentration was noted in A2780 (42 ug/g) 24 h post the treatment. ELISA was also used to detect and semi-quantify cisplatin-induced DNA adducts in the chemosensitive and chemoresistant cells following cisplatin treatment, as shown in Figure 3.3.3B. The chemosensitive cells tend to have crosslinks more than the chemoresistant cell post cisplatin treatment.



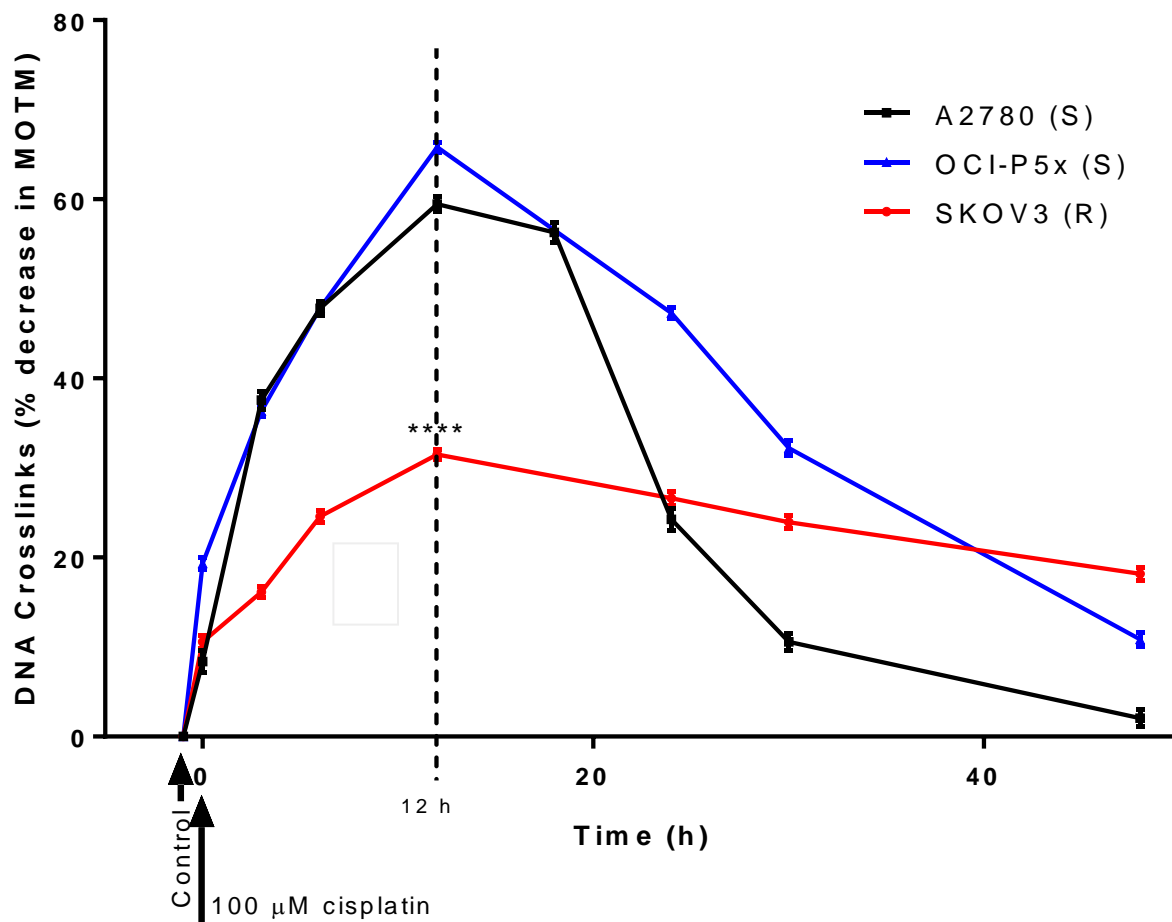


**Figure 3.3.2 Chemoresistant tumor cells are refractory to the formation of cisplatin-induced DNA crosslinks.** Modified comet assays (single cell gel electrophoresis) was used to measure interstrand cross-link (ICL) formation and repair. Cells were treated with cisplatin for 1 h at 100  $\mu$ M and then placed in drug free media for different time points. After cisplatin treatment, DNA damage was induced by 50  $\mu$ M hydrogen peroxide treatment, on ice, for 30 min. Data represent mean  $\pm$  SEM from three experiments. \*\*\*\*  $P < 0.0001$ .

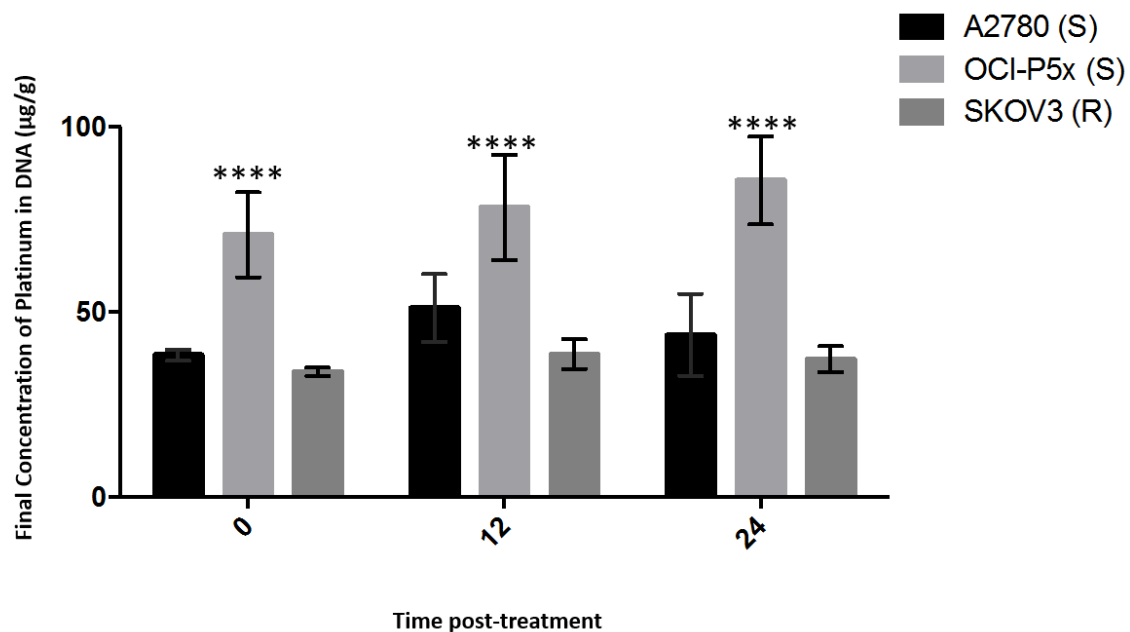


**Figure 3.3.3A Quantification of platinum in DNA using ICP-MS in chemoresistant and chemosensitive ovarian cancer cells.** Cells were treated with cisplatin for 1 h with 100  $\mu$ M and then placed in drug free media for different time points. DNA was then isolated, and samples were directly analyzed by ICP-MS. Data represent mean  $\pm$  SEM from three experiments. \*\*\*\* P < 0.0001.

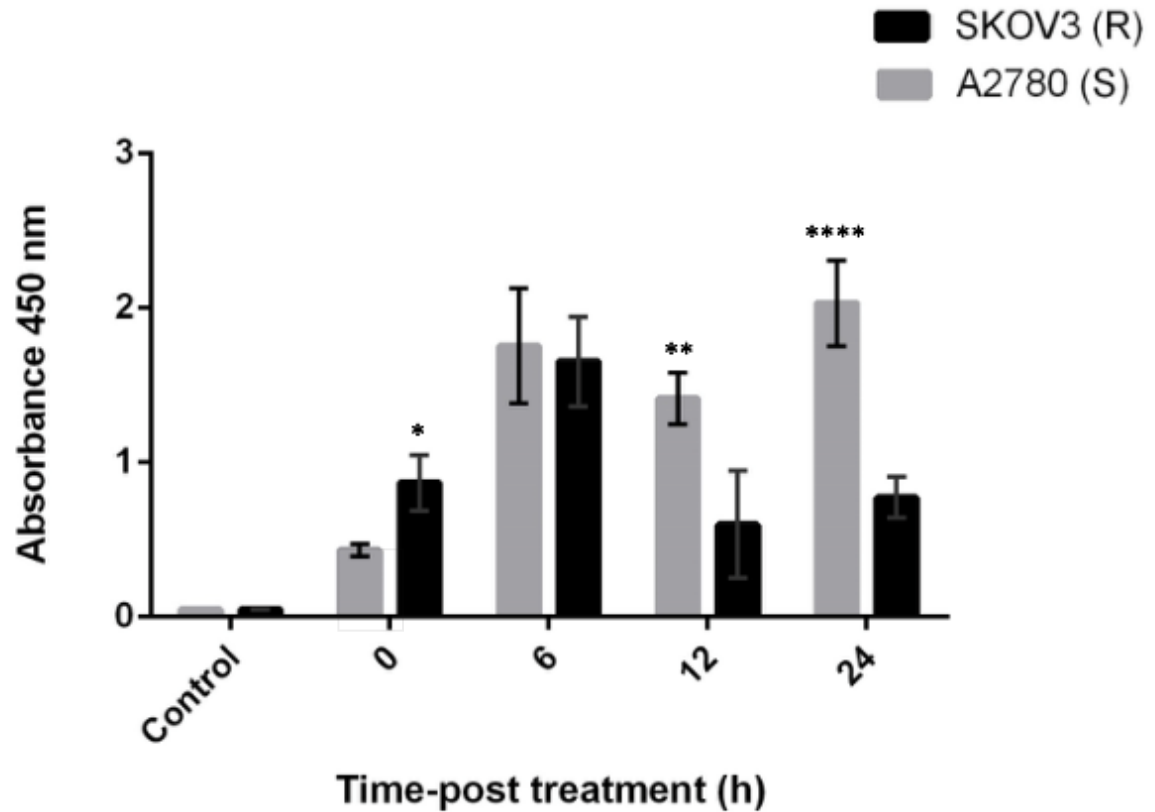


**Figure 3.3.3B Formation of DNA crosslinks and repair in ovarian tumor cells measured by ELISA.** Cells were treated with cisplatin for 1 h (100  $\mu$ M) and DNA was isolated at different time intervals (0, 6, 12, 18, and 24 h). Primary Ab (1:250, 0.004 mg/mL), and secondary Ab (1:5000, 0.16  $\mu$ g/mL) were used. Data represent mean  $\pm$  SEM of 3 replicates

### **3.3.4 Both cells and nucleoid bodies from chemoresistant cells are refractory to crosslinks formation.**

The crosslink formation was assessed by the alkaline comet assay and was used to study the role of nuclear organization on DNA damage formation, through comparison of response in nucleoid bodies and intact cells. As Figure 3.3.4 shows, the results demonstrated the same rank order of dose-response in nucleoid bodies as in intact cells, but with chemoresistant cells being considerably more resistant to damage formation, at all doses cisplatin.

In intact cells, the chemoresistant cells (SKOV3) showed a lower percentage of DNA crosslinks compared to the chemosensitive cell lines (A2780 and OCI-P5X) with increasing concentrations of cisplatin. The percentage of DNA crosslinks in SKOV3 was around 19 % (\*\*\*) ( $P < 0.001$ ) following treatment with the highest concentration of cisplatin, while the percentage of DNA crosslinks in A2780 and OCI-P5X was 33 % and 31 %, respectively at the same concentration of cisplatin.

Moreover, the results showed a similar rank order of dose-response in nucleoid bodies as in intact cells. Correspondingly, SKOV3 had low percentages of DNA crosslinks with increasing concentrations of cisplatin comparing to A2780 and OCI-P5X. At the highest dose of cisplatin, SKOV3 showed a significantly lower percentage 37 % of DNA crosslinks (\*\*\*) ( $P < 0.001$ ) compared to A2780 64 % and OCI-P5X 58.67 %.

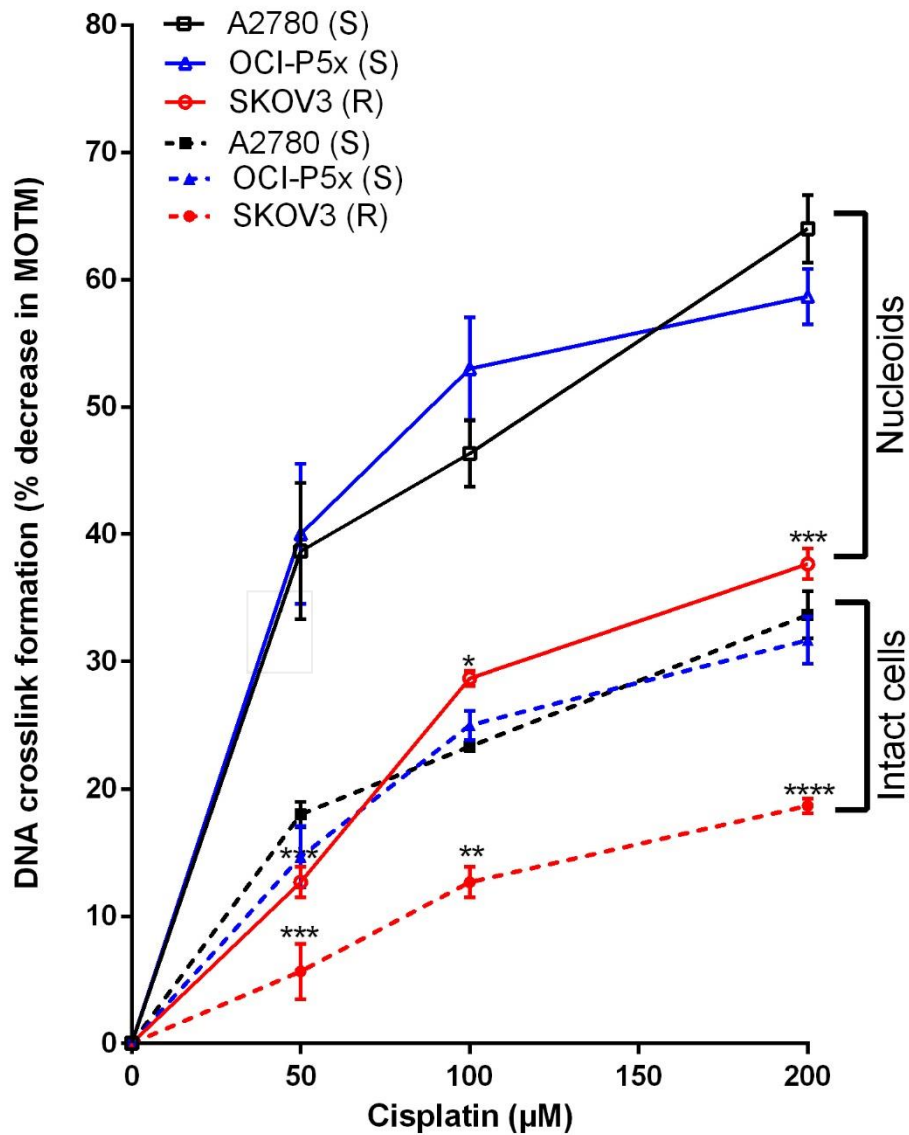


**Figure 3.3.4 The differential response to cisplatin treatment derives from proportion associated with the nucleoid body.** DNA crosslink formation was determined by variant of the comet assay in cisplatin treated cells or nucleoid bodies. Data represent mean +/- SEM from three experiments. The stars represent the statistical analysis comparing to the chemosensitive cell lines. \*\*\*\* P < 0.0001, \*\*\* P < 0.001, \*\* P < 0.01.

### 3.3.5 Optimization of PI concentration

The staining step is a critical step in the comet assay; therefore, it was important to optimize the PI concentration to increase the accuracy of the software for having a better detection during capturing the comets. During this experiment, increase concentrations of the PI were used, as shown in Figure 3.3.5; and the optimum concentration of PI was 2.5  $\mu\text{g}/\text{mL}$ . There was no significant difference among all the concentrations following the exposure with different doses of UVB; however, using higher concentrations showed some issues of detecting the comets. As shown in the Figure 3.3.6, (A-B) software partially recognizes comets with using a high concentration of PI 3.5 and 4.0  $\mu\text{g}/\text{mL}$  following the exposure to 0.5  $\text{J}/\text{cm}^2$ ; (C-D) comets display intense brightness more difficult to differentiate nucleus with using a high concentration of PI 3.5 and 4.0  $\mu\text{g}/\text{mL}$  following the exposure to 1.0  $\text{J}/\text{cm}^2$

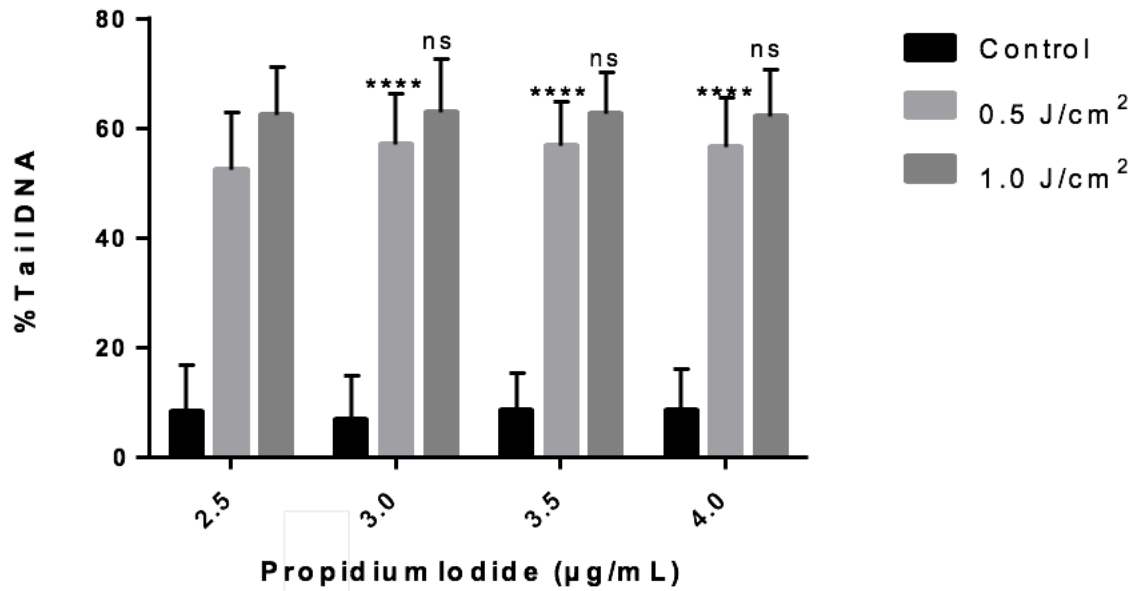


**Figure 3.3.5 Levels of DNA damage in HaCaTs irradiated with UVB determined by alkaline comet assay.** Cells were irradiated with 0.5 J/cm<sup>2</sup> or 1.0 J/cm<sup>2</sup> UVB on ice prior to undergoing alkaline comet assay and stained with various concentrations of P.I. to assess % tail DNA. Data represent the mean +/- SEM from three experiments. \*\*\*\* p < 0.0001

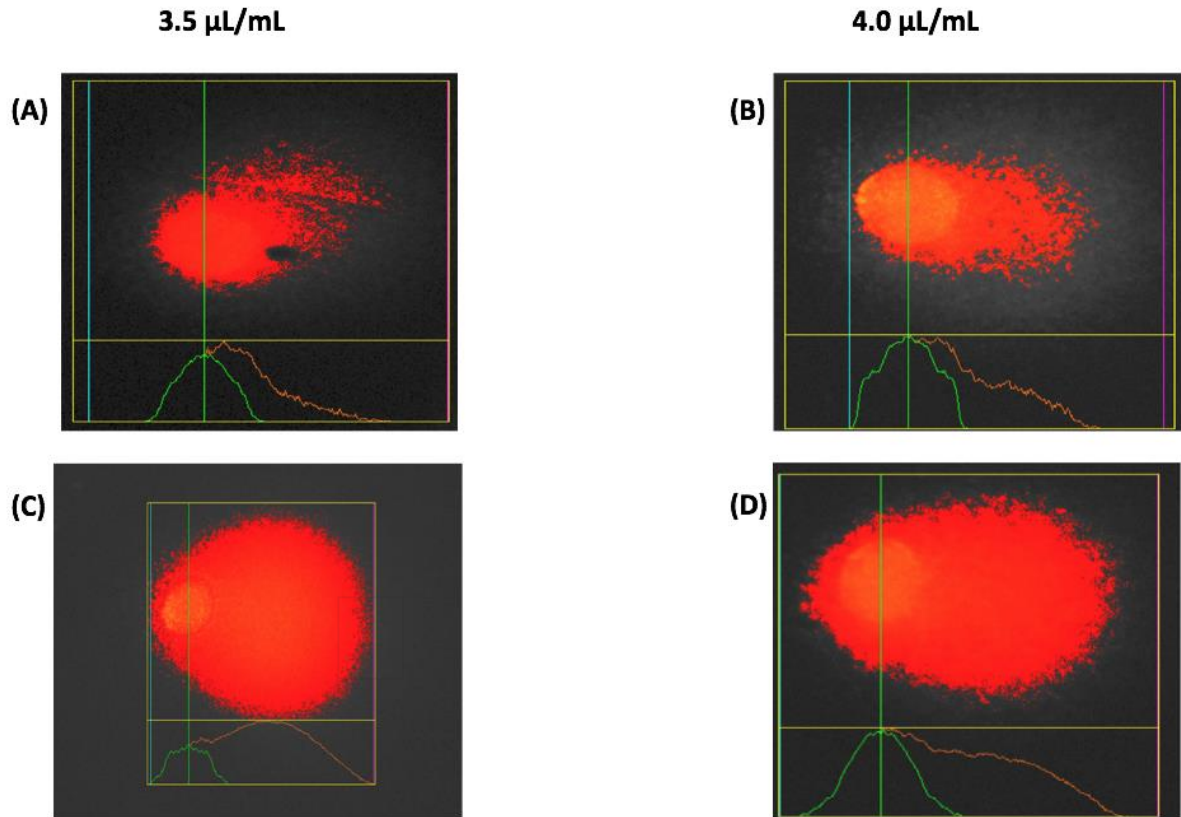


**Figure 3.3.6 Potential limitation of using high concentrations of P.I.** Cells were irradiated with  $0.5 \text{ J/cm}^2$  or  $1.0 \text{ J/cm}^2$  UVB on ice prior to undergoing alkaline comet assay. Cells were stained with high concentration of P.I (3.5, 4.0  $\mu\text{g/mL}$ ) to examine the ability of Comet Assay VI software to detect the DNA damage. (A-B) software partially recognizes comets with using high concentration of PI 3.5 and 4.0  $\mu\text{g/mL}$  following the exposure to  $0.5 \text{ J/cm}^2$ ; (C-D) comets display intense brightness more difficult to differentiate nucleus with using high concentration of PI 3.5 and 4.0  $\mu\text{g/mL}$  following the exposure to  $1.0 \text{ J/cm}^2$

### **3.3.7 Optimization of hOGG1 concentration for ovarian cell lines**

The optimum conditions for hOGG1 enzyme required to be determined for the ovarian cancer cell lines. The results in Figure 3.3.7 demonstrated that the level of DNA damage was increased with the increased concentrations of hOGG1 enzyme. Treatment with increased concentrations of H<sub>2</sub>O<sub>2</sub> led to a significant increase in levels of oxidized purine ( $P < 0.0001$ ) and SB/ALS ( $P < 0.0001$ ) for the chemosensitive and chemoresistant cell lines. As shown in Figure 3.3.7, treatment with hOGG1 enzyme led to a significant increase in levels of oxidized purine and SB/ALS in all ovarian cell lines. The optimum concentration of hOGG1 enzyme was 4.0 U/mL and was used for the detection of the oxidized purine induced on the DNA of ovarian cell lines. Control samples which were not irradiated and were incubated with the same concentrations of hOGG1 enzyme showed no significant difference following the treatment. Moreover, the amount of oxidized purine and SB/ALS were assessed using the modified comet assay at each concentration of the enzyme. It was observed high amounts of oxidized purine at 4.0 U/mL and 8.0 U/mL in the ovarian cancer cell lines.

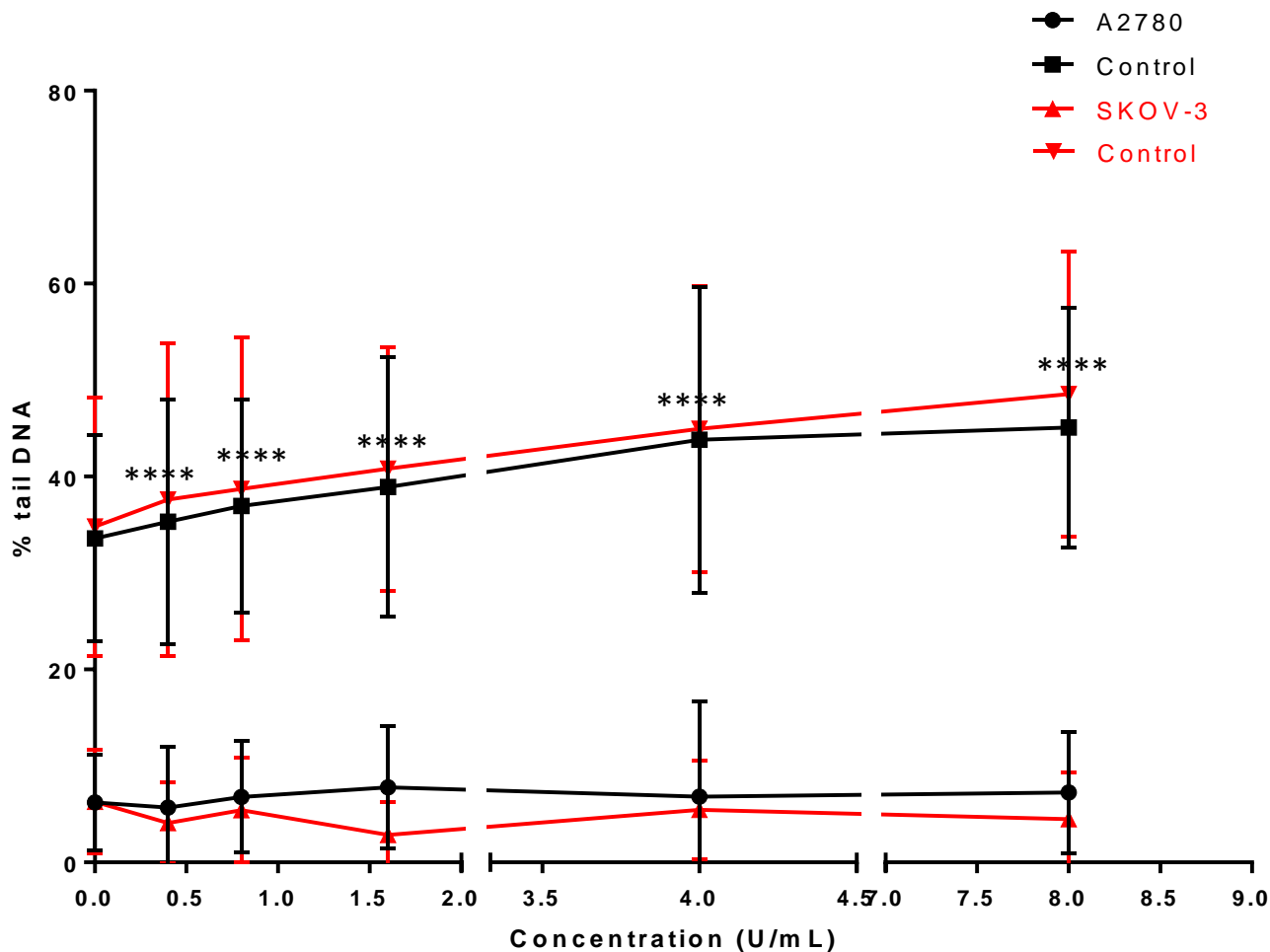


**Figure 3.3.7 Induction of DNA breaks and the amount of 8-oxodG in A2780 and SKOV-3 following treatment with H<sub>2</sub>O<sub>2</sub> (50 μM) determined by hOGG1-modified comet assay.** Cells were treated with increased concentration hOGG1 enzyme (0, 0.4, 0.8, 1.6, 4.0, 8.0 U/mL). The control samples were not treated with H<sub>2</sub>O<sub>2</sub>.

### **3.3.8 Equivalent BER ability occurs in chemosensitive and chemoresistant ovarian tumor cells**

The hOGG1-modified comet assay was carried out to assess the kinetics of BER after hydrogen peroxide treatment. The remaining percentage of tail DNA was detected at different time points. As Figure 3.3.8 shows, the amount of DNA damage remaining for all cells at the 1 h post treatment was around 30 %. This level was decreased below 25 % at 2 h post treatment for all cell lines. At 6 h post the treatment, all cell lines showed a major decline of the amount of DNA damage remaining. This result shows the complete repair of DNA damage produced by hydrogen peroxide treatment. The data showed that no significant differences in BER were noted among all the cell lines.

Moreover, all cell lines had increased levels of oxidized purine and SB/ALS at the first three time points post treatment, Figure 3.3.9. Treatment with 50  $\mu\text{M}$  of  $\text{H}_2\text{O}_2$  led to a significant increase in levels of oxidized purine ( $P < 0.0001$ ) and SB/ALS ( $P < 0.0001$ ) for A2780 at 0 h post treatment, comparing to the control. These levels significantly declined after 6 h post treatment in the same cell line as shown in Figure 3.3.9A; however, the levels of oxidized purine and SB/ALS at these time points (1 h, 2 h, and 6 h post treatment) were still high and significantly different from the control.

Similarly, OCIP5X and SKOV3 had increased levels of oxidized purines ( $P < 0.0001$ ) and SB/ALS ( $P < 0.0001$ ) at 0 h post treatment, comparing to the control. These levels were also significantly declined at 1 h and 2 h post treatment in the same cell line, however, these levels were still high and significantly different from the control. Moreover, OCIP5X and SKOV3 completely repaired all oxidized purines after 6 h, but A2780 were fully repaired after 24 h., as demonstrated in Figure 3.3.9.

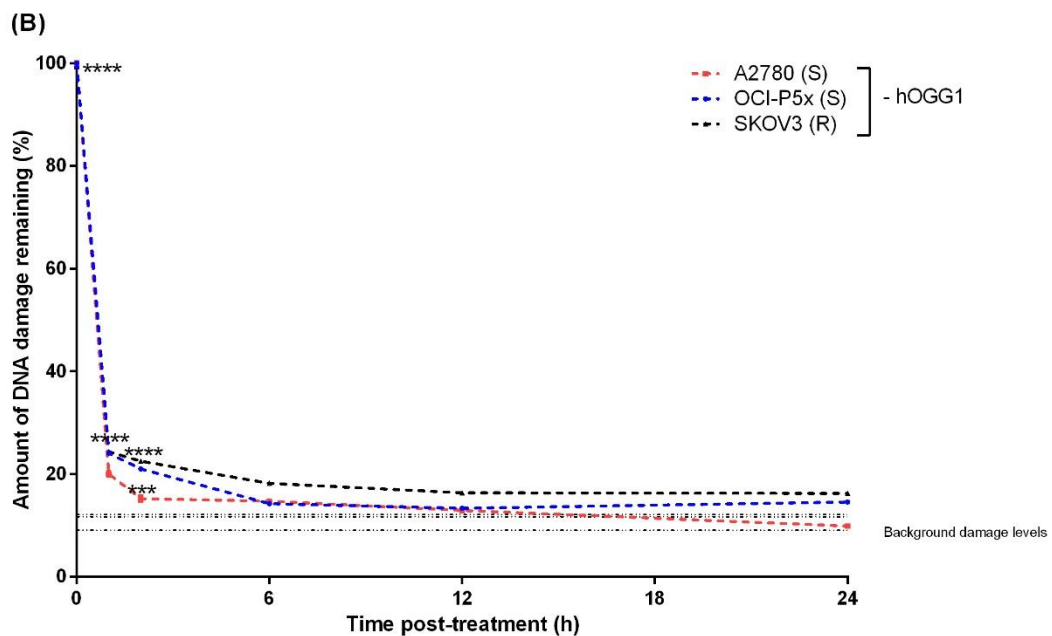
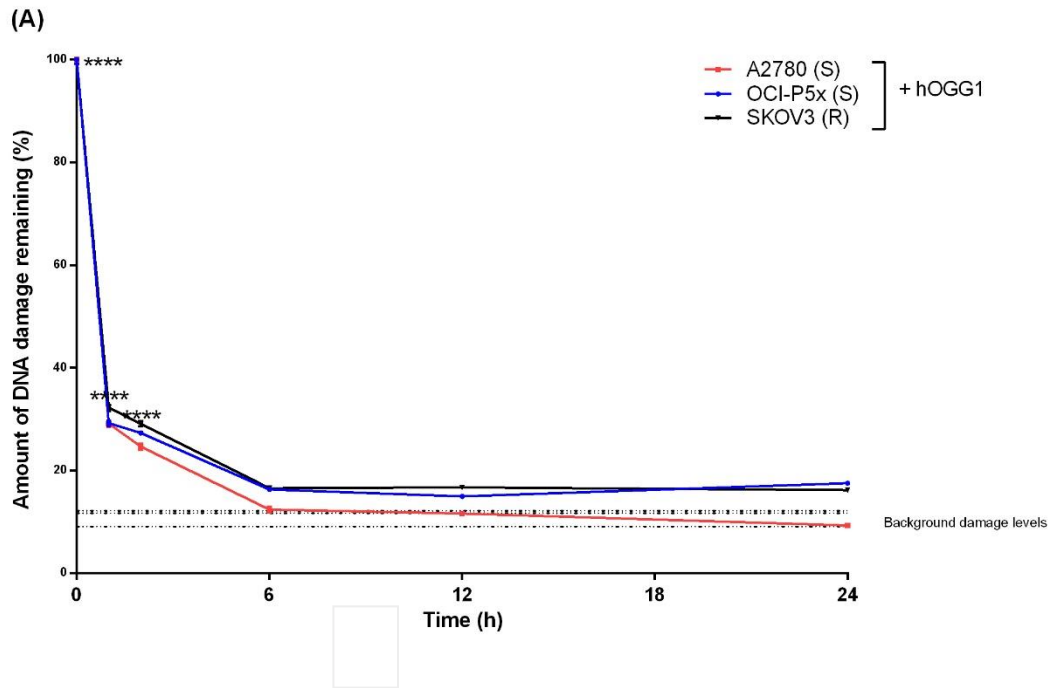


**Figure 3.3.8 kinetics of BER of oxidized purines (A) (+ hOGG1) and repair of strand breaks (B) (- hOGG1) does not differ between chemosensitive and chemoresistant ovarian cells.** Following 50  $\mu\text{M}$   $\text{H}_2\text{O}_2$  treatment for 30 min, on ice, cells left, in the incubator, to repair for different times (0 h, 1 h, 2 h, 6 h, 12 h or 24 h). Data represent mean  $\pm$  SEM from three experiments. Statistical analysis was used to compare every individual cell line, at each point, to their background level, in present or absent of hOGG1. \*\*\*\* P < 0.0001. Background levels were detected as follow; A2780 (9.08 %), OCI-P5x (12.11%), and SKOV3 (11.67 %)

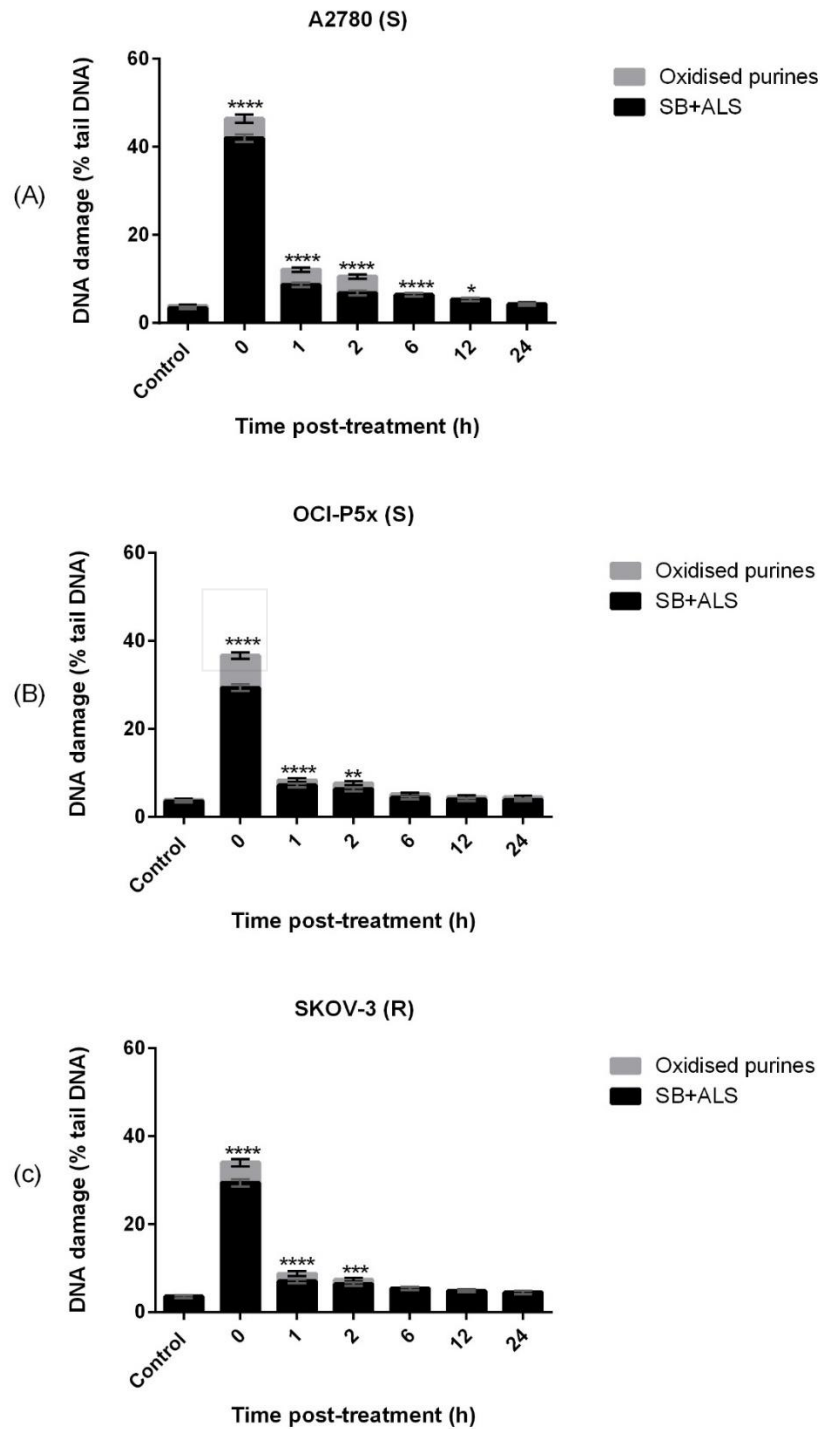


**Figure 3.3.9 Significant levels of oxidized purines + SB/ALS were induced by H<sub>2</sub>O<sub>2</sub> in ovarian cancer cells.** BER ability does not vary between sensitive and resistant ovarian cells. Following 50  $\mu$ M H<sub>2</sub>O<sub>2</sub> treatment for 30 min, on ice, cells left in the incubator to repair for different times (0 h, 1 h, 2 h, 6 h, 12 h or 24 h). Data represent mean  $\pm$  SEM from three experiments. (A) Chemosensitive cell line, A2780; (B) Chemosensitive cell line, OCIP5X; (C) Chemoresistant cell line, SKOV3.

### 3.3.9 UVB dose response

The comet assay was carried out to measure the level of DNA damage induced by different doses of UVB, as shown in Figure 3.3.10. Exposure to different doses of UVB led to a significant increase in levels of DNA damage, which were represented as % tail DNA. Treatment with T4endoV enzyme led to a significant increase in levels of CPD and SB/ALS in all ovarian cancer cell lines.

As Figure 3.3.10 shows, A2780 cells showed slightly higher DNA damage levels (SB/ALS) comparing to other cell lines; at 0.25 J/cm<sup>2</sup> had 38.66 % while, OCI-P5x showed 34.12% and 32.12% was the level of damage level detected in SKOV3. Following exposure to 0.5 J/cm<sup>2</sup>, A2780 had 49.28 % of DNA damage, while OCIP5x showed 48.99 %, and the chemoresistant cells, SKOV3, had 45.25 % of DNA damage. These percentages were increased using the T4endoV enzyme which indicated the amount of the CPD following the exposure to the UVB. The amount of CPD in A2780 following the exposure to 0.5 J/cm<sup>2</sup> was 13.66 %, while the amount of CPD in OCI-P5X was 11.13 %. The chemoresistant cell line had 11.93 % of CPD levels following exposure to UVB. The optimum UVB dose, to use in the other experiments, was 0.5 J/cm<sup>2</sup>. The pictures of the comets representing the DNA damage levels in ovarian cancer cells, following the exposure to 0.5 J/cm<sup>2</sup> UVB, were represented in Figure 3.3.11.

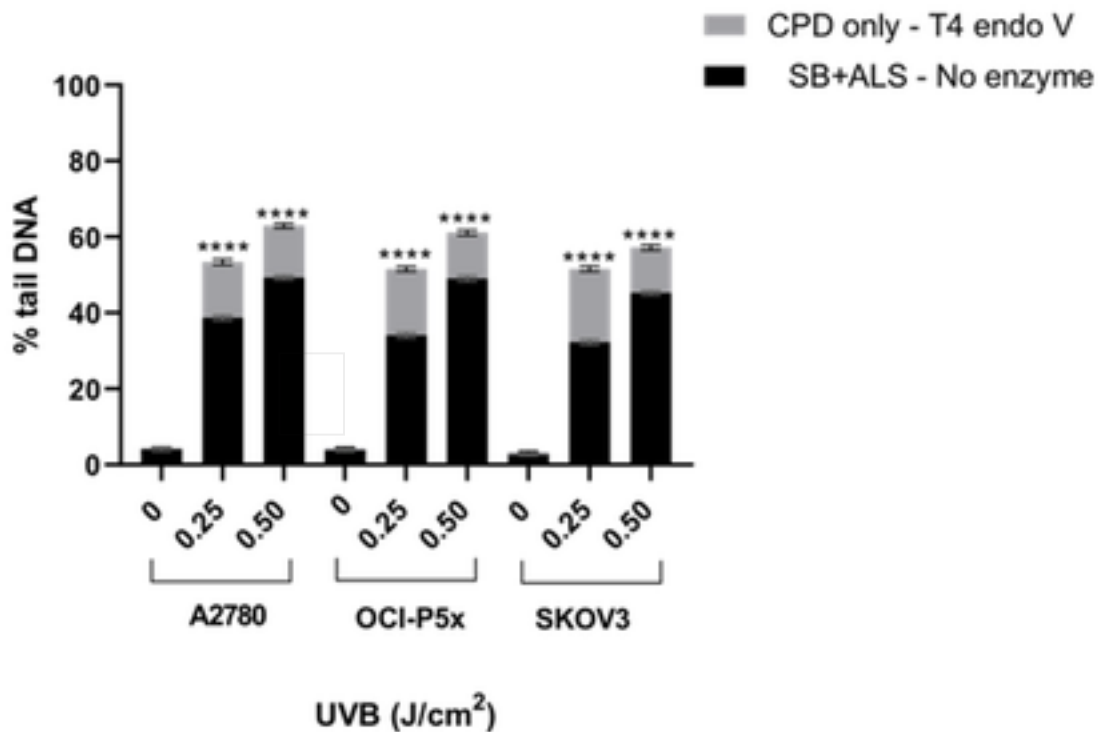


**Figure 3.3.10 Induction of DNA breaks in ovarian cancer cells following the exposure to UVB.** Induction of DNA breaks were measured, following UVB exposure (0.25 and 0.5 J/cm<sup>2</sup>), by T4endoV-modified comet assay. Data represent mean +/- SEM from three experiments (100 individual determinations each).

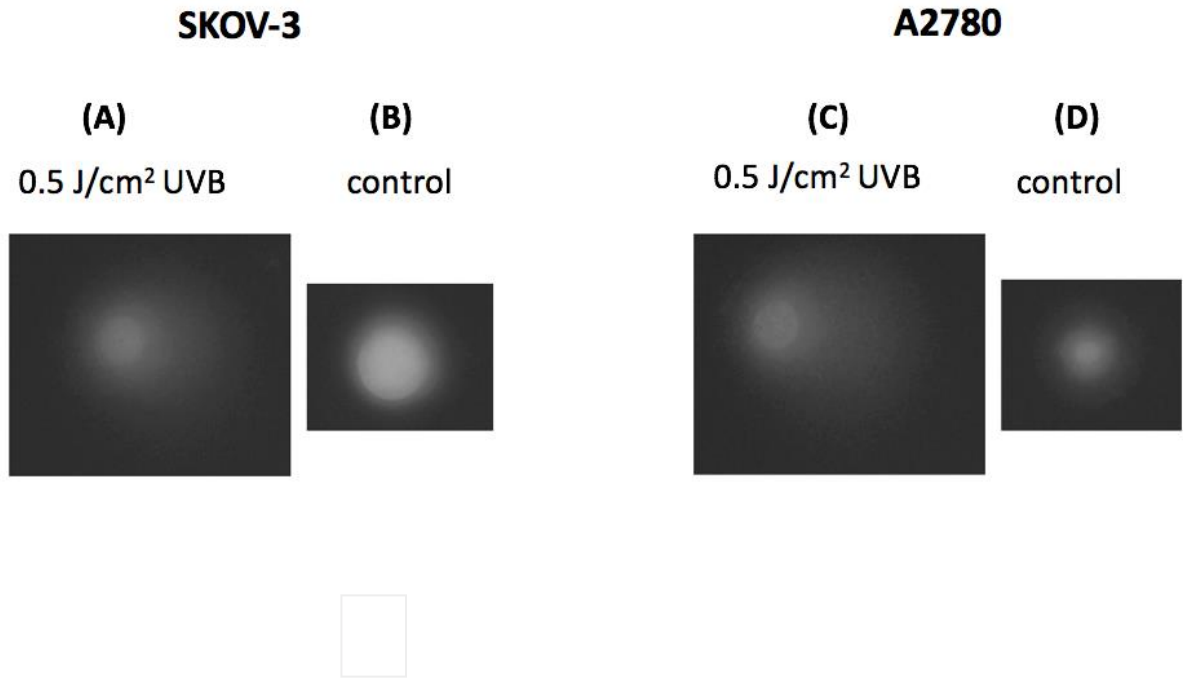


**Figure 3.3.11 Representation of comet pictures of DNA damage following the exposure to UVB in ovarian cancer cells.** Cells were irradiated with 0.5 J/cm<sup>2</sup> UVB on ice prior to undergoing alkaline comet assay, and the indication of DNA breaks were then measured. Example of comet images using comet assay IV software. (A-C) After the UVB exposure, DNA strand breaks allowed the migration of the DNA (under electrophoresis) away from the nucleoid body something along these lines, whereas in (B-D) control had minimal levels of DNA strand breaks, so the DNA remains complexed with the nucleoid body.

### 3.3.10 UVC dose response

The comet assay was carried out to measure the level of DNA damage induced by different doses of UVB, as shown in Figure 3.3.12. Exposure to different doses of UVC led to a significant increase in levels of DNA damage, comparing to the control, in all ovarian cancer cells. Following the exposure to 0.025 J/cm<sup>2</sup> UVC, a significant increase levels DNA damage (around 25 %) was noted in all cell lines. The percentage of tail DNA was the damage parameter used to illustrate the level of the DNA damage. Following the exposure to 0.05 J/cm<sup>2</sup> UVC, SKOV-3 showed significant resistance to DNA damage comparing to the chemosensitive cell lines ( $p < 0.001$ ). At dose of 0.1 J/cm<sup>2</sup> UVC, SKOV-3 also showed a slight resistance to DNA damage when compared to the chemosensitive cell lines.

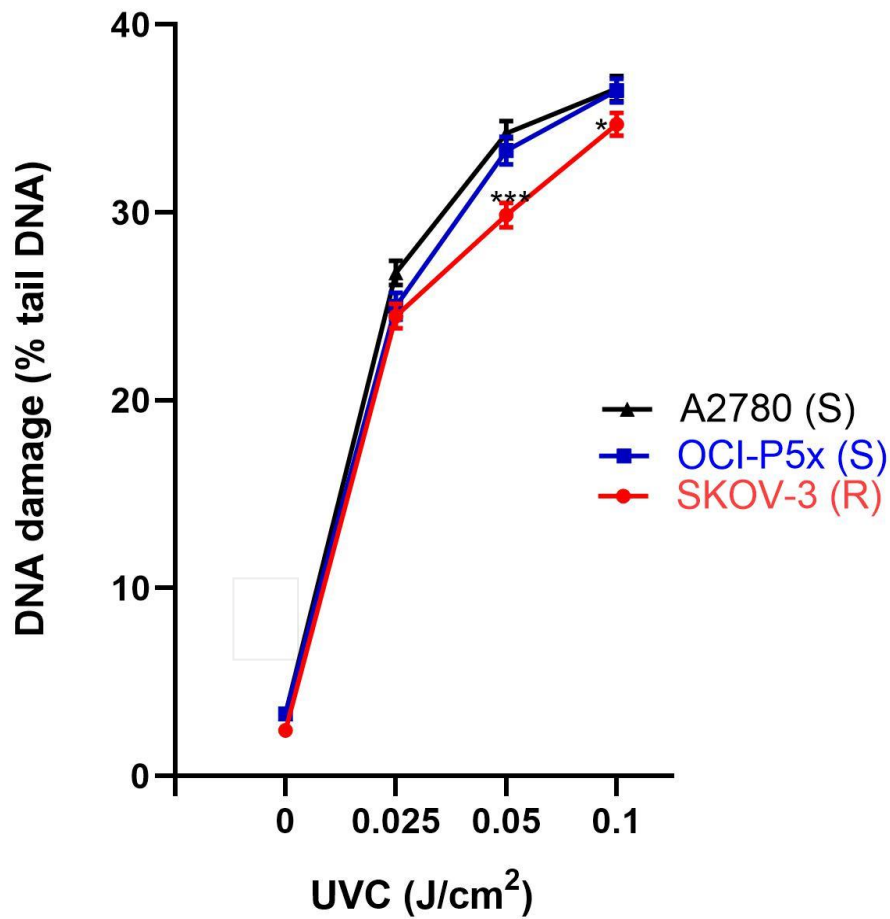


**Figure 3.3.12 Induction of DNA damage in ovarian cancer cells following exposure to UVC.** Cells were UVC exposed, on ice, and then processed for alkaline comet assay. Data illustrate the mean  $\pm$  SEM from three independent experiments. Mann Whitney test was used to compare the chemoresistant cell line, SKOV-3, to the chemosensitive cell lines. The stars represent the statistical analysis. \*\*\*  $P < 0.001$ , \*  $P < 0.05$ .

### **3.3.11 Optimization of T4endoV concentration for ovarian cell lines**

During the optimization of T4endoV concentration for the NER assay it was noted that incubation of SKOV3 cells with the enzyme at concentrations typically used in the T4endoV modified comet assay, led to the formation of higher comets compared to the control. Figure 3.3.13A shows that increasing dilution of the T4endoV leads to the formation of fewer comets in UVB irritated cells. In contrast, no comets are formed by incubation with T4endoV at any concentration in unirradiated cells. This phenomenon was also noted for A2780 (Figure 3.3.13B). This finding led us to speculate that the bottle of T4endoV that we had received was highly concentrated or did not represent the U/ $\mu$ L stated. Support for this hypothesis came from the experiments which showed we needed to further dilute the enzyme, to levels unreported in the literature to be effective, and demonstrated the expected results based upon past experiments in our laboratory (Figure 3.3.14). Again, unirradiated cells showed no increase in comet tail when incubated with T4endoV (Figure 3.3.14B); however, irritated cells showed a significant increase in % tail DNA when incubated in the absence of T4endoV (Figure 3.3.14A). Treatment with a low concentration of T4endoV (0.0001 U/ $\mu$ L) increased the levels of DNA damage, as shown in Figure 3.3.14B.

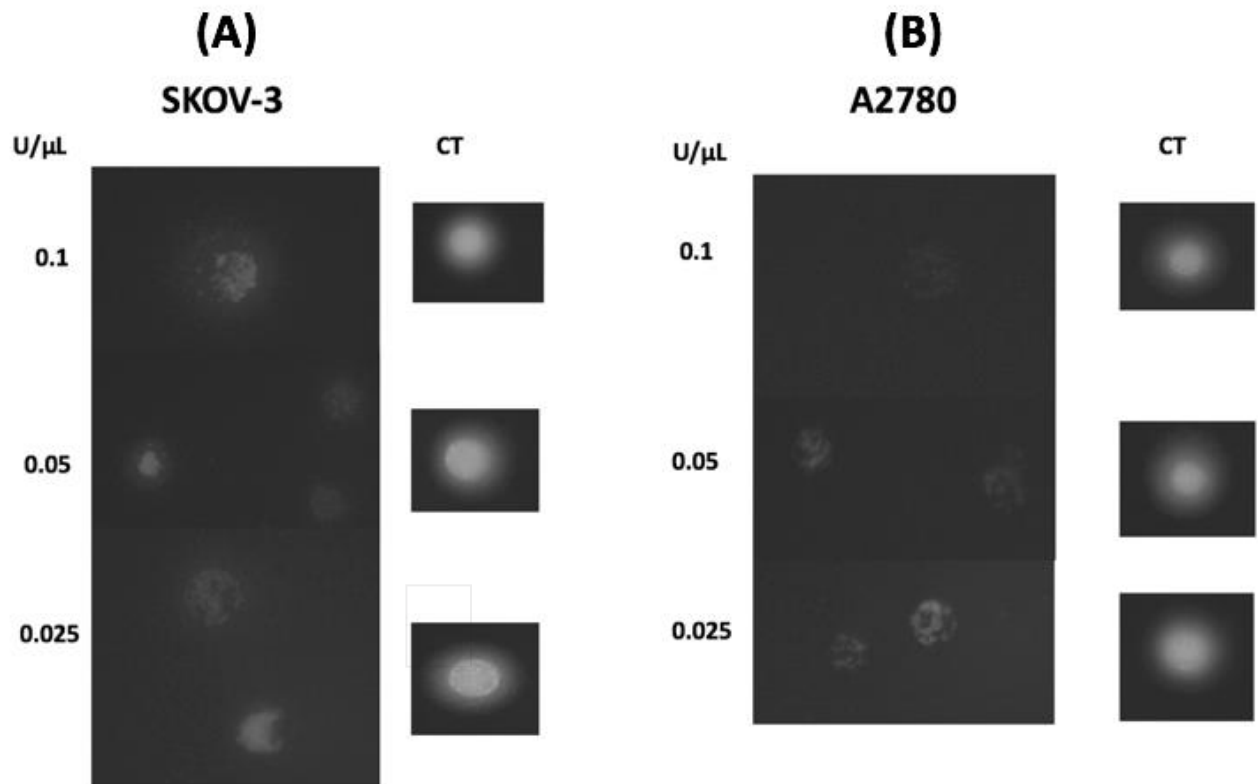


**Figure 3.3.13 Damaged comet images from SKOV-3 and A2780 cells following the treatment with different concentrations of T4endoV enzyme.** Ovarian cancer cells were exposed to  $0.5 \text{ J/cm}^2$  of UVB and cell were then processed using the T4endoV-modified comet assay. This experiment was repeated three times and these concentrations were rapturing the comets in every individual experiment.

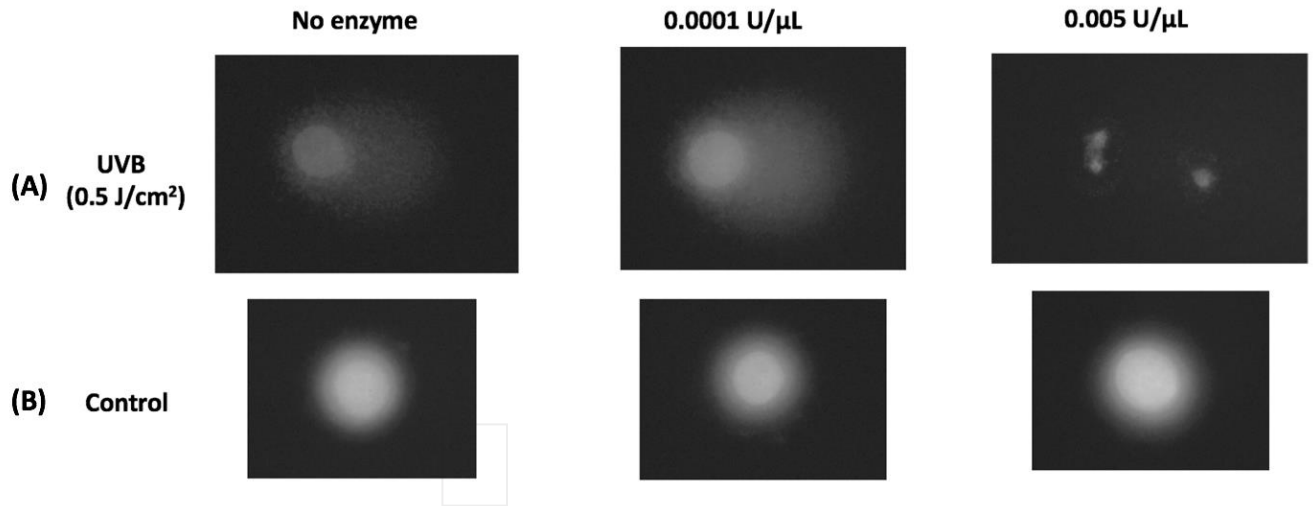


**Figure 3.3.14** Typical comet images from SKOV-3 cells following the treatment with the optimum concentration of T4endoV for removal of CPD from ovarian cells. Ovarian cells were exposed to 0.5 J/cm<sup>2</sup> with 0.5 J/cm<sup>2</sup> of UVB and cell were then processed using the T4endoV-modified comet assay.

### 3.3.12 NER repair of UV radiation-induced CPD in ovarian cells

The T4endoV-modified comet assay was performed to measure the kinetics of NER following the UVB irradiation. As shown in Figure 3.3.15, the remaining percentage of tail DNA was detected at different time points. The amount of DNA damage remaining at 1 h and 2 h post irradiation was around 95 % in all ovarian cancer cells. At 6 h post irradiation, all cell lines showed a slight decline in the amount of DNA damage remaining, around 80 %. Moreover, the amount of CPD and SB/ALS was also determined at each time point, as shown in Figure 3.3.16. Exposure to 0.5 J/cm<sup>2</sup> of UVB led to a significant increase in levels of CPD ( $p < 0.0001$ ) and SB/ALS ( $p < 0.0001$ ) for all the cell lines at all time points, compared to the control. These levels remained significantly high and not fully repaired even at 30 h post irradiation, as shown in Figure 3.3.15 and 3.3.16.

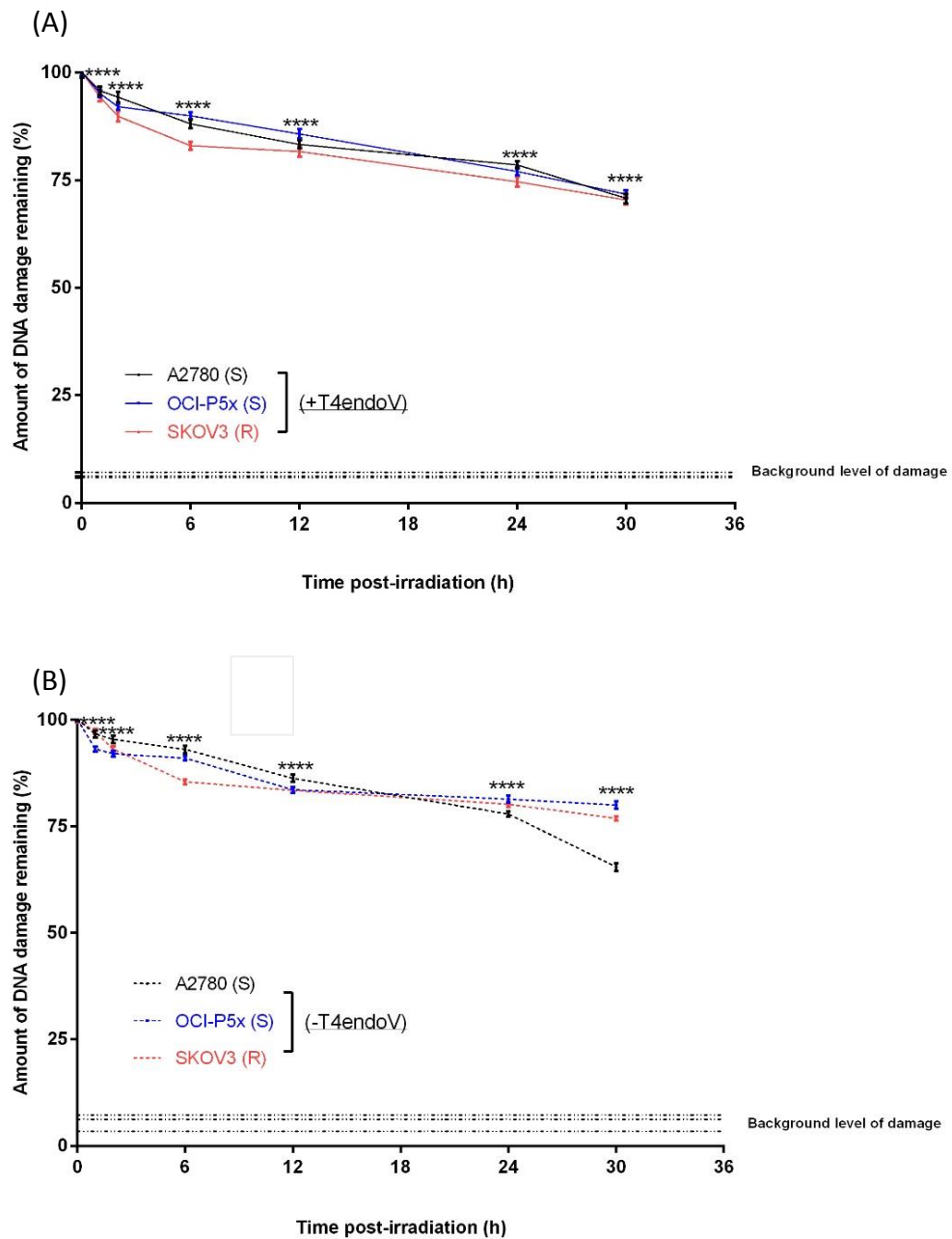


**Figure 3.3.15 kinetics of nucleotide repair of CPD (+ T4endoV) and strand breaks (- T4endoV) in ovarian cancer cells.** Ovarian cells were exposed to 0.5 J/cm<sup>2</sup> of UVB and allowed to repair in the incubator for different time points (0, 1, 2, 6, 12, 24, or 30 h). The control samples were not irradiated. (A) The percentage of amount of DNA damage remaining in ovarian cancer cells following the treatment of T4endoV enzyme (0.0001 U/ $\mu$ L). (B) The percentage of amount of DNA damage remaining in ovarian cancer cells in the absent of T4endoV enzyme; Data represent mean  $\pm$  SEM from three experiments. Statistical analysis was used to compare every individual cell line, at each point, to their background level, in present or absent of T4endoV. \*\*\*\* P < 0.0001. Background levels were detected as follow; A2780 (6.18 %), OCI-P5x (5.86%), and SKOV3 (7.13 %).

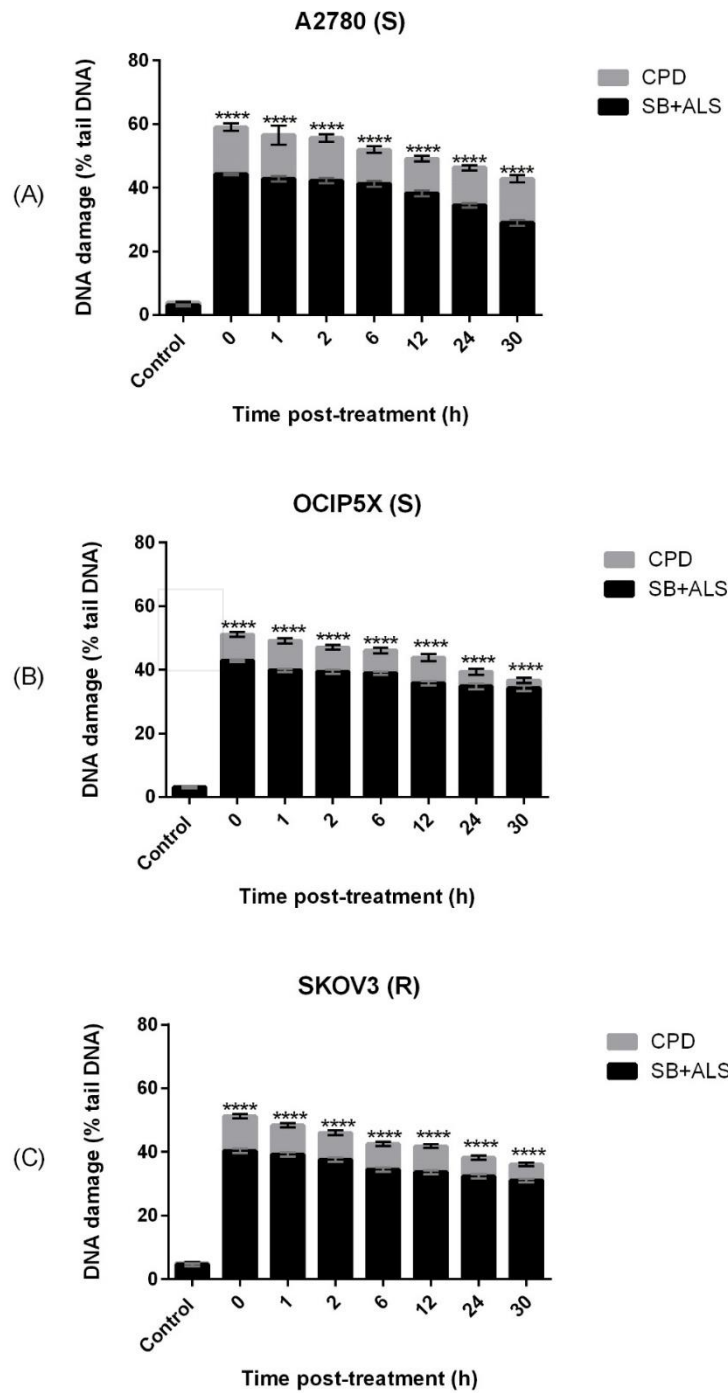


**Figure 3.3.16 significant levels of CPD + SB/ALS were induced by UVB in ovarian cancer cells.** Repair of the CPD in ovarian cells measured by the T4endoV-modified comet assay. Cells were exposed to 0.5 J/cm<sup>2</sup> of UVB and allowed to repair in the incubator for different time points (0, 1, 2, 6, 12, 24, or 30 h). The control samples were not irradiated. (A) Chemosensitive cell line, A2780; (B) Chemosensitive cell line, OCIP5X; (C) Chemoresistant cell line, SKOV3. Data represent mean +/- SEM from three experiments. \*\*\*\* P < 0.0001

### **3.3.13 Examination of ovarian cancer cells response to environmental and chemical agents**

The comet assay was carried out to measure the level of DNA damage induced by different doses of cisplatin and formaldehyde. Following the treatment with the cisplatin/formaldehyde, cells were exposed to 0.5 J/cm<sup>2</sup> UVB to induce DNA damage. In the absence of cisplatin/formaldehyde, the DNA breaks migrate with the current forming the comet shape. However, in the presence of the treatment the tail becomes shorter as a result of the formation of crosslinks. As Figure 3.3.17, the control samples showed a low level of DNA damage (below 5 %). All ovarian cancer cells showed a significant reduction ( $p < 0.0001$ ) in % tail DNA following the treatment with cisplatin or formaldehyde, compared to irritated damaged cells (UVB only). Following cisplatin treatment, a reduction in DNA damage levels was demonstrated with the increase of cisplatin concentrations in all ovarian cancer cells, Figure 3.3.17. Cisplatin was more effective in the chemosensitive cells with increased dosage compared to the formaldehyde; while the chemoresistant cells are more resistant to form DNA crosslinks following the treatment with cisplatin/formaldehyde. The reduction of DNA damage induced by cisplatin treatment were significantly different ( $p < 0.0001$ ) in A2780 than formaldehyde treatment, as shown in Figure 3.3.17A. Likewise, this finding was also noted in OCIP5X following the treatment with 50  $\mu$ M and 100  $\mu$ M. of cisplatin the DNA damage level were significantly reduced comparing to formaldehyde treatment, Figure 3.3.17B. Following the treatment with 50  $\mu$ M of cisplatin/formaldehyde, the chemoresistant cells showed less reduction of DNA damage levels ( $p < 0.05$ ) which indicated less DNA crosslinks formed comparing to the chemosensitive cells, Figure 3.3.17C.

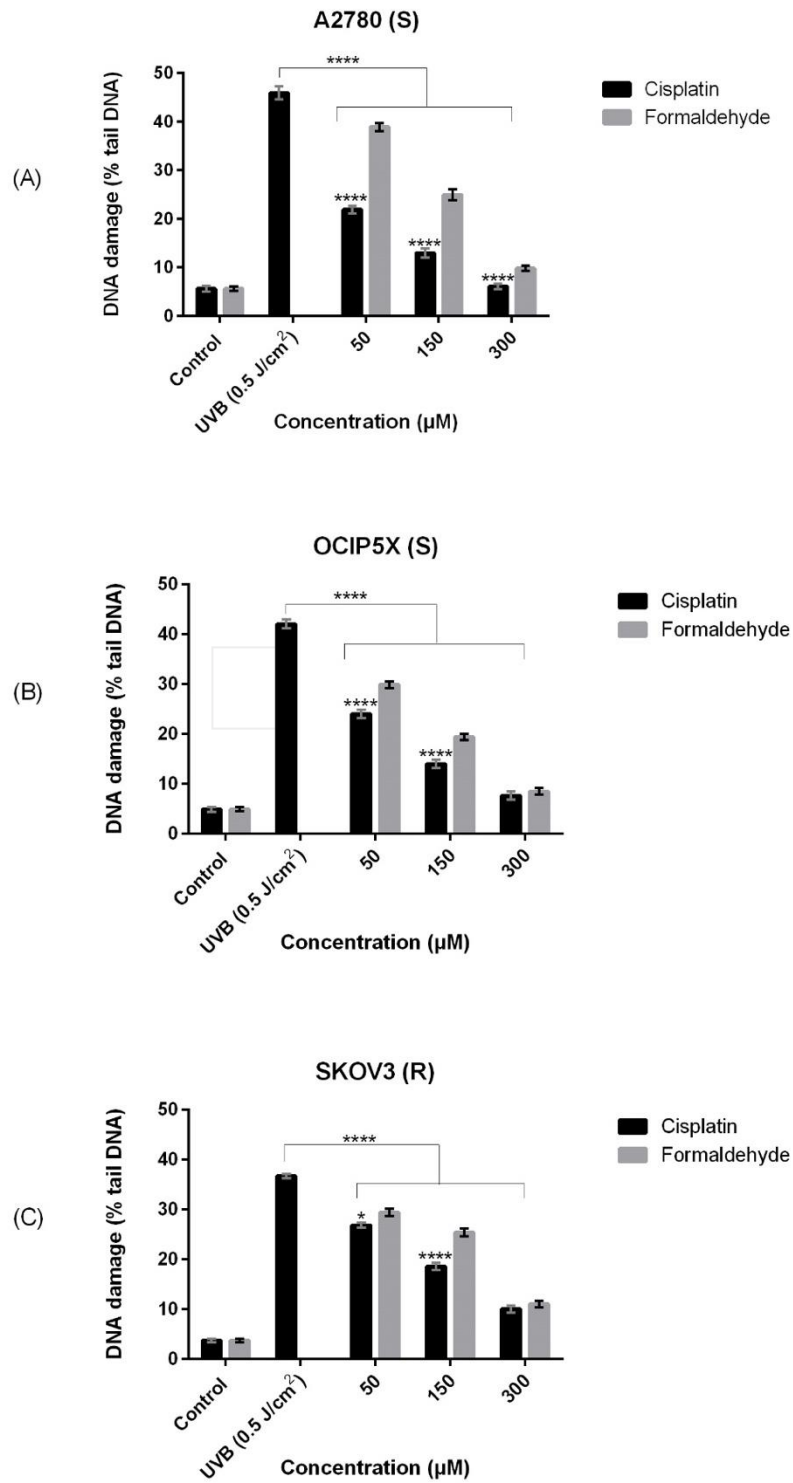


**Figure 3.3.17 Chemoresistant cells are more resistant to ICL formation from cisplatin + formaldehyde, a representation environmental crosslinks agent.** Induction of DNA damage following the treatment with increase concentration of formaldehyde/cisplatin. Data represent mean +/- SEM from three experiments. Exposure to UVB was used to induce the damage

### 3.4 Discussion

A growing number of women around the world are getting diagnosed with ovarian cancers every year. Unfortunately, most of these cancer patients are usually not identified until related complications are already developed. Generally, there is only an approximated five years of survival with even less than a 50% chance of favorable outcome. Cisplatin is considered as a very dynamic medication for the treatment of ovarian disease throughout the past forty years, and the medical findings for female patients with malignant ovarian growth can be characterized by the tumor reaction to cisplatin. The results of this chapter demonstrated a clear observation of the molecular differences between the chemosensitive and chemoresistant cells. Chemoresistant cells have a significantly higher cell survival in response to cisplatin compared to chemosensitive cell lines. This suggests that chemoresistant cells could have a mechanism that helps to tolerate cisplatin chemotherapy. Unhooking the formed crosslinks could be one of the strategies to reduce the cisplatin affects. Chemoresistant tumor cells are refractory to the formation of cisplatin-induced DNA crosslinks. It was noticed that SKOV 3 had a low percentage of ICL following cisplatin treatment comparing to the chemosensitive cell lines. This result was conducted by modified comet assays were used to measure ICL formation. Further approaches, ICP-MS and ELISA, were used to confirm that SKOV3 was more resistant to the ICL formation following cisplatin treatment compared to the chemosensitive cells, as demonstrated in Figure 3.3.2 and 3.3.3. The formation of cisplatin-DNA adducts, in the chemosensitive and chemoresistant cells, was measured by determining the platinum concentration in DNA with ICP-MS and by using anti-cisplatin-DNA with ELISA. This can lead to understanding the mechanisms of drug-DNA interactions in ovarian cancer cells. One of the major defects

□ □ □

that accompany cisplatin use in treating cancer is the development associated with drug resistance, which was correlated with a reduced intracellular accumulation of cisplatin. Therefore, the intracellular platinum concentration can be used as an indicator of the resistance of cisplatin.

Additional theories that may be involved in the development of chemoresistance is the effectiveness of the repair systems in the cell lines. Therefore, studying the repair kinetics was essential. Equivalent BER ability occurs in chemosensitive and chemoresistant ovarian tumor cells were demonstrated; however, significant levels of oxidized purines + SB/ALS were observed in ovarian cancer cells, Figure 3.3.9. Moreover, the kinetics of nucleotide repair of CPD and strand breaks in ovarian cancer cells were conducted. Interestingly, it was noticed that exposure to 0.5 J/cm<sup>2</sup> of UVB led to a significant increase in levels of CPD and SB/ALS for all the cell lines at all time points. These levels remained significantly high and were not fully repaired even at 30 h post-irradiation.

Generally, cisplatin is an effective chemotherapeutic agent that induces DNA damage; however, it is less effective with the inference of the process of DNA repair systems. Some of the processes involved in the repair process include NER, MMR, HR, FA pathway, NHEJ, and BER. Therefore, further investigations are needed in order to have a better understanding of the repair system involvement in the chemoresistance (reviewed in section 1.4).

Principally, the key mechanism to cisplatin activity is the formation of DNA crosslinks, which interrupts the proper functioning of cellular DNA, which subsequently induces apoptosis. Therefore, investigating the response of ovarian cancer cells to different crosslinking agents was essential in this study. As Figure 3.3.17 shows, chemoresistant

cells are more resistant to ICL formation from cisplatin and formaldehyde, a representative environmental crosslinking agent. Based on the previous findings, and the response to the environmental crosslinking agent, the assumption that chemoresistant cells have a mechanism to resist the formation of crosslinks was developed. Therefore, further investigations were required to have a better understanding of the chemoresistance. One of the novel approaches used was to study the DNA damage response in different cell substrates. This approach investigated the basis of this differential DNA damage response by examining the potential role of nuclear organization, via the comparison of damage induction in nucleoid bodies versus intact cells. The results demonstrated the same rank order of dose-response in nucleoid bodies as observed in intact cells, with chemoresistant cells being considerably more resistant to damage formation, at all doses of cisplatin. These data provide a basis for further studies to improve our understanding of the differential DNA damage response associated with chemosensitive and chemoresistant ovarian cells. Therefore, isolation and characterization of associated nuclear proteins in ovarian cancer cells and study their involvement in the chemoresistance is one of the future directions for this thesis.

## **CHAPTER 4**

# **EVALUATION OF GENE POSITIONING AND COPY NUMBER CHANGES IN CHEMOSENSITIVE AND CHEMORESISTANT OVARIAN CANCER CELL LINES**

## 4.1 Introduction

Ovarian cancer is the leading cause of gynecologic cancer-related deaths among women. This cancer rarely has specific symptoms making early detection challenging, and there are limited chemotherapeutic options, with many patients developing resistance to treatment, eventually succumbing to the disease. In 2020, an estimated 21,750 women will be diagnosed with ovarian cancer, and 13,940 women will die from the disease in the US, according to the American Cancer Society [8]. It is hypothesized that there is a difference in the organization of chromatin in chemosensitive (CS) and chemoresistant (CR) ovarian cancer cell lines, and gene repositioning and copy number changes are associated with resistance to chemotherapy in ovarian cancer cell lines. Basically, genomic organization applies to the linear order of DNA components and their division into chromosomes. The human genome is divided into 46 chromosomes, which are packaged in order to fit inside the nucleus. At the chromosome level, the organization is defined in preferential territories filled by chromosomes. In eukaryotic cells the genome is highly spatially organized. Functional relevance of higher order genome organization is implied by the fact that specific genes, and even whole chromosomes, alter spatial position in concert with functional changes within the nucleus, for example with modifications to chromatin or transcription [178].

While global genome organization patterns remain largely conserved in disease, some genes and chromosomes occupy distinct nuclear positions in diseased cells compared to their normal counterparts, with the patterns of reorganization differing between diseases. Importantly, mapping the spatial positioning patterns of specific genomic loci can distinguish cancerous tissue from benign with high accuracy. Genome positioning is an

□ □ □

attractive novel biomarker since additional quantitative biomarkers are urgently required in many cancer types [179]. Therefore, this study was important to investigate the difference in organization of genes in chemosensitive and chemoresistant cell lines.

Hence, it was essential to investigate whether the exposure to cisplatin chemotherapy is altering gene positioning; also, to evaluate the copy number changes in ovarian cancer cells. This study aims to explore the correlation between gene positioning prior to and following exposure to cisplatin chemotherapy in CS and CR ovarian cancer cell lines. It well established that chromosomes and genes occupy distinct cell-type-specific and evolutionarily conserved locations in interphase nuclei. This organization of chromatin in the nucleus is hypothesized to be additional level of epigenetic regulation of the genome [178, 181]. The packaging and organization of the genome into discrete chromosome territories in interphase nuclei is hypothesized to be involved in regulating important genome functions [178, 181]. In the majority of cell types, gene-rich chromosomes are preferentially located more towards the nuclear interior, with gene-poor chromosomes localized toward the nuclear periphery. Additionally, within each cell-type, how the DNA is packaged within the chromosome territory may differ, with expressed genes often localized at, or near the periphery of the chromosome territory. The nuclear localization of chromosome territories and the position of individual genes within individual chromosome territories likely plays an important role in various genome functions (e.g., gene expression, DNA damage induction, recognition, and repair etc.). Numerous studies have demonstrated alterations in the nuclear position of chromosomes and/or genes following altered gene expression, induction of DNA damage, and in a number of diseases including laminopathies and cancer [179-184]. Altered chromatin organization is accompanied with

functional changes such as changes in gene transcription and modifications to chromatin [179] At present, the regulation of how chromosome and gene positioning is determined in the nucleus remains to be discovered. However, chromosome and/or gene organization is increasingly recognized as a potential marker for disease and new diagnostic tool [179,183]. Altered gene positioning may play an important role in the molecular difference between chemoresistant and chemosensitive ovarian cell lines. In order to study gene positioning and assess copy number changes, fluorescence in situ Hybridization was used. FISH is a cytogenetic technique that allows the nuclear localization of target regions to be established and the detection of chromosomal abnormalities using commercially available fluorescent probes that bind to DNA with a high degree of sequence complementarity. As discussed in Foster and Bridge (2005), the spatial and temporal organization of genomes in their nuclear environment helps to control their function and behavior is becoming widely accepted, especially when we see genome mis-organization in disease cells such as cancer and nuclear envelope diseases such as laminopathies [183]. Studies on functional genome organization should include how the genome interacts with the underlying architecture making up the nucleus. Thus, understanding aspects of the genome and its interphase home in 4D will lead to 21st century treatments and therapies for a range of ills from cancer to ageing. In this chapter, FISH was used to map specific genes potentially involved in cancer formation and/or progression to determine if the targeted genes are randomly or nonrandomly organized in ovarian cancer cell lines (A2780, OCI-P5X, and SKOV3). Differences in gene positioning of the selected genes and copy number changes were evaluated in the two chemosensitive ovarian cell lines (A2780 and OCI-P5X) and the chemoresistant ovarian cell line (SKOV3) and following exposure to cisplatin

□ □ □

chemotherapy. It is hypothesized that gene positioning will be non-random for the investigated genes. Additionally, that gene positioning and gene copy number may differ between CS and CR ovarian cancer cell lines, and gene positioning may be altered following cisplatin chemotherapy exposure.

## **4.2 Methods**

### **4.2.1 Ovarian cancer cell lines**

Three ovarian cancer cell lines were used in this study; two cell lines are sensitive to cisplatin chemotherapy (A2780 and OCI-P5X), and one is resistant (SKOV-3). All cells were cultured according to the supplier's recommended media and condition for each cell line (section 2.2.1 to section 2.2.4). Briefly, all cells were cultured in T25 cell culture flask and allowed to grow with the manufacturers recommended cell culture media at 37 °C in a 5% CO<sub>2</sub> and humidified atmosphere. For each cell line, two experimental groups were prepared, one control group (no cisplatin treatment), and the other treated with cisplatin.

### **4.2.2 Cisplatin treatment**

For the treated groups, all investigated cell lines were treated with cisplatin at the same time when they become confluent enough to perform the treatment (section 2.2.15.1). Briefly, treated groups were treated with cisplatin (100 µM) for 1 h at 37 °C in a 5% CO<sub>2</sub> and humidified atmosphere. Subsequently, the cell culture media containing the cisplatin was removed and replaced with drug-free media for 12 h at 37 °C in a 5% CO<sub>2</sub> and humidified atmosphere. All groups were then trypsinized and transferred to a 15 mL centrifuge tubes, which were centrifuged at 9000 rpm for 5 mins. The supernatant was removed, and the cell pellet was fixed by resuspending the pellet dropwise with a total of

□ □ □

5 mL of 3:1 methanol: acetic acid. Resuspension of the pellet was performed after each drop of the fixative to minimize cell clumping. Samples were centrifuged and the fixation and resuspension step were repeated two further times. Samples were subsequently stored at – 20 °C until required for experiments.

### **4.2.3 Dual color FISH**

The FISH protocol has been prescribed in detail previously in section 2.2.15.2. Briefly, following the fixation step from the previous section, the pellet was centrifuged and the supernatant was removed to 1 – 2 mL depending on the size of the cell pellet. The cell pellet was then resuspended and 1-5  $\mu$ L of the cell suspension depending on the pellet size was placed onto a glass microscope slide. Slides were visualized under a phase contrast microscope to confirm the optimal cell density (200 - 500 cells not overlapping). Slides were then washed with PBS and dehydrated in an ethanol series (70%, 80%, and 100%) for five min each and air-dried. Slides were then washed in ddH<sub>2</sub>O followed by rinsing in PBS before incubation in 4% paraformaldehyde/PBS at 4 °C for 10 min; slides were then rinsed with PBS followed by ddH<sub>2</sub>O at room temperature, and another ethanol series was carried out at room temperature for 2 min each and the slides air-dried. FISH probes complementary to specific genes used in this study are provided in Table 2.2.1. Seventeen genes were selected to be targeted in this study, genes were selected based on their involvement in cancer formation and progression, (e.g., known driver mutation, altered gene expression etc.). The name of the gene, known function and chromosome locations have been described in detail in Table 4.4.1, FISH probes were either labelled with TRITC (red) or FITC (green) fluorescent dyes and allowed evaluation of 2 FISH probes simultaneously. The FISH probe mix of the two different genes and hybridization mix was

prepared as per the manufacturer's guidelines. Once mixed the FISH probes were then vortexed and pulse microfuged and subsequently pre-denatured at 73 °C for 10 min in a water bath. Following denaturation of the FISH probes in hybridization mix, 1 µL of the probe was added to the slide, and a 5 mm round coverslip was placed on the slide; and sealed with rubber cement. The microscope slides with the predenatured FISH probes were placed in a hybrite (Vysis) at 75 °C, for 90 sec to denature the DNA in conjunction with the FISH probes. Subsequently, the DNA and FISH probes were allowed to hybridize overnight (16 h) at 37 °C in a humidified chamber. Once the hybridization period was completed, the slides were washed in 0.4X SSC-0.3% tween to remove the coverslips at room temperature. Then, the slides were placed in a pre-warmed solution of 0.4 X SSC-0.3% Tween-20 at 73 °C and washed for 90 seconds to remove the excess probe. Slides were then placed in 2X SSC-0.1% tween for a 1 min wash at room temperature followed by an ethanol series (2 min each). Finally, slides were air-dried and counterstained with DAPI to stain all DNA to allow identification of the interphase nucleus. Subsequently, slides were stored at 4 °C until ready for capturing.

**Table 4.4.1 Descriptive table of all genes used in the study (Gene Cards Human Gene Database)**

<b>Gene</b>	<b>Gene Function</b>	<b>Chromosome Location</b>
<b>AKT Serine/Threonine Kinase 3</b> <i>(AKT3)</i>	Involved in cell proliferation	1
<b>Alpha-1,3 Glucosyltransferase</b> <i>(ALG8)</i>	Part of enzyme family that adds glucose residue to necessary proteins to maintain normal function	11
<b>B-Raf Proto-Oncogene, Serine/Threonine Kinase</b> <i>(BRAF)</i>	Regulates a pathway cell division and differentiation	7
<b>Breast cancer type 1</b> <i>(BRCA1)</i>	Maintains genomic stability; tumor suppressor	17
<b>Breast cancer type 1</b> <i>(BRCA2)</i>	Maintains genomic stability; tumor suppressor gene, active in HR pathway.	13
<b>Cyclin E1 (CCNE1)</b>	CDK kinase regulating mitotic cycle	19

<b>Catenin Beta 1</b> <i>(CTNNB1)</i>	Involved in maintaining growth and adhesions between epithelial cell layers	3
<b>Folate Receptor 1</b> <i>(FOLR1)</i>	Transport folate derivatives into cells	11
<b>KRAS Proto-Oncogene</b> <i>(KRAS)</i>	Involved in the regulation of cell proliferation	12
<b>MDS1 and EVI1 Complex Locus</b> <i>(MECOM)</i>	Involved in hematopoiesis, apoptosis; and differentiation;	3
<b>Nucleus Accumbens Associated 2</b> <i>(NACCI)</i>	Involved in regulating apoptosis and proliferation	19
<b>Neurofibromin 1</b> <i>(NF1)</i>	Involved in cell communication mainly in regard to growth factors	17
<b>Paired Box 3</b> <i>(PAX3)</i>	Regulates transcription	2
<b>Phosphatase and Tensin Homolog</b> <i>(PTEN)</i>	Tumor suppressor	10

<b>RB Transcriptional Corepressor 1</b> <i>(RB1)</i>	Cell cycle regulator; genomic stabilizer	13
<b>SRY-Box 17</b> <i>(SOX17)</i>	Regulates transcription	8
<b>Tumor Protein 53</b> <i>(TP53)</i>	Tumor suppressor protein; regulates transcription; regulates DNA repair mechanisms	17

#### **4.2.4 FISH image capture**

The image capture process is described previously in Section 2.2.15.3. In brief, Slides were examined on an Olympus BX-61 epifluorescence microscope supplied with a cooled CCD camera and fluorescence filters for FITC, TRITC, and DAPI. Images were captured using SmartCapture 3 software. A minimum of 100 individual (non-overlapping) cells were analyzed per FISH probe, per cell line, per condition (cisplatin treated and untreated).

#### **4.2.5 Assessment of gene copy number**

The copy number of each gene was assessed when capturing FISH images. The number of fluorescent signals (red or green) were scored in each individual cell to assess the copy number of each gene in each cell, in each cell line and following cisplatin treatment. A strict scoring criteria was used to assess copy number. All signals had to be similar in size and intensity and signals had to be at least one signal distance apart to be counted as two individual signals, (rather than a split signal).

#### **4.2.6 Radial assessment of gene positioning in interphase nuclei**

To evaluate the gene positioning in interphase nuclei previously published methodologies were utilized [180]. Assessment of gene localization within the interphase nucleus was established using a custom script written for Image J. This script allows for the separation of each image into the three individual color channels (TRITC [red], FITC [green], which correspond to the FISH probes and DAPI (blue) for the DNA counterstain). The software converts the DAPI fluorescence to a binary mask that allows for the creation of five rings of equal area based on the DAPI fluorescence intensity. The software then measures to amount of red and green fluorescence corresponding to each targeted gene located in each

□ □ □

of the five rings (of equal area), relative to the total signal for the area that is covered by the ring, as shown in Figure 2.2.6 Data is collected and normalized against the different DNA content (DAPI counterstain) in the nucleus to compensate for the fact that a 3D object is observed under two-dimensions. The amount of red and green fluorescence in each of the five rings of equal area can then be displayed in a histogram to display the nuclear localization of each gene in the 100 cells analyzed per gene, per cell line, per treatment (control or cisplatin treated).

#### **4.2.7 Assessment of nonrandom gene positioning in interphase nuclei and statistical analysis**

Based on the radial organization software data it is possible to determine the nuclear localization of the targeted genes within the interphase nuclei. The histograms produced can indicate whether a gene is preferentially nonrandomly or randomly organized and where the gene tends to be localized. For example, if more red or green fluorescence is detected in the inner most rings the gene is more interiorly located, versus peripherally located if more fluorescence is detected in peripheral rings. In both of these cases, it would indicate a nonrandom localization of the gene. However, if the red or green fluorescence is roughly equally distributed in all of the rings it suggests a more random organization. Whether the nuclear organization of a gene was nonrandomly or randomly organized was confirmed using the Chi-squared goodness of fit ( $\chi^2$ ) ( $p < 0.05$ ) as per previously published studies [180, 185]. This statistical test was also utilized to determine whether gene positioning differed [180, 185] between the CS and CR lines and whether genes were repositioned following cisplatin treatment within the same cell line.

## 4.3 Results

### 4.3.1 Nonrandom gene positioning in ovarian cancer cell lines

The nuclear localization of 17 different genes (Table 4.4.1) was examined in three ovarian cancer cell lines (A2780, OCI-P5X, and SKOV3) in control (no cisplatin treatment; Table 4.4.2A) and cisplatin treated cell lines (Table 4.4.2 B). Of the 17 genes tested, eight genes (47.06%) (*ALG8*, *BRCA1*, *BRCA2*, *CNNE1*, *FOLR1*, *NACCI*, *NF1*, and *TP53*) demonstrated nonrandom organization in all cell lines and in all conditions (cisplatin treated and untreated).

In the A2780 cell line, 10 genes (58.82%) were found to be nonrandomly organized in the control untreated cells (additional genes included *KRAS* and *SOX17*). In the cisplatin treated A2780 cells, nine genes (52.94%) were nonrandomly organized. Compared to the control A2780 cells cisplatin treatment resulted in nonrandom positioning of *RBI* and random positioning of *KRAS* and *SOX17*.

In the OCI-P5X cell line, 13 genes (76.47%) were found to be nonrandomly organized in the control untreated cells (additional genes included *CTNNB1*, *KRAS*, *PAX3*, *RBI* and *SOX17*). In the cisplatin treated OCI-P5X cells, 15 genes (88.24%) were nonrandomly organized. Compared to the control OCI-P5X cells cisplatin treatment resulted in nonrandom positioning of *MECOM* and *PTEN*.

In the SKOV3 cell line, 15 genes (88.24%) were found to be nonrandomly organized in the control untreated cells (additional genes included *AKT3*, *BRAF*, *CTNNB1*, *KRAS*, *PAX3*, *RBI* and *SOX17*). In the cisplatin treated SKOV3 cells, 14 genes (82.35%) were nonrandomly organized. Compared to the control SKOV3 cells cisplatin treatment resulted in random positioning of *CTNNB1*.

Between the CS and CR cell lines, two genes (*AKT3*, and *BRAF*) were found to be randomly organized in CS cell lines and nonrandomly organized in the CR cell line in both control and cisplatin treated cells (Figure 4.4.1).



**Table 4.4.2 Nonrandom gene positioning in control and cisplatin treated A2780, OCI-P5X, and SKOV3 ovarian cancer cell lines**

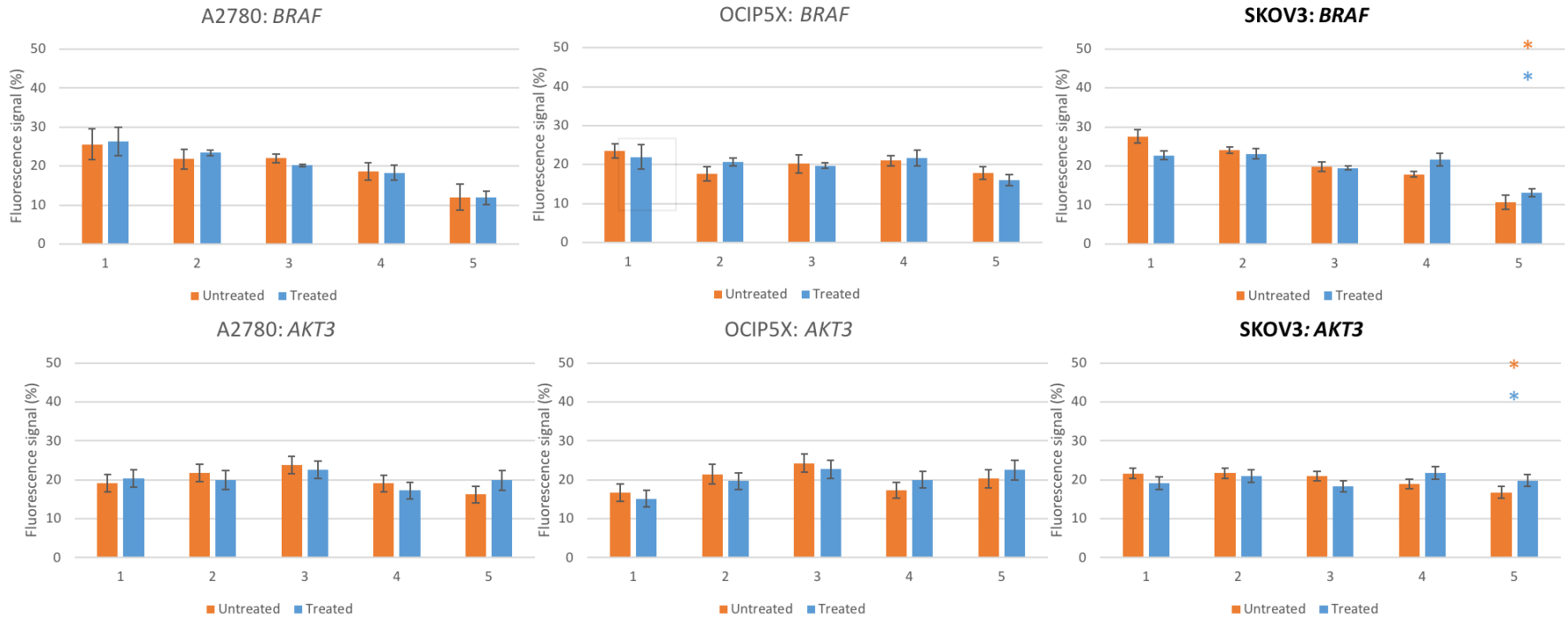
(A) Control (no cisplatin treatment)				(B) Cisplatin treated cells			
Genes	A2780 (CS)	OCI-P5X (CS)	SKOV3 (CR)	Genes	A2780 (CS)	OCI-P5X (CS)	SKOV3 (CR)
<i>AKT3</i>				<i>AKT3</i>			
<i>ALG8</i>				<i>ALG8</i>			
<i>BRAF</i>				<i>BRAF</i>			
<i>BRCA1</i>				<i>BRCA1</i>			
<i>BRCA2</i>				<i>BRCA2</i>			
<i>CNNE1</i>				<i>CNNE1</i>			
<i>CTNNB1</i>				<i>CTNNB1</i>			
<i>FOLR1</i>				<i>FOLR1</i>			
<i>KRAS</i>				<i>KRAS</i>			
<i>MECOM</i>				<i>MECOM</i>			
<i>NACC1</i>				<i>NACC1</i>			
<i>NF1</i>				<i>NF1</i>			
<i>PAX3</i>				<i>PAX3</i>			
<i>PTEN</i>				<i>PTEN</i>			
<i>RB1</i>				<i>RB1</i>			
<i>SOX17</i>				<i>SOX17</i>			
<i>TP53</i>				<i>TP53</i>			

	Non-randomly organized
	Randomly organized

Table 4.4.2 displays genes found to be statistically significantly nonrandomly positioned ( $p < 0.05$ ; cells shaded blue) in the interphase nucleus of three different ovarian cancer cell lines without (A) and with cisplatin treatment (B). Genes found to be randomly organized are indicated by white boxes ( $p > 0.05$ ).

- *BRAF* and *AKT3* were randomly organized in CS (A2780/OCIP5X) and non-randomly organized in CR (SKOV3)



**Figure 4.4.1 Differences in gene positioning (*BRAF/AKT3*) between CS and CR ovarian cell lines.** Example of data obtained from 2 different genes (*BRAF/AKT3*) in the three cell lines. Graphs display percentage of fluorescence for each gene from the nuclear interior (1) to the nuclear periphery (5) within the three cell lines. Error bars represent the standard error of the mean. Statistically significant findings  $p < 0.05$  \* non-random organization untreated cells; \* non-random organization cisplatin treated cells.

- *KRAS* and *SOX17* were randomly organized only in CS (A2780)

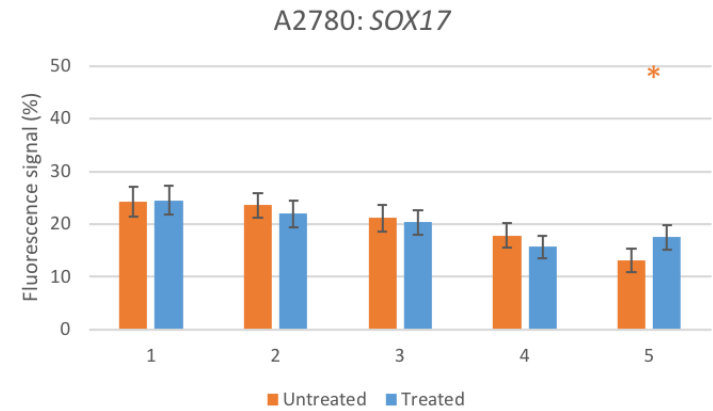
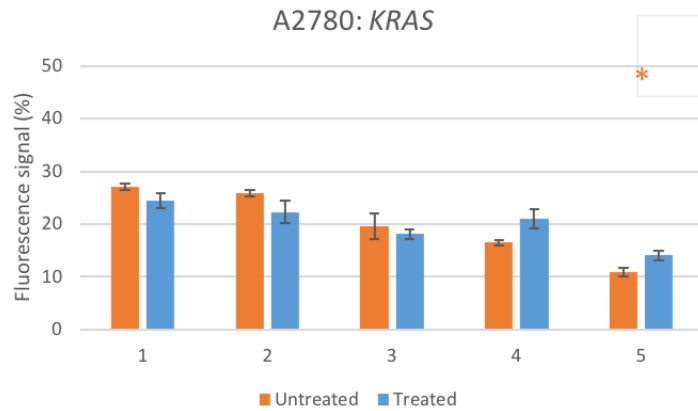


**Figure 4.4.2** *KRAS* and *SOX17* were randomly organized only in A2780. Example of data obtained from 2 different genes (*KRAS*/*SOX17*) in A2780. Graphs display percentage of fluorescence for each gene from the nuclear interior (1) to the nuclear periphery (5) within the three cell lines. Error bars represent the standard error of the mean. Statistically significant findings  $p < 0.05$   
 \* non-random organization untreated cells; \* non-random organization cisplatin treated cells.

- ***RB1* was randomly organized only in CS (A2780)**

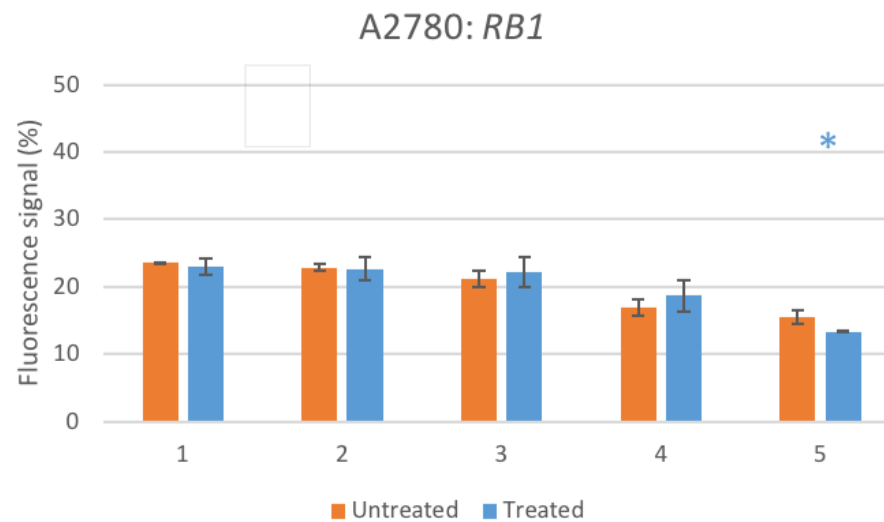


**Figure 4.4.3 *RB1* was randomly organized only in A2780.** Example of data obtained from one gene (*RB1*) in A2780. Graphs display percentage of fluorescence for *RB1* from the nuclear interior (1) to the nuclear periphery (5) within the three cell lines. Error bars represent the standard error of the mean. Statistically significant findings  $p < 0.05$  \* non-random organization untreated cells; \* non-random organization cisplatin treated cells.

- ***PAX3* was randomly organized in CS (A2780)**

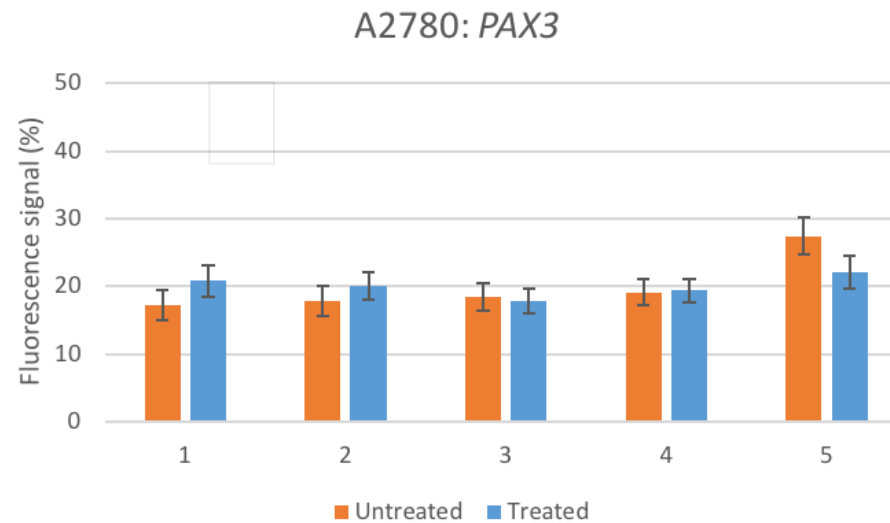


**Figure 4.4.4 *PAX3* was randomly organized in A2780.** Example of data obtained from one gene (*PAX3*) in A2780. Graphs display percentage of fluorescence for *PAX3* from the nuclear interior (1) to the nuclear periphery (5) within the three cell lines. Error bars represent the standard error of the mean.

- **MECOM** and **PTEN** were randomly organized in CS (A2780/OCIP5X) and CR (SKOV3)

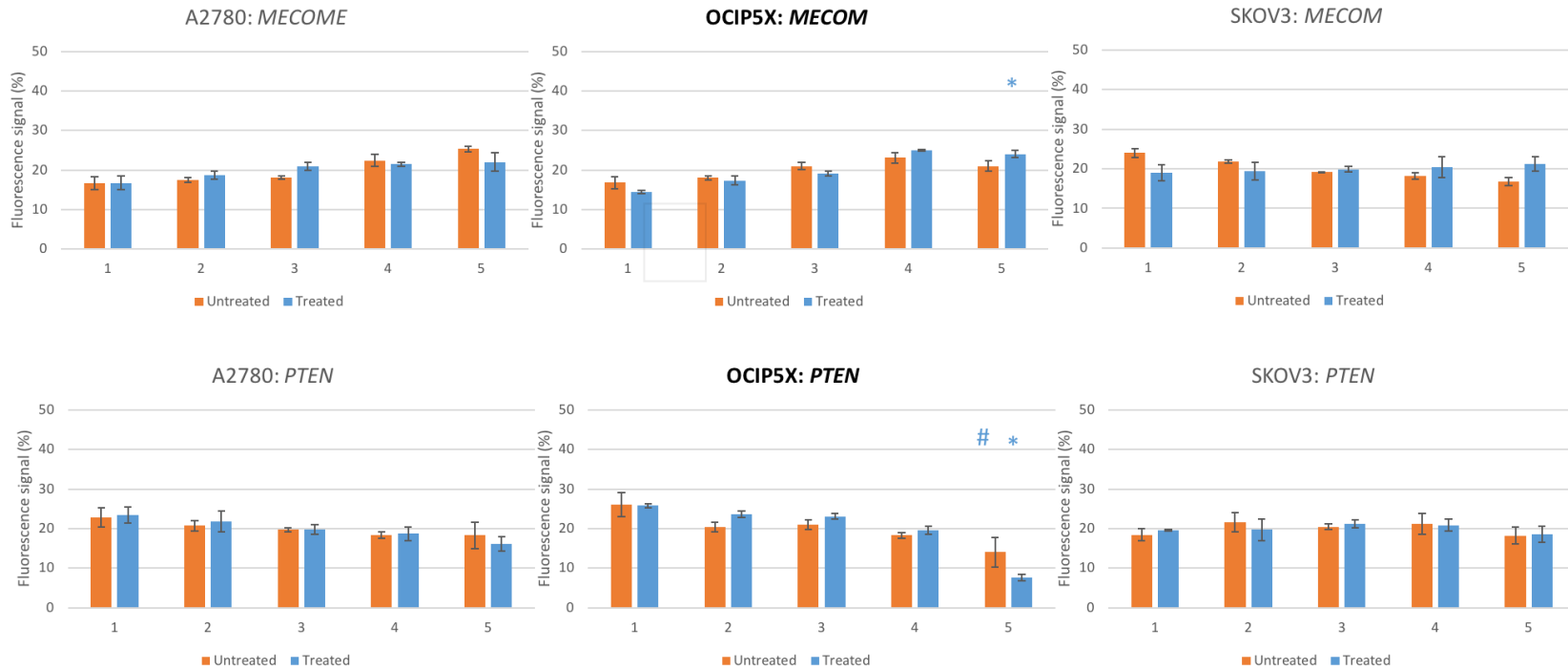


**Figure 4.4.5 Differences in gene positioning (*MECOM/PTEN*) between CS and CR ovarian cell lines.** Example of data obtained from 2 different genes (*MECOM/PTEN*) in all three cell lines. Graphs display percentage of fluorescence for each gene from the nuclear interior (1) to the nuclear periphery (5) within the three cell lines. Error bars represent the standard error of the mean. Statistically significant findings  $p < 0.05$  \* non-random organization untreated cells; \* non-random organization cisplatin treated cells. # difference in gene positioning between CR and CS cell line

### 4.3.2 Differences in the nuclear localization of genes in chemosensitive and chemoresistant cell lines

In addition to assessing whether the 17 investigated genes displayed random or nonrandom organization, the nuclear position of each of the genes in the interphase nucleus was compared between CS and CR cell lines. Differences in the nuclear position of genes between CS and CR cell lines could potentially be used to predict whether a patient's ovarian cancer might be CS or CR which may offer important prognostic information and potentially alter treatment and or management of the patient. Three genes displayed altered patterns of nuclear position in at least one CS cell line and the CR cell line. Specifically, *CCNE1* was positioned preferentially toward the nuclear interior in both the CS cell lines A2780 and OCI-P5X, whereas, in the CR cell line SKOV3 it was positioned more intermediately in the nucleus (Figure 4.4.6). A difference in the nuclear of *FOLR1* was also observed between A2780 and SKOV3, with the gene being much more interior in SKOV3 versus A2780. However, this gene in OCI-P5X was not found to be significantly differently positioned than in SKOV3 displaying a position in between that found in the A2780 and OCI-P5X cell line (Figure 4.4.7). A significant difference in the position of the *NFI* gene was also observed between the OCI-P5X cell line and SKOV3, but no difference was observed for A2780 cell line. With the *NFI* gene being positioned more toward the nuclear interior in the SKOV3 cell line versus the OCI-P5X cell line (Figure 4.4.8).

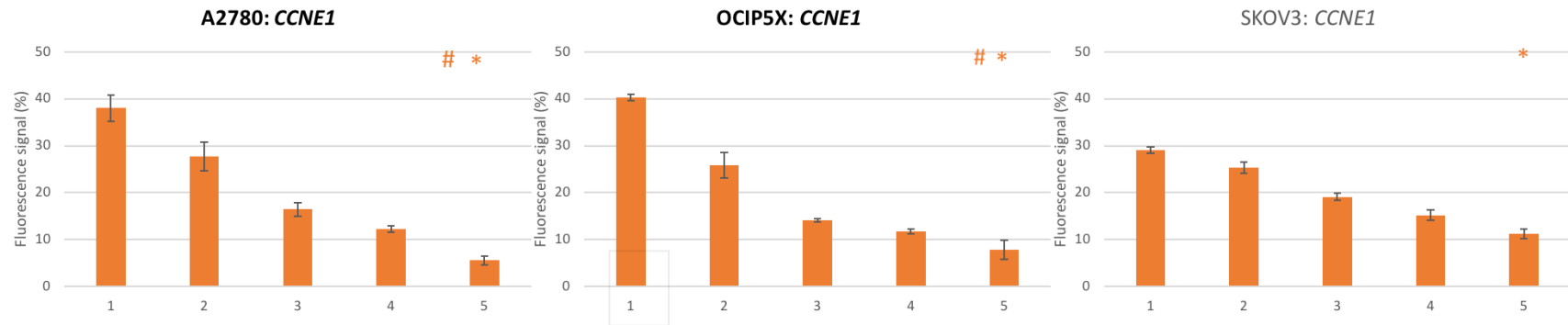


**Figure 4.4.6 Differences in gene positioning (*CCNE1*) between CS and CR ovarian cell lines.** Example of data obtained from *CCNE1* in all three cell lines. Graphs display percentage of fluorescence for the gene from the nuclear interior (1) to the nuclear periphery (5) within the three cell lines. Error bars represent the standard error of the mean. Statistically significant findings  $p < 0.05$   
 # non-random organization # difference in gene positioning between CR and CS cell line  
 \* non-random organization

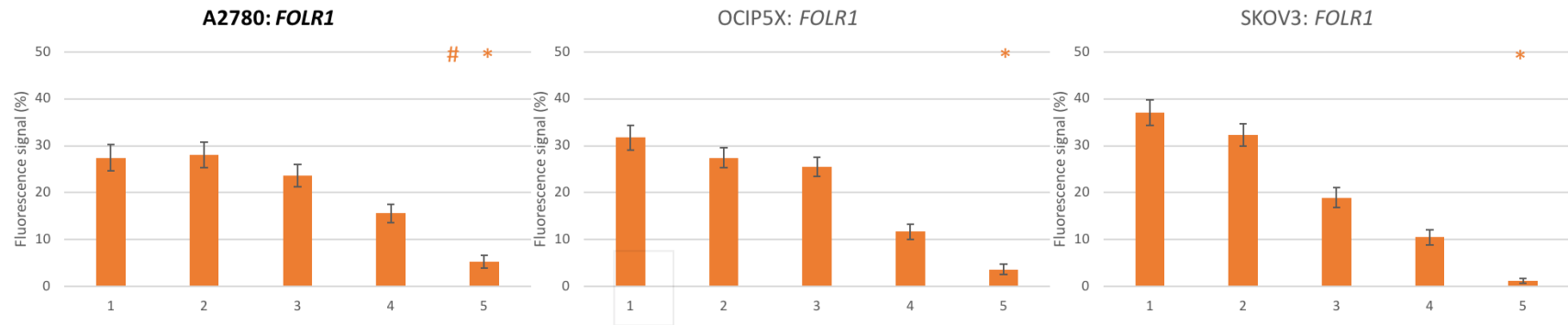


**Figure 4.4.7 Differences in gene positioning (*FOLR1*) between CS and CR ovarian cell lines.** Example of data obtained from *FOLR1* in all three cell lines. Graphs display percentage of fluorescence for the gene from the nuclear interior (1) to the nuclear periphery (5) within the three cell lines. Error bars represent the standard error of the mean. Statistically significant findings  $p < 0.05$   
 # non-random organization. # difference in gene positioning between CR and CS cell line

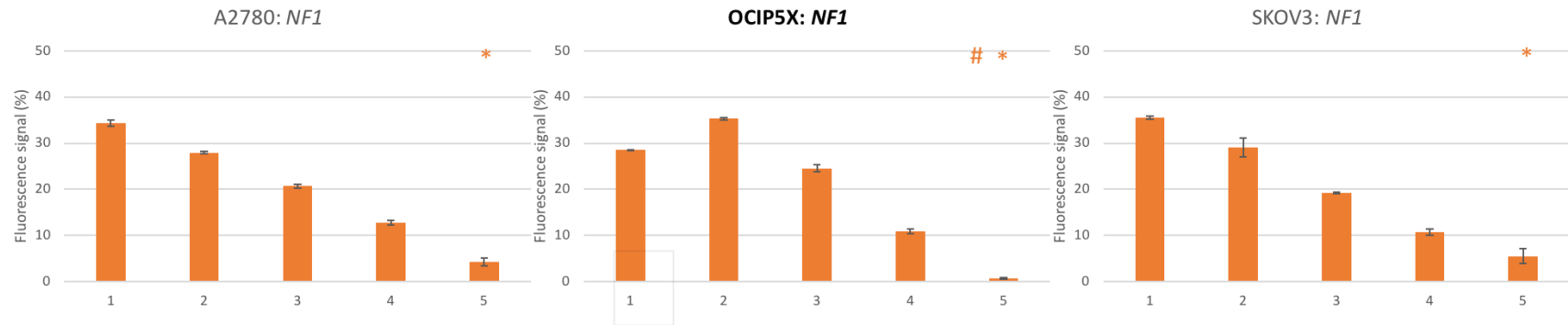


**Figure 4.4.8 Differences in gene positioning (*NF1*) between CS and CR ovarian cell lines.** Example of data obtained from *NF1* in all three cell lines. Graphs display percentage of fluorescence for the gene from the nuclear interior (1) to the nuclear periphery (5) within the three cell lines. Error bars represent the standard error of the mean. Statistically significant findings  $p < 0.05$  \* non-random organization. # difference in gene positioning between CR and CS cell line

### 4.3.3 Copy number changes in chemoresistant and chemosensitive cell lines.

The use of FISH also allowed verification of the copy number of each of the 17 investigated genes in each of the three investigated cell lines (Figure 4.4.6). The average copy number observed in each gene is presented in (Figure 4.4.7 to Figure 4.4.9). In the normal situation, it would be expected that each cell would contain two (diploid) copies of each gene. This is largely the case for the CS cell line A2780 for all investigated genes (Figure 4.4.7). The other two cell lines had a more heterogeneous population in terms of copy number changes. The expected diploid copy number was observed for the following genes: *AKT3*, *BRCA1*, *BRCA2*, *BRAF*, *CTNNB1*, and *PTEN* in the CS cell line OCI-P5X, with *RBI*, and *NF1* displaying slightly less than the expected two signals. The remaining genes displayed greater than the expected signals (Figure 4.4.8 and Figure 4.4.9). However, the CR SKOV3 cell line exhibited significant copy number changes with the exception of *PTEN* and *TP53* (Figure 4.4.9). Statistical analysis was performed using GraphPad Prism. The copy number changes were analyzed using non-parametric t-tests (Mann Whitney) to compare the values between the groups. The results are represented as mean  $\pm$  SEM.

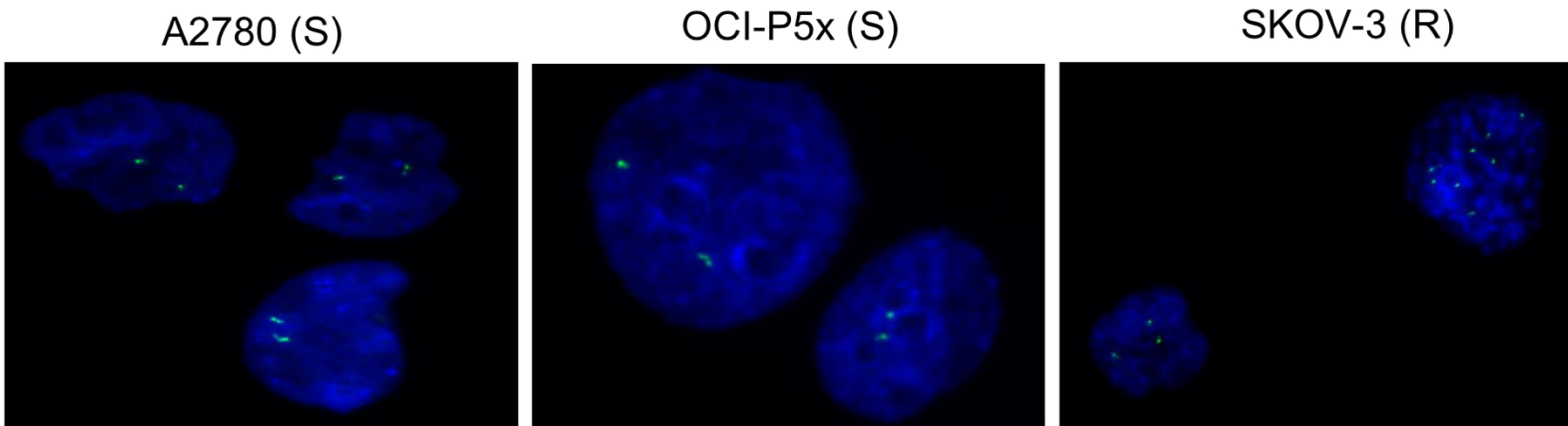


**Figure 4.4.9 The highest increase in copy number was observed in CR cell line SKOV-3.** Chemoresistant cell line shows abnormal numbers of copies of the *NF1* gene (green signals) compared to the chemosensitive cell lines. The expected diploid number in healthy cells is two copies. Up to 8 copies were found in the chemoresistant cells, SKOV-3. A minimum of 100 cells were captured and analyzed per gene per cell type. commercially available fluorescent probes that bind to DNA with a high degree of sequence complementarity to *NF1* only were used.

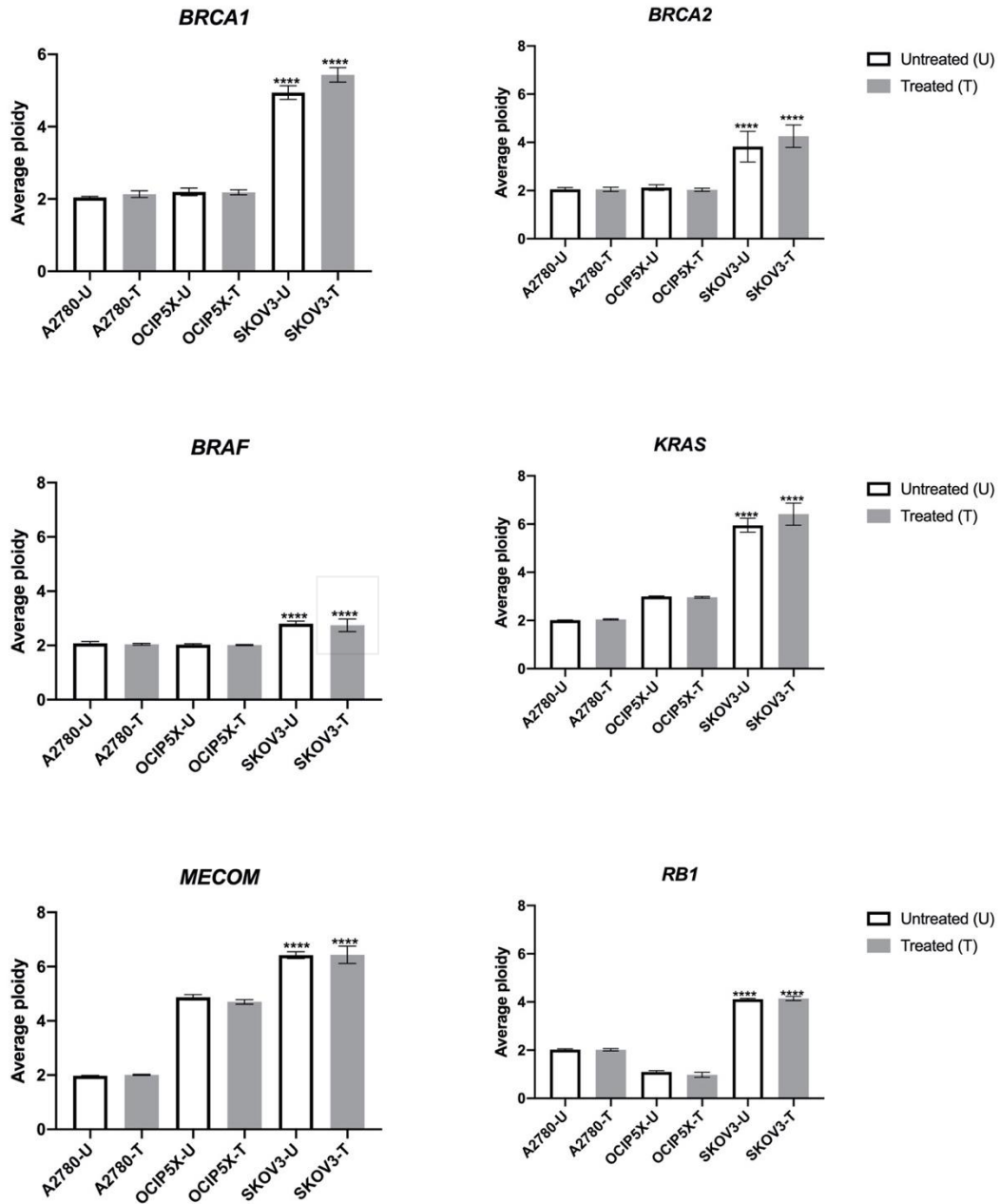


**Figure 4.4.10** There was a significantly increased copy number observed in CR cell line (SKOV3) compared to the CS (A2780 and OCIP5X). SKOV3 showed a higher average ploidy in *BRCA1*, *BRCA2*, *BRAF*, *KRAS*, *MECOM*, and *RB1*. A minimum of 100 cells were captured and analyzed per gene per cell type for every experiment. The copy number changes were analyzed using non-parametric t-tests (Mann Whitney) to compare the values between the groups. The results are represented as mean  $\pm$  SEM. \*\*\*\* P < 0.0001

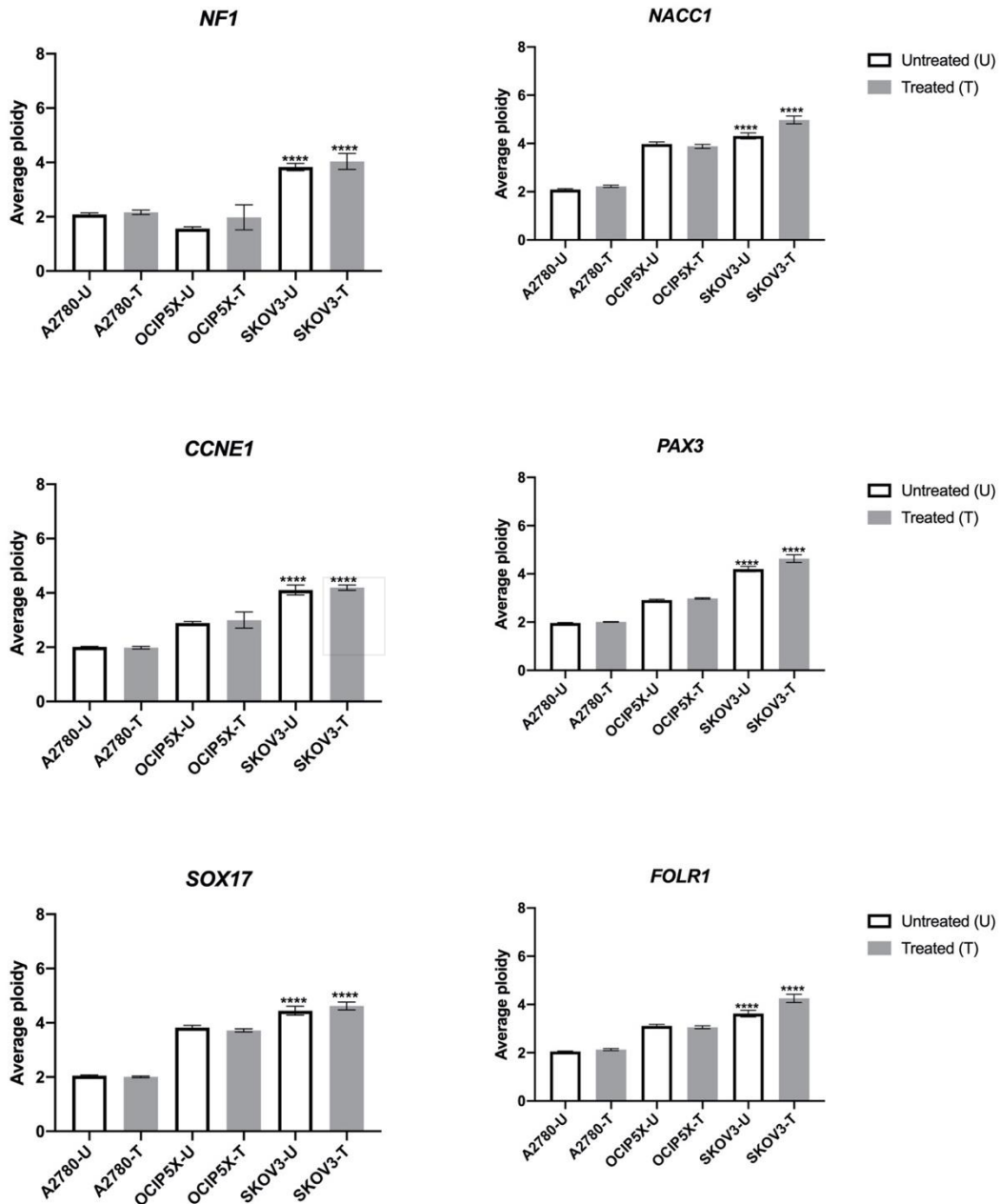


**Figure 4.4.11** There was a significantly increased copy number observed in CR cell line (SKOV3) compared to the CS (A2780 and OCIP5X). SKOV3 showed a higher average ploidy of *NF1*, *NACC1*, *CCNE1*, *PAX3*, *SOX17*, and *FOLR1*. A minimum of 100 cells were captured and analyzed per gene per cell type for every experiment. The copy number changes were analyzed using non-parametric t-tests (Mann Whitney) to compare the values between the groups. The results are represented as mean  $\pm$  SEM. \*\*\*\*  $P < 0.0001$

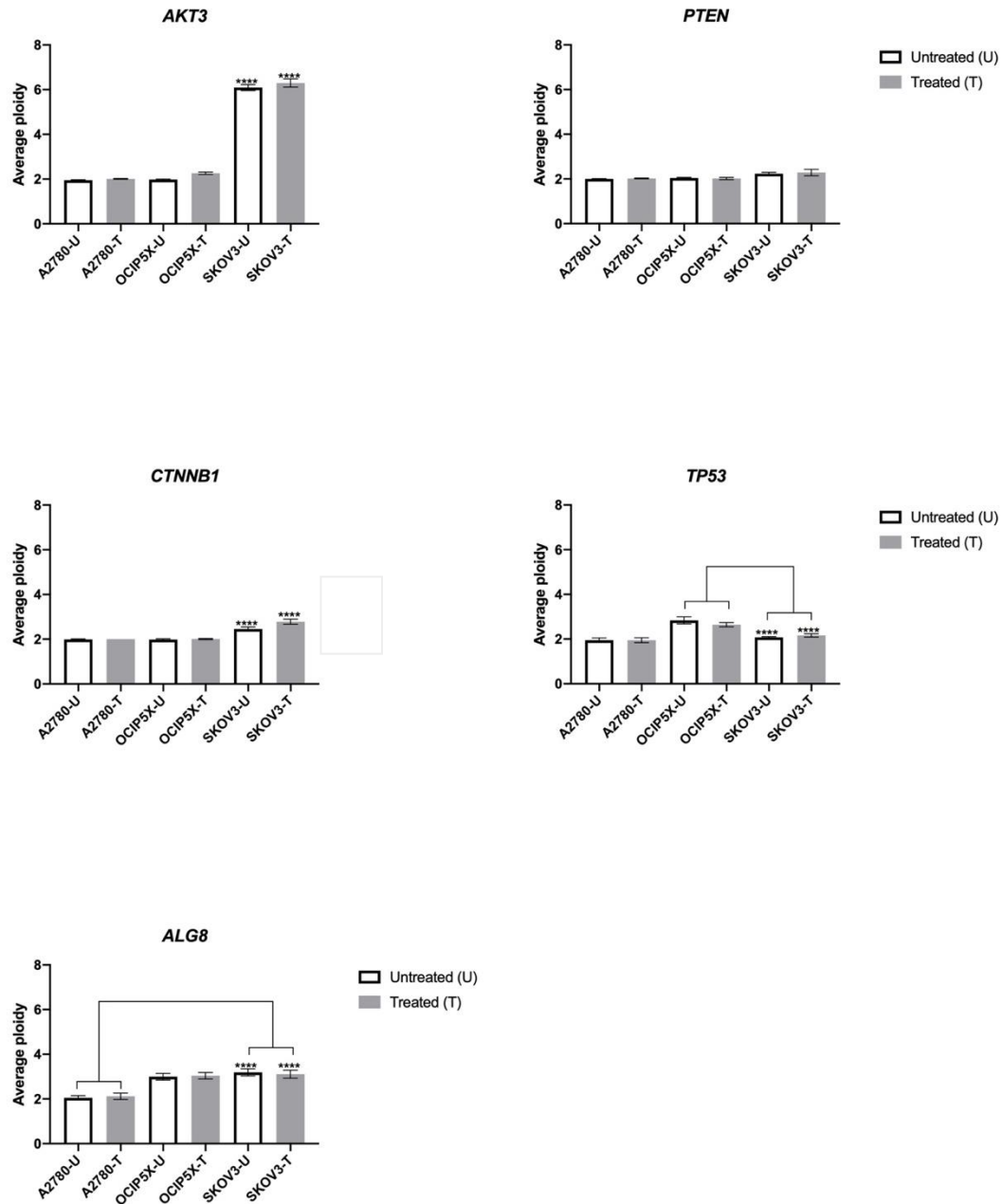


**Figure 4.4.12** There was a significantly increased copy number observed in CR cell line (SKOV3) compared to the CS (A2780 and OCIP5X). SKOV3 showed a higher average ploidy of *AKT3*, *PTEN*, and *CTNNB1*. There were no significant differences observed between SKOV3 and OCIP5X in *ALG8* and *TP53* genes. A minimum of 100 cells were captured and analyzed per gene per cell type for every experiment. The copy number changes were analyzed using non-parametric t-tests (Mann Whitney) to compare the values between the groups. The results are represented as mean  $\pm$  SEM. \*\*\*\* P < 0.0001

#### 4.0 Discussion

The aim of this study was to evaluate the nuclear organization of genes selected due to their involvement in cancer formation and progression. Seventeen genes were studied, and the nuclear position of these genes was evaluated in three ovarian cancer cell lines, two sensitive to cisplatin chemotherapy (A2780 and OCIP5X) and one chemoresistant (SKOV3). Additionally, the nuclear organization of the targeted genes was evaluated in the three cell lines following cisplatin treatment (treated) and without cisplatin treatment (control), to establish whether exposure to the chemotherapeutic agent was able to induce changes in the nuclear organization of the tested genes. The nuclear position was evaluated using a widely used approach that assesses the 2D radial distribution of FISH probes within the nucleus [186]. The chi-squared goodness-of-fit statistical analysis was utilized to examine differences in the radial distribution of the genes to determine whether genes were randomly or nonrandomly organized and whether there were significant differences in gene positioning between the different cell lines. Several genes showed nonrandom organization in all cell lines in the presence of absent of cisplatin treatment; *ALG8*, *BRCA1*, *BRCA2*, *CNNE1*, *FOLR1*, *NACCI*, *NF1*, and *TP53*. In terms of nonrandom versus random organization in the control (untreated) cell lines the A2780 cell line showed the highest number of genes to be randomly organized (7 out of 17; 41.18%), followed by OCI-P5X (4 out of 17; 23.53%) and SKOV3 (2/17; 11.76%). When comparing nonrandom versus random organization in the cisplatin treated cell lines, small changes were observed for a handful of genes in all cell lines. These changes included several genes that were nonrandomly organized in control cells becoming randomly organized following cisplatin treatment and vice versa. These results demonstrate that the majority of genes tested

display nonrandom organization, however the number of genes that were nonrandomly organized varied between cell lines. Moreover, evidence was provided to suggest that cisplatin treatment has the ability to potentially alter the gene positioning observed in control cell lines. Moreover, *AKT3*, and *BRAF* were found to be randomly organized in CS cell lines and nonrandomly organized in the CR cell line in both control and cisplatin treated cells, suggesting that the organization pattern of these genes may be useful to differentiate between CS and CR tumors. However, clearly more work is needed to confirm these findings.

To have better understanding about chemoresistance, the nuclear positioning of genes was compared to determine if any genes displayed a significant difference in gene positioning between CR (SKOV3) and CS cell lines. The gene *CNNE1* showed a significant difference in nuclear position in both CS cell lines A2780 and OCI-P5X compared to SKOV3. Additionally, two genes *FOLR1* and *NFI* showed a difference in organization between one of the CS cell lines and the CR SKOV3 cell line, specifically A2780 (*FOLR1*) and OCI-P5X (*NFI*). These results suggest that it may be possible to identify genes that occupy different positions in CS and CR cells for example *CNNE1* as shown in this study. These results provide pilot data that suggest it may be possible identify individual genes that could provide valuable diagnostic and prognostic information for patients with ovarian cancer, to determine whether their tumors are CS or CR. These findings need to be confirmed in future studies with additional cell lines, genes and patient tumor samples.

Interestingly, the chemoresistant cell line showed abnormal increases in copy number changes for many genes compared to the chemosensitive cell lines. Up to 8 copies of *NFI* were demonstrated, as shown Figure 4.4.6, while an average of two copies were found in

□ □ □

the chemosensitive cell lines. This finding of altered and increased copy number was also demonstrated for the majority of the seventeen genes, Figure 4.4.9. The expected diploid copy number was observed for the majority of the 17 investigated genes in the A2780 cell line, whereas the OCI-P5X cell line had a little more variation in the copy number of certain genes but significantly less than the CR SKOV3 cell line. Two genes, *ALG8* and *TP53* were not significantly different in SKOV3 and OCIP5X. This study provides evidence of non-random gene positioning in both sensitive and resistant ovarian cancer cell lines. The chemosensitive cells, A2780, was the most well controlled as it is almost perfectly diploid (Figure 4.4.9). Both of the CS cell lines were more likely to be diploid than the CR cell line, OCI-P5X averages to just above diploid.

These results suggest that for the investigated genes the SKOV3 CR cell line has significantly more accumulated mutations as measured by copy number changes compared to the CS cell lines.

Furthermore, the chemoresistant cell line has an abnormal increase in copy number, compared to A2780 or OCI-P5X, the two sensitive cell lines. Chromosome aneuploidy and copy number changes are consistently observed in most cancers [182,187,188]. It has been observed in different types of cancer the increasing aneuploidy and copy number changes, which could be associated with the chemoresistance [187]. These factors, increasing aneuploidy and copy number changes, were observed; however, further investigation required to approve the causation of the chemoresistance. It has been reported that copy number changes are often increased in aggressive tumors. [184, 189, 190, 191, 192].

There was a small decrease in the organization of genes in the cisplatin treated cell lines, as presented in Table 4.4.2. However, this could be as result of the duration of cisplatin

treatment; therefore, a time course would be one of the future directions of this study. Furthermore, future research should give repeated chemotherapy treatment to cells and continuously check the location to see if genes reorganize. Further investigations should use cancer cells with the similar characters of A2780, OCI-P5X, and SKOV3 to fully understand the real difference in response to the treatment. Therefore, A2780cis, the parent cisplatin-sensitive A2780 cell line, will be used to study the gene repositioning in the presence and absence of cisplatin. Importantly, this study will provide informative data that will help to provide a better understanding about cisplatin chemoresistance. These findings suggest that that it may be possible to utilize gene positioning as a novel diagnostic and prognostic tool in ovarian cancer that may be able to differentiate between CS and CR tumors. If future studies confirm and expand these findings, they may ultimately lead to better patient counseling and altered patient management which may lead to better patient outcomes.



## **CHAPTER 5**

### **CONCLUSION AND DIRECTIONS FOR FUTURE RESEARCH**

## **5.1 Conclusion**

This thesis aimed to investigate DNA damage and genomic organization in the cellular response to platinum chemotherapy in ovarian cancer cell lines. The outcomes from this thesis distinguished the DNA damage response and repair in chemoresistant and chemosensitive ovarian cell lines. The DNA crosslink formations were evaluated between the chemosensitive and chemoresistant cells following the cisplatin chemotherapy. Moreover, in this dissertation, the evaluation of gene positioning and copy number changes in chemosensitive and chemoresistant ovarian cancer cell lines were conducted. The outcome indicated differences in the nuclear position of potential genes between chemosensitive and chemoresistant. The results also demonstrated copy number changes, which tended to be abnormal in chemoresistant cells compared to the chemoresistant cell lines.

Consequently, this thesis's future directions will help to understand the chemoresistance in ovarian cancer cells better. However, further investigations are needed to distinguish the foundation of chemoresistance fully. There is a requirement to develop novel strategies for ovarian cancer treatment. Perhaps the most remarkable contributions to understanding this phenomenon at a cellular level are the development of various macromolecules, for example, DNA, messenger RNA, and proteins, to evaluate the response of ovarian cancer to chemotherapy.

## **5.2 Directions for future research**

By providing a foundation of cisplatin and the molecular basis of chemoresistance in ovarian cancer, further investigations are needed to understand better how ovarian cancer cells acquire chemoresistance. This dissertation's results are intended to open the way for

different strategies for further investigations of cisplatin and the molecular basis of chemoresistance. In this study, different approaches have been initiated and used to introduce the next phase of this project. There are three main directions to achieve: (1) Isolation and characterization of nuclear associated proteins in ovarian cancer cells and study their involvement in the chemoresistance. (2) Investigation of factors that can enhance the chemotherapy treatment's effectiveness, like 8-TrzdG and 8-TrzdA, which were reported to be beneficial [175] and [176]. (3) To identify regions of the genome in which preferential repair of, and/or resistance to DNA damage results in gene “drivers” of chemoresistance. Identifying the regions will help to find the critical genes to study the gene positioning in chemosensitive and chemoresistant ovarian cancer cell lines. The following procedures and data demonstrated the initial steps to investigate these three main directions (section 5.2.1, 5.2.2, and 5.2.3).

### **5.2.1 Isolation and characterization of nuclear associated proteins in the chemosensitive and chemoresistant cells.**

Further investigation was required to have a better understanding of the significant differences between the chemosensitive and the chemoresistant cells that were found in different cell-DNA substrates. Protein enzymatic digest analysis was used to study the role of proteins involved in chemoresistant and chemosensitive ovarian cell lines.

Pellet preparation was achieved by Jesenia Perez (Florida International University, Miami, FL, USA). Samples were delivered to the advanced mass spectrometry facility (Florida International University, Miami, FL, USA) as white protein pellets stored in plastic Eppendorf tubes. In-solution digestion was preformed utilizing the Thermo Scientific

digestion kit protocol number 89895, without reduction, alkylation, or guanidination of the proteins.

The protein enzymatic digest analysis demonstrated 522 of the total top protein found in the samples, as shown in Figure 5.5.1. There were 327 proteins shared between chemosensitive and chemoresistant cells. A total of 171 proteins were found in A2780, while 24 proteins were found in SKOV3. The names and functions of these proteins were described in Table 5.5.1, Table 5.5.2, and Table 5.5.3. Further investigations are required to examine the protein involvement in the acquired chemoresistance. This approach will be one of the main future directions in this study.





**Figure 5.5.1** Number of top proteins identified after mass spectrometry analysis in the chemosensitive and chemoresistant cells.

**Table 5.5.1 Proteins shared between A2780 and SKOV3 nucleoids**

<b>Accession #</b>	<b>Name</b>	<b>Location</b>	<b>Function</b>
P08670	Vimentin	nucleus, cytosol, ER, mitochondria	intermediate filaments; cytoskeleton
P41219	Peripherin	cytosol, ECM or secreted	intermediate filament (neuronal); cytoskeleton
P17661	Desmin	plasma membrane, nucleus	cytoskeleton
P60709	Actin	cytosol, nucleus	cytoskeleton
P07437	Tubulin	cytosol	cytoskeleton
P10809	Heat shock protein	mitochondria	mito protein import and macromol assembly; facilitates correct folding
P68104	Elongation factors	plasma membrane, nucleus	ribosome protein biosynthesis, transcription factor
P04406	Glyceraldehyde-3-phosphate dehydrogenase (GAPDH)	cytosol, nucleus	cytoskeleton, nuclear functions
P06576	ATP Synthase	mitochondria	ATP production
P23528	Cofilin	nucleus, plasma membrane, cytosol	cytoskeleton, regulation of morphology

**Table 5.5.2 Proteins were found only in A2780.**

<b>Accession #</b>	<b>Name</b>	<b>Location</b>	<b>Function</b>
Q32P51	Heterogenous nuclear ribonucleoprotein	nucleus	package pre-mRNA, transport poly(A) mRNA to cytoplasm, splice site selection
P19338	Nucleolin	nucleus	chromatin decondensation, transcriptional elongation
P48681	Nestin	cytosol	cytoskeleton disassemble vimentin intermediate filaments during mitosis
P05387	60S acidic ribosomal protein P2	cytosol, ECM	elongation step of protein synthesis.
P61978	Heterogeneous nuclear ribonucleoprotein K	nucleus	pre-mRNA binding proteins; p53 response; transcription activation and repression

**Table 5.5.3 Proteins were found only in SKOV3.**

<b>Accession #</b>	<b>Name</b>	<b>Location</b>	<b>Function</b>
P07355	Annexin A2	ECM	calcium-regulated membrane binding protein
P08729	Keratin, type II cytoskeletal 7	NA	stimulates DNA synthesis; involved in transcriptional regulation of HPV
Q6NZI2	Caveolae-associated protein 1	cytosol, ER, nucleus, mitochondrion	caveolae formation; caveolae biogenesis (required for secretions of protein)
P26038	Moesin	cytosol, plasma membrane	connects cytoskeleton to plasma membrane
Q8IVF2	Protein AHNAK2	nucleus	regulation of RNA splicing

### **5.2.2 Measuring cell toxicity of triazole-modified nucleosides and/or their enhancement with cisplatin efficiency in ovarian cell line**

Triazole-modified nucleosides (8-(1-H-1,2,3-triazol-4-yl)-2'-deoxyadenosine (8-TrzdA) and 8-(1-H-1,2,3-triazol-4-yl)-2'-deoxyguanosine (8-TrzdG)) are chemical compounds that have a fluorescent property. These compounds were obtained from Dr. Stanislaw F. Wnuk (Florida International University, Miami, FL, USA). Using these chemical compounds in the presence of cisplatin is reported to enhance the effectiveness of the chemotherapy treatment. Cell toxicity of triazole-modified nucleosides was measured. Their enhancement with cisplatin efficacy in ovarian cell lines was measured using CCK-8 (section 2.2.12.2). As Figure 5.5.2 shown, using increased concentrations of the 8-TrzdG showed no significant difference compared to the negative control. These findings illustrate that there was no cytotoxicity was observed using this chemical compound. However, following cisplatin treatment on the other cells group, an observed reduction was demonstrated with all concentrations. This reduction was not significantly different from cells, which were only treated with cisplatin, as shown in Figure 5.5.2. This result might support the fact that this chemical compound was not able to enter the cell or did not incorporate into DNA.

Therefore, it was important to use different methods to incorporate DNA and the chemical compound. A2780 cells were treated with the highest concentration of 8-TrzdG (204.8  $\mu\text{g/mL}$ ). DNA was then isolated and divided into two groups, genomic DNA and sonicated DNA. The reason for doing that is to demonstrate if treating cells with 8-TrzdG will increase the size of DNA when the samples run on the gel or not. As Figure 5.5.3 shown, there were no significant differences in the DNA size using gDNA and sonicated DNA in

both treated and untreated samples. This implies there was not enough evidence support that this chemical compound has incorporated into the DNA or not. Therefore, altered methods are required to investigate the presence of 8-TrzdG in DNA samples, like HPLC.



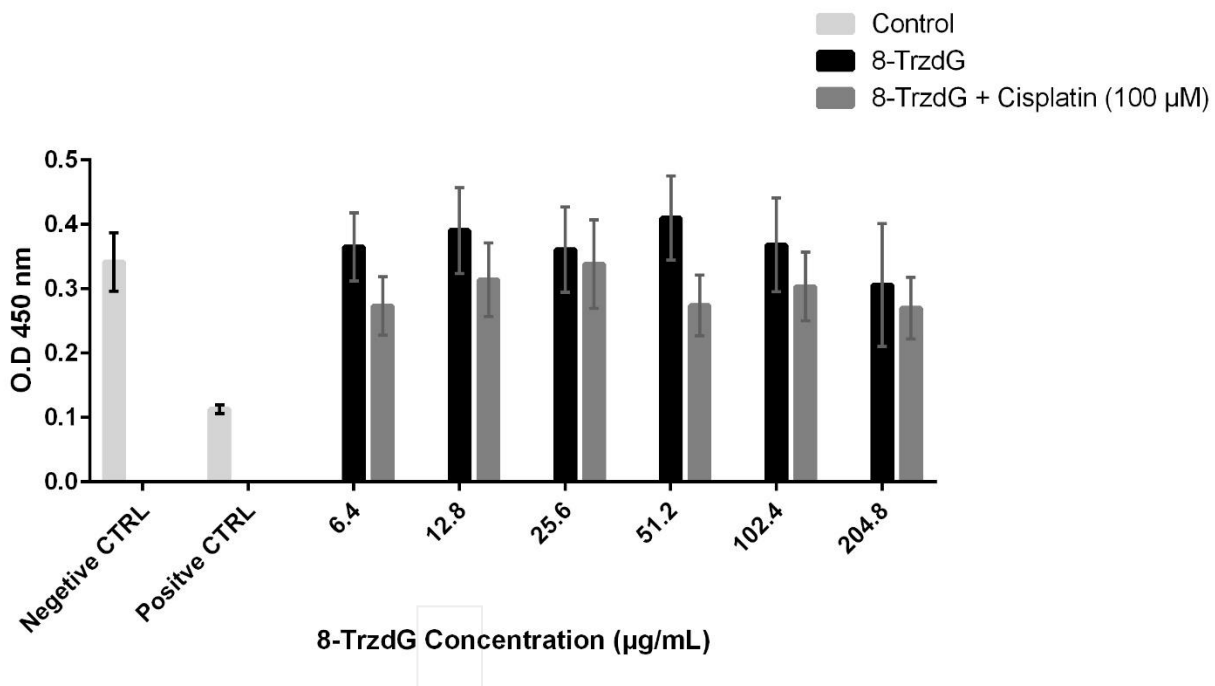


**Figure 5.5.2 Cell viability as measured by WST-8 assay using A2780 cells after 24 h of incubation with 8-TrzdG of different concentrations.** A group of cells were also treated with cisplatin (100 µM) for 1 h and placed after in drug-free media for 3 h. Negative control (no 8-TrzdG/ no cisplatin), while positive control cells were treated with high concentration of cisplatin (1 mM cisplatin), cells treated also with only cisplatin (100 µM) and were used as a control. Data were expressed as mean ± SEM. from three experiments.

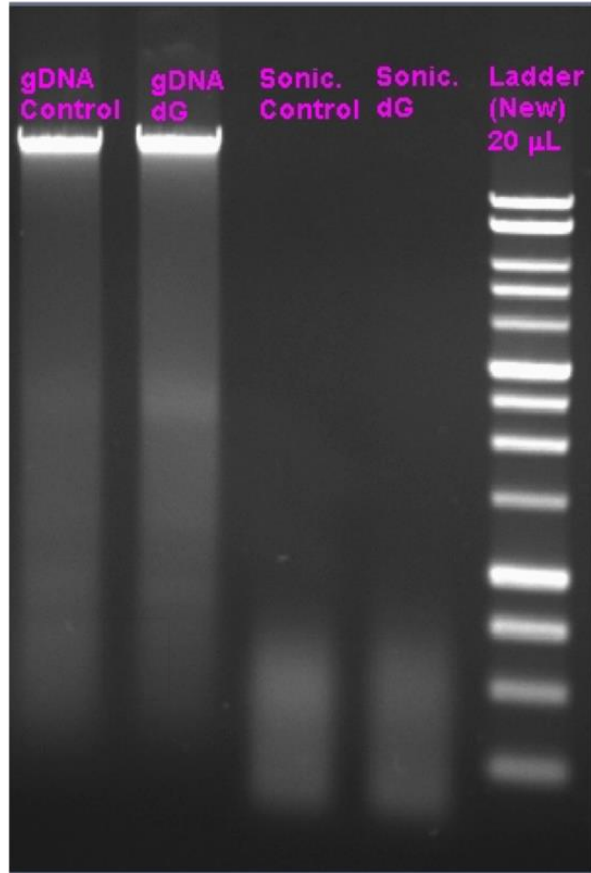


**Figure 5.5.3 Gel electrophoresis of A2780 cell line after the treatment of 8-TrzdG.** Cells were treated with 8-TrzdG (204.8  $\mu\text{g}/\text{mL}$ ) for 24 h, DNA was then isolated, and samples were fragmented using sonicator for different cycle (30 sec ON/Off). DNA samples were loaded in 1 % agarose gel. Ladder (Promega, 1 kb DNA Ladder Molecular, Fisher).

### **5.2.3 Examination changes in the DNA damage response with acquired chemoresistance**

To examine changes in the DNA damage response with acquired chemoresistance, the chemosensitive cell line, A2780, was used to develop A2780cis in our laboratory by chronic exposure of the parent cisplatin-sensitive A2780 cell line to increasing concentrations of cisplatin. After six months of the chronic exposure to increasing concentrations of cisplatin, cell viability assay (CCK8) was performed to measure the difference between A2780 and A2780cis (section 2.2.12.1). Briefly, Cells were seeded in a 96 well plate (5000 cells/well) and incubated overnight at 37 °C, 5% CO<sub>2</sub>. Cells were then treated with increasing concentrations of cisplatin (0.05, 0.1, 0.2, 0.4, 0.8 1.6, and 3.2 μM). After incubation for 24 h, CCK-8 mixture (10 μL) was added to every well and the plates were placed for 4 h at 37 °C, 5% CO<sub>2</sub>. The plate was read at 450 nm in a Biotech plate reader (Winooski, VT, USA). There was no significant difference observed between A2780 and A2780cis in all concentrations, (data not shown). This finding can be explained the need of A2780CIS for more chronic exposure of cisplatin in order to acquire chemoresistance. Therefore, we have obtained recently a commercial A2780cis (ECACC catalogue no. 93112517). As one of the future directions, it will be important to examine changes in the DNA damage response with acquired chemoresistance. This will play an essential role to have a better understanding of the DNA damage response with acquired chemoresistance.

#### **5.2.4 Optimization of sonication procedure and number of cycles**

As future directions also in this study, it will be essential to identify the genomic regions associated with DNA damage and repair in chemoresistant and chemosensitive ovarian cancer cells. This will require advance approaches like chromatin immunoprecipitation sequencing (chip-seq) and DNA immunoprecipitation sequencing. Using these approaches, DNA should be sheared into small fragments in the 100–300 bp range. Therefore, it was essential to optimize the sonication step prior performing the assay using ovarian cell lines. Briefly, cells were treated with 100  $\mu$ M of cisplatin for 1 h and then incubated in drug-free media for 12 h. DNA was then isolated, and samples were fragmented using different methods including Bioruptor Sonicator from Diagenode (Diagenode Inc., Sparta, NJ) (data not shown) dsDNA fragmentase from New England Biolabs (Beverly, MA, USA) ( data not shown), sonicator (probes) from Tekmar (Tekmar Model TM50, 50W) (Figure 5.5.4 and 5.5.5) and from Misonix (Misonix Model XL2000, 100W) (Figure 5.5.4). Depending on the type of the procedure, different cycles were used, between (8- 60 cycles) for 15 sec ON/Off. For the Bioruptor Sonicator, 30 sec ON/Off was used for every cycle. Afterwards, samples were loaded in 1.5 % agarose gel.

From all the procedures that been used (data not shown), the optimum sonicator system to shear the DNA for the ovarian cancer cell lines was the one from Tekmar (60 cycle, 15 sec ON/Off), which produced the desired 300 bp length, as shown in Figure 5.5.4. For the other procedures, DNA was smeared but was not at located at the desired size as showed with using the Bioruptor Sonicator from Diagenode. Same was observed with using the enzymatic way using dsDNA fragmentase from New England Biolabs. Using sonicator (probes) from Misonix was the closet procedure to have DNA sheared at the desired size

but was not showing clear bands at the desired size (300 bp) comparing to the sonicator (probes) from Tekmar.



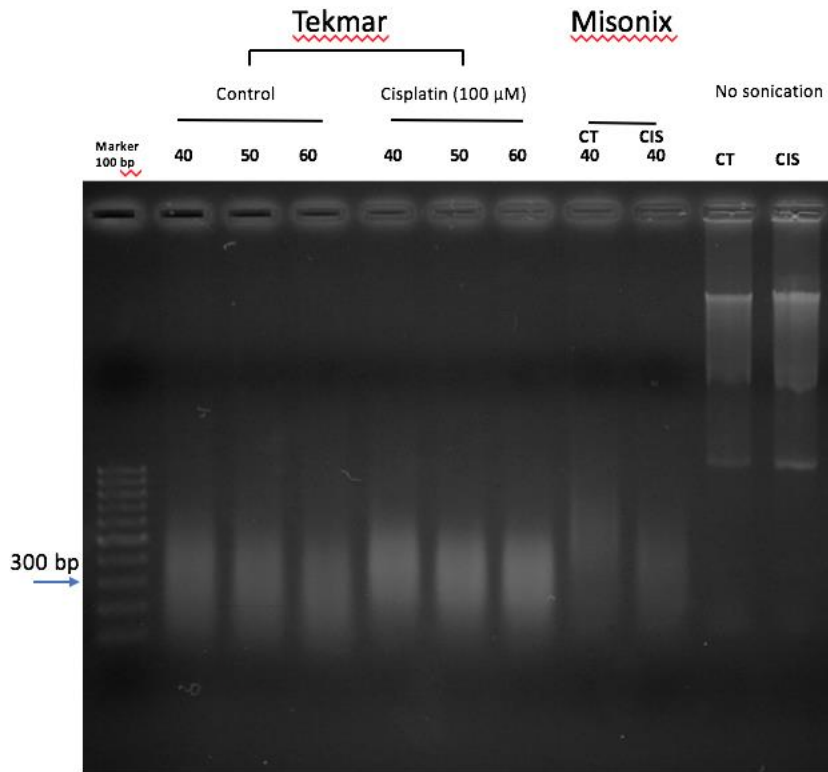


**Figure 5.5.4 DNA sonication of SKOV-3 using a sonicator (Probes).** Cells were treated with 100  $\mu\text{M}$  of cisplatin for 1 h and then incubated in drug-free media for 12 h. DNA was then isolated, and samples were fragmented using sonicator (probes) for different cycle (15 sec ON/Off). DNA samples were loaded in 1.5 % agarose gel. Data analysis was then performed using ImageJ Software. Bands intensity were measured around 500-200 bp. Two probe sonicators were used (Tekmar Model TM50, 50W) and (Misonix Model XL2000, 100W)

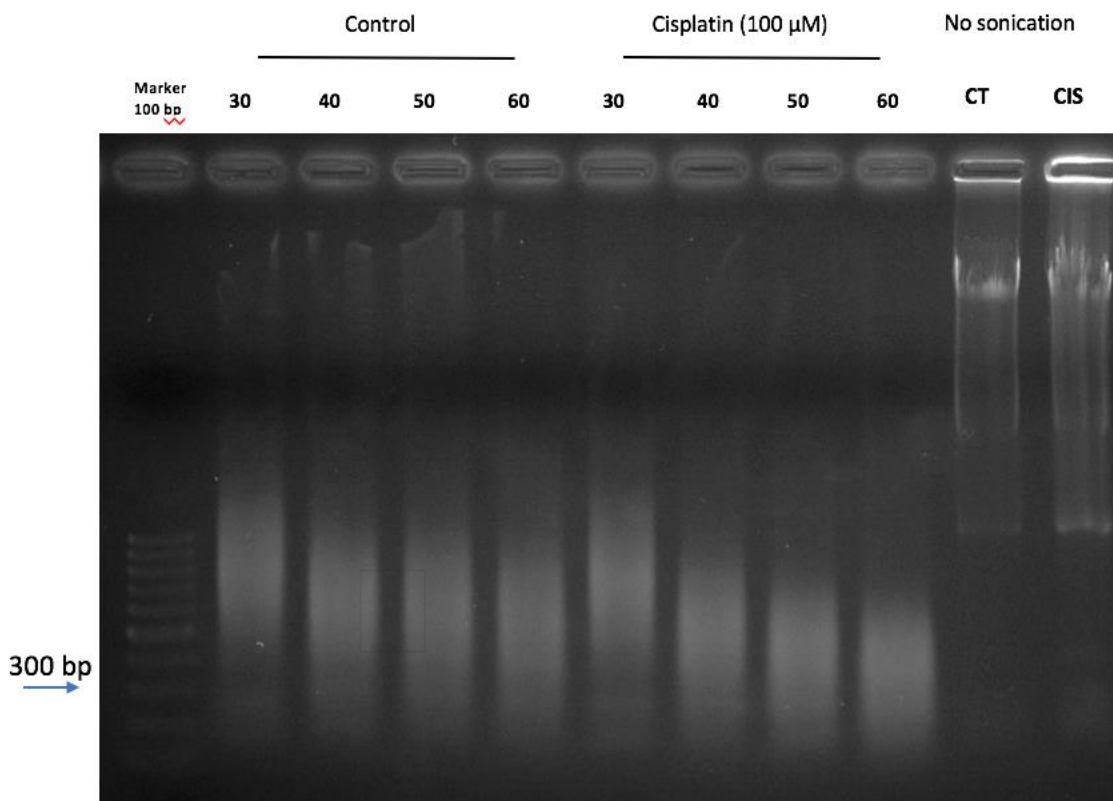


**Figure 5.5.5 DNA sonication of SKOV-3 using a sonicator (Probes).** Cells were treated with 100  $\mu$ M of cisplatin for 1 h and then incubated in drug-free media for 12 h. DNA was then isolated, and samples were fragmented using sonicator (probes) for different cycle (15 sec ON/Off). DNA samples were loaded in 1.5 % agarose gel. Data analysis was then performed using ImageJ Software. Bands intensity were measured around 500-300 bp. Sonicator by Tekmark was used (Tekmar Model TM50, 50W).

## REFERENCES

1. Siegel, R. L., Miller, K. D., & Jemal, A. (2015). Cancer statistics, 2015. *CA: A Cancer Journal for Clinicians*, *65*(1), 5–29. <https://doi.org/10.3322/caac.21254>
2. Reed, E., Ozols, R. F., Tarone, R., Yuspa, S. H., & Poirier, M. C. (1987). Platinum-DNA adducts in leukocyte DNA correlate with disease response in ovarian cancer patients receiving platinum-based chemotherapy. *Proceedings of the National Academy of Sciences of the United States of America*, *84*(14), 5024–5028. <https://doi.org/10.1073/pnas.84.14.5024>
3. Bristow, R. E., Tomacruz, R. S., Armstrong, D. K., Trimble, E. L., & Montz, F. J. (2002). Survival effect of maximal cytoreductive surgery for advanced ovarian carcinoma during the platinum era: A meta-analysis. *Journal of Clinical Oncology*, *20*(5), 1248–1259. <https://doi.org/10.1200/JCO.20.5.1248>
4. Muggia, F. M., Braly, P. S., Brady, M. F., Sutton, G., Niemann, T. H., Lentz, S. L., ... Small, J. M. (2000). Phase III randomized study of cisplatin versus paclitaxel versus cisplatin and paclitaxel in patients with suboptimal stage III or IV ovarian cancer: A Gynecologic Oncology Group study. *Journal of Clinical Oncology*, *18*(1), 106–115. <https://doi.org/10.1200/jco.2000.18.1.106>
5. Ozols, R. F., Bundy, B. N., Greer, B. E., Fowler, J. M., Clarke-Pearson, D., Burger, R. A., ... Mackey, D. (2003). Phase III trial of carboplatin and paclitaxel compared with cisplatin and paclitaxel in patients with optimally resected stage III ovarian cancer: A Gynecologic Oncology Group study. *Journal of Clinical Oncology*, *21*(17), 3194–3200. <https://doi.org/10.1200/JCO.2003.02.153>
6. Thigpen, J. T., Vance, R. B., & Khansur, T. (1993). Second-line chemotherapy for recurrent carcinoma of the ovary. *Cancer*, *71*(4 S), 1559–1564. <https://doi.org/10.1002/cncr.2820710422>
7. Du Bois, A., Quinn, M., Thigpen, T., Vermorken, J., Avall-Lundqvist, E., Bookman, M., ... Wagner, U. (2005). 2004 consensus statements on the management of ovarian cancer: Final document of the 3rd International Gynecologic Cancer Intergroup Ovarian Cancer Consensus Conference (GCIIG OCCC 2004). *Annals of Oncology*, *16*(SUPPL. 8). <https://doi.org/10.1093/annonc/mdi961>

8. American Cancer Society. (2019). American Cancer Society. Facts & Figures 2019. In *American Cancer Society*. Retrieved from <https://www.cancer.org/content/dam/cancer-org/research/cancer-facts-and-statistics/annual-cancer-facts-and-figures/2019/cancer-facts-and-figures-2019.pdf>
9. Foley, O. W., Rauh-Hain, J. A., & del Carmen, M. G. (2013). Recurrent epithelial ovarian cancer: an update on treatment. *Oncology (Williston Park, N.Y.)*, 27(4), 288–298.
10. Howell, S. B. (Ed.). (1991). *Platinum and Other Metal Coordination Compounds in Cancer Chemotherapy* (Vol. 1). Springer Science & Business Media. <https://doi.org/10.1007/978-1-4899-0738-7>
11. Mandic, A., Hansson, J., Linder, S., & Shoshan, M. C. (2003). Cisplatin induces endoplasmic reticulum stress and nucleus-independent apoptotic signaling. *Journal of Biological Chemistry*, 278(11), 9100–9106. <https://doi.org/10.1074/jbc.M210284200>
12. Zamble, D. B., & Lippard, S. J. (1995). Cisplatin and DNA repair in cancer chemotherapy. *Trends in Biochemical Sciences*, 20(10), 435–439. [https://doi.org/10.1016/S0968-0004\(00\)89095-7](https://doi.org/10.1016/S0968-0004(00)89095-7)
13. Vitale, I., Galluzzi, L., Castedo, M., & Kroemer, G. (2011). Mitotic catastrophe: a mechanism for avoiding genomic instability. *Nature Reviews. Molecular Cell Biology*, 12(6), 385–392. <https://doi.org/10.1038/nrm3115>
14. Chaney, S. G., & Sancar, A. (1996). DNA repair: Enzymatic mechanisms and relevance to drug response. *Journal of the National Cancer Institute*, 88(19), 1346–1360. <https://doi.org/10.1093/jnci/88.19.1346>
15. Vermorken, J. B., Ten Bokkel Huinink, W. W., Eisenhauer, E. A., Favalli, G., Belpomme, D., Conte, P. F., & Kaye, S. B. (1993). Carboplatin versus cisplatin. *Annals of Oncology*, 4(SUPPL. 4). [https://doi.org/10.1093/annonc/4.suppl\\_4.S41](https://doi.org/10.1093/annonc/4.suppl_4.S41)
16. Cobo, M., Isla, D., Massuti, B., Montes, A., Sanchez, J. M., Provencio, M., ... Rosell, R. (2007). Customizing cisplatin based on quantitative excision repair cross-complementing 1 mRNA expression: A phase III trial in non-small-cell lung cancer. *Journal of Clinical Oncology*, 25(19), 2747–2754. <https://doi.org/10.1200/JCO.2006.09.7915>
17. Fraser, M., Leung, B., Jahani-Asl, A., Yan, X., Thompson, W. E., & Tsang, B. K. (2003). Chemoresistance in human ovarian cancer: The role of apoptotic regulators. *Reproductive Biology and Endocrinology*, Vol. 1. <https://doi.org/10.1186/1477-7827-1-66>

- □ □
18. Holzer, A. K., Manorek, G. H., & Howell, S. B. (2006). Contribution of the major copper influx transporter CTR1 to the cellular accumulation of cisplatin, carboplatin, and oxaliplatin. *Molecular Pharmacology*, *70*(4), 1390–1394. <https://doi.org/10.1124/mol.106.022624>
  19. Song, I. S., Savaraj, N., Siddik, Z. H., Liu, P., Wei, Y., Wu, C. J., & Kuo, M. T. (2004). Role of human copper transporter Ctr1 in the transport of platinum-based antitumor agents in cisplatin-sensitive and cisplatin-resistant cells. *Molecular Cancer Therapeutics*, *3*(12), 1543–1549.
  20. Kelland L. (2007). The resurgence of platinum-based cancer chemotherapy. *Nature reviews. Cancer*, *7*(8), 573–584. <https://doi.org/10.1038/nrc2167>
  21. Sakamoto, M., Kondo, A., Kawasaki, K., Goto, T., Sakamoto, H., Miyake, K., ... Tenjin, Y. (2001). Analysis of gene expression profiles associated with cisplatin resistance in human ovarian cancer cell lines and tissues using cDNA microarray. *Human Cell : Official Journal of Human Cell Research Society*, *14*(4), 305–315.
  22. Li, M., Balch, C., Montgomery, J. S., Jeong, M., Chung, J. H., Yan, P., ... Nephew, K. P. (2009). Integrated analysis of DNA methylation and gene expression reveals specific signaling pathways associated with platinum resistance in ovarian cancer. *BMC Medical Genomics*, *2*. <https://doi.org/10.1186/1755-8794-2-34>
  23. Reed, E. (1998). Platinum-DNA adduct, nucleotide excision repair and platinum based anti-cancer chemotherapy. *Cancer Treatment Reviews*, *24*(5), 331–344. [https://doi.org/10.1016/S0305-7372\(98\)90056-1](https://doi.org/10.1016/S0305-7372(98)90056-1)
  24. Martin, L. P., Hamilton, T. C., & Schilder, R. J. (2008). Platinum resistance: the role of DNA repair pathways. *Clinical cancer research*, *14*(5), 1291-1295. <https://doi.org/10.1158/1078-0432.CCR-07-2238>
  25. Deans, A. J., & West, S. C. (2011). DNA interstrand crosslink repair and cancer. *Nature reviews cancer*, *11*(7), 467-480. <https://doi.org/10.1038/nrc3088>
  26. Spivak, G. (2015). Nucleotide excision repair in humans. *DNA repair*, *36*, 13-18. <https://doi.org/10.1016/j.dnarep.2015.09.003>
  27. Arora, S., Kothandapani, A., Tillison, K., Kalman-Maltese, V., & Patrick, S. M. (2010). Downregulation of XPF-ERCC1 enhances cisplatin efficacy in cancer cells. *DNA Repair*, *9*(7), 745–753. <https://doi.org/10.1016/j.dnarep.2010.03.010>

- □ □
28. Furuta, T., Ueda, T., Aune, G., Sarasin, A., Kraemer, K. H., & Pommier, Y. (2002). Transcription-coupled nucleotide excision repair as a determinant of cisplatin sensitivity of human cells. *Cancer Research*, *62*(17), 4899–4902
  29. Ferry, K. V., Hamilton, T. C., & Johnson, S. W. (2000). Increased nucleotide excision repair in cisplatin-resistant ovarian cancer cells: Role of ERCC1-XPF. *Biochemical Pharmacology*, *60*(9), 1305–1313. [https://doi.org/10.1016/S0006-2952\(00\)00441-X](https://doi.org/10.1016/S0006-2952(00)00441-X)
  30. Takahara, P. M., Rosenzweig, A. C., Frederick, C. A., & Lippard, S. J. (1995). Crystal structure of double-stranded DNA containing the major adduct of the anticancer drug cisplatin. *Nature*, *377*(6550), 649–652. <https://doi.org/10.1038/377649a0>
  31. Bessho, T., Sancar, A., Thompson, L. H., & Thelen, M. P. (1997). Reconstitution of human excision nuclease with recombinant XPF-ERCC1 complex. *Journal of Biological Chemistry*, *272*(6), 3833–3837. <https://doi.org/10.1074/jbc.272.6.3833>
  32. Niedernhofer, L. J., Odijk, H., Budzowska, M., van Drunen, E., Maas, A., Theil, A. F., ... Kanaar, R. (2004). The Structure-Specific Endonuclease Ercc1-Xpf Is Required To Resolve DNA Interstrand Cross-Link-Induced Double-Strand Breaks. *Molecular and Cellular Biology*, *24*(13), 5776–5787. <https://doi.org/10.1128/mcb.24.13.5776-5787.2004>
  33. McKay, B. C., Becerril, C., & Ljungman, M. (2001). P53 plays a protective role against UV- and cisplatin-induced apoptosis in transcription-coupled repair proficient fibroblasts. *Oncogene*, *20*(46), 6805–6808. <https://doi.org/10.1038/sj.onc.1204901>
  34. Welsh, C., Day, R., McGurk, C., Masters, J. R. W., Wood, R. D., & Köberle, B. (2004). Reduced levels of XPA, ERCC1 and XPF DNA repair proteins in testis tumor cell lines. *International Journal of Cancer*, *110*(3), 352–361. <https://doi.org/10.1002/ijc.20134>
  35. Köberle, B., Masters, J. R. W., Hartley, J. A., & Wood, R. D. (1999). Defective repair of cisplatin-induced DNA damage caused by reduced XPA protein in testicular germ cell tumours. *Current Biology*, *9*(5), 273–278. [https://doi.org/10.1016/S0960-9822\(99\)80118-3](https://doi.org/10.1016/S0960-9822(99)80118-3)
  36. Wu, X., Fan, W., Xu, S., & Zhou, Y. (2003). Sensitization to the Cytotoxicity of Cisplatin by Transfection with Nucleotide Excision Repair Gene Xeroderma Pigmentosum Group A Antisense RNA in Human Lung Adenocarcinoma Cells. *Clinical Cancer Research*, *9*(16 I), 5874–5879.

- □ □
37. Chen, H. Y., Shao, C. J., Chen, F. R., Kwan, A. L., & Chen, Z. P. (2010). Role of ERCCI promoter hypermethylation in drug resistance to cisplatin in human gliomas. *International Journal of Cancer*, 126(8), 1944–1954. <https://doi.org/10.1002/ijc.24772>
  38. Orelli, B., McClendon, T. B., Tsodikov, O. V., Ellenberger, T., Niedernhofer, L. J., & Schärer, O. D. (2010). The XPA-binding domain of ERCC1 is required for nucleotide excision repair but not other DNA repair pathways. *Journal of Biological Chemistry*, 285(6), 3705–3712. <https://doi.org/10.1074/jbc.M109.067538>
  39. Kunkel, T. A., & Erie, D. A. (2005). DNA mismatch repair. *Annu. Rev. Biochem.*, 74, 681-710. <https://doi.org/10.1146/annurev.biochem.74.082803.133243>
  40. Jascur, T., & Boland, C. R. (2006). Structure and function of the components of the human DNA mismatch repair system. *International Journal of Cancer*, 119(9), 2030-2035. <https://doi.org/10.1002/ijc.22023>
  41. Peltomäki, P. (2001). DNA mismatch repair and cancer. *Mutation Research/Reviews in Mutation Research*, 488(1), 77-85. [https://doi.org/10.1016/S1383-5742\(00\)00058-2](https://doi.org/10.1016/S1383-5742(00)00058-2)
  42. Peltomaki, P. (2003). Role of DNA mismatch repair defects in the pathogenesis of human cancer. *Journal of clinical oncology*, 21(6), 1174-1179. <https://doi.org/10.1200/JCO.2003.04.060>
  43. Esteller, M. (2000). Epigenetic lesions causing genetic lesions in human cancer: promoter hypermethylation of DNA repair genes. *European journal of cancer*, 36(18), 2294-2300. [https://doi.org/10.1016/S0959-8049\(00\)00303-8](https://doi.org/10.1016/S0959-8049(00)00303-8)
  44. Suzuki, H., Itoh, F., Toyota, M., Kikuchi, T., Kakiuchi, H., Hinoda, Y., & Imai, K. (1999). Distinct methylation pattern and microsatellite instability in sporadic gastric cancer. *International Journal of Cancer*, 83(3), 309–313. [https://doi.org/10.1002/\(SICI\)1097-0215\(19991029\)83:3<309::AID-IJC4>3.0.CO;2-Z](https://doi.org/10.1002/(SICI)1097-0215(19991029)83:3<309::AID-IJC4>3.0.CO;2-Z)
  45. Rhyu, M. S. (1996). Molecular mechanisms underlying hereditary nonpolyposis colorectal carcinoma. *JNCI: Journal of the National Cancer Institute*, 88(5), 240-251. <https://doi.org/10.1093/jnci/88.5.240>
  46. Strathdee, G., MacKean, M. J., Illand, M., & Brown, R. (1999). A role for methylation of the hMLH1 promoter in loss of hMLH1 expression and drug resistance in ovarian cancer. *Oncogene*, 18(14), 2335–2341. <https://doi.org/10.1038/sj.onc.1202540>

47. Geisler, J. P., Goodheart, M. J., Sood, A. K., Holmes, R. J., Hatterman-Zogg, M. A., & Buller, R. E. (2003). Mismatch Repair Gene Expression Defects Contribute to Microsatellite Instability in Ovarian Carcinoma. *Cancer*, 98(10), 2199–2206. <https://doi.org/10.1002/cncr.11770>
48. Bignami, M., Casorelli, I., & Karran, P. (2003). Mismatch repair and response to DNA-damaging antitumour therapies. *European Journal of Cancer*, 39(15), 2142–2149. [https://doi.org/10.1016/S0959-8049\(03\)00569-0](https://doi.org/10.1016/S0959-8049(03)00569-0)
49. Topping, R. P., Wilkinson, J. C., & Scarpinato, D. (2009). Mismatch repair protein deficiency compromises cisplatin-induced apoptotic signaling. *Journal of Biological Chemistry*, 284(21), 14029–14039. <https://doi.org/10.1074/jbc.M809303200>
50. Ding, X., Mohd, A. B., Huang, Z., Baba, T., Bernardini, M. Q., Lyerly, H. K., ... Devi, G. R. (2009). MLH1 expression sensitises ovarian cancer cells to cell death mediated by XIAP inhibition. *British Journal of Cancer*, 101(2), 269–277. <https://doi.org/10.1038/sj.bjc.6605180>
51. Fink, D., Aebi, S., & Howell, S. B. (1998). The role of DNA mismatch repair in drug resistance. *Clinical Cancer Research*, 4(1), 1-6.
52. Drummond, J. T., Anthony, A., Brown, R., & Modrich, P. (1996). Cisplatin and adriamycin resistance are associated with MutL $\alpha$  and mismatch repair deficiency in an ovarian tumor cell line. *Journal of Biological Chemistry*, 271(33), 19645–19648. <https://doi.org/10.1074/jbc.271.33.19645>
53. Brown, R., Hirst, G. L., Gallagher, W. M., McIlwrath, A. J., Margison, G. P., Van Der Zee, A. G. J., & Anthony, D. A. (1997). hMLH1 expression and cellular responses of ovarian tumour cells to treatment with cytotoxic anticancer agents. *Oncogene*, 15(1), 45–52. <https://doi.org/10.1038/sj.onc.1201167>
54. Galluzzi, L., Vitale, I., Michels, J., Brenner, C., Szabadkai, G., Harel-Bellan, A., ... & Kroemer, G. (2013). Systems biology of cisplatin resistance: past, present and future. *Cell Death Dis.* 2014; 5: e1257. <https://doi.org/10.1038/cddis.2013.428>
55. Vaisman, A., Varchenko, M., Umar, A., Kunkel, T. A., Risinger, J. I., Barrett, J. C., ... Chaney, S. G. (1998). The role of hMLH1, hMSH3, and hMSH6 defects in cisplatin and oxaliplatin resistance: Correlation with replicative bypass of platinum-DNA adducts. *Cancer Research*, 58(16), 3579–3585.

- □ □
56. Her, J., & Bunting, S. F. (2018). How cells ensure correct repair of DNA double-strand breaks. *Journal of Biological Chemistry*, 293(27), 10502-10511. <https://doi.org/10.1074/jbc.TM118.000371>
  57. Wright, W. D., Shah, S. S., & Heyer, W. D. (2018). Homologous recombination and the repair of DNA double-strand breaks. *Journal of Biological Chemistry*, 293(27), 10524-10535.
  58. Jasin, M., & Rothstein, R. (2013). Repair of strand breaks by homologous recombination. *Cold Spring Harbor Perspectives in Biology*, 5(11). <https://doi.org/10.1101/cshperspect.a012740>
  59. Sakai, W., Swisher, E. M., Jacquemont, C., Chandramohan, K. V., Couch, F. J., Langdon, S. P., ... Taniguchi, T. (2009). Functional restoration of BRCA2 protein by secondary BRCA2 mutations in BRCA2-mutated ovarian carcinoma. *Cancer Research*, 69(16), 6381–6386. <https://doi.org/10.1158/0008-5472.CAN-09-1178>
  60. Moynahan, M. E., Pierce, A. J., & Jasin, M. (2001). BRCA2 is required for homology-directed repair of chromosomal breaks. *Molecular Cell*, 7(2), 263–272. [https://doi.org/10.1016/S1097-2765\(01\)00174-5](https://doi.org/10.1016/S1097-2765(01)00174-5)
  61. Chetrit, A., Hirsh-Yechezkel, G., Ben-David, Y., Lubin, F., Friedman, E., & Sadetzki, S. (2008). Effect of BRCA1/2 mutations on long-term survival of patients with invasive ovarian cancer: The National Israeli Study of Ovarian Cancer. *Journal of Clinical Oncology*, 26(1), 20–25. <https://doi.org/10.1200/JCO.2007.11.6905>
  62. De Picciotto, N., Cacheux, W., Roth, A., Chappuis, P. O., & Labidi-Galy, S. I. (2016). Ovarian cancer: status of homologous recombination pathway as a predictor of drug response. *Critical Reviews in Oncology/Hematology*, 101, 50-59. <https://doi.org/10.1016/j.critrevonc.2016.02.014>
  63. Liu, G., Yang, D., Sun, Y., Shmulevich, I., Xue, F., Sood, A. K., & Zhang, W. (2012). Differing clinical impact of BRCA1 and BRCA2 mutations in serous ovarian cancer. *Pharmacogenomics*, 13(13), 1523-1535. <https://doi.org/10.2217/pgs.12.137>
  64. Lees-Miller, S. P., & Meek, K. (2003). Repair of DNA double strand breaks by non-homologous end joining. *Biochimie*, 85(11), 1161-1173. <https://doi.org/10.1016/j.biochi.2003.10.011>

65. Buscemi, G., Savio, C., Zannini, L., Miccichè, F., Masnada, D., Nakanishi, M., ... Delia, D. (2001). Chk2 Activation Dependence on Nbs1 after DNA Damage. *Molecular and Cellular Biology*, 21(15), 5214–5222. <https://doi.org/10.1128/mcb.21.15.5214-5222.2001>
66. Meek, K., Gupta, S., Ramsden, D. A., & Lees-Miller, S. P. (2004). The DNA-dependent protein kinase: the director at the end. *Immunological reviews*, 200(1), 132-141. <https://doi.org/10.1111/j.0105-2896.2004.00162.x>
67. Boeckman, H. J., Trego, K. S., & Turchi, J. J. (2005). Cisplatin sensitizes cancer cells to ionizing radiation via inhibition of nonhomologous end joining. *Molecular Cancer Research*, 3(5), 277–285. <https://doi.org/10.1158/1541-7786.MCR-04-0032>
68. Sand-Dejmek, J., Adelmant, G., Sobhian, B., Calkins, A. S., Marto, J., Iglehart, D. J., & Lazaro, J. B. (2011). Concordant and opposite roles of DNA-PK and the “facilitator of chromatin transcription” (FACT) in DNA repair, apoptosis and necrosis after cisplatin. *Molecular Cancer*, 10. <https://doi.org/10.1186/1476-4598-10-74>
69. Wang, L. C., & Gautier, J. (2010). The Fanconi anemia pathway and ICL repair: implications for cancer therapy. *Critical reviews in biochemistry and molecular biology*, 45(5), 424-439. <https://doi.org/10.3109/10409238.2010.502166>
70. Taylor, S. J., Arends, M. J., & Langdon, S. P. (2020). Inhibitors of the Fanconi anaemia pathway as potential antitumour agents for ovarian cancer. *Exploration of Targeted Anti-Tumor Therapy*, 1(1), 26–52. <https://doi.org/10.37349/etat.2020.00003>
71. Nalepa, G., & Clapp, D. W. (2018). Fanconi anaemia and cancer: an intricate relationship. *Nature Reviews Cancer*, 18(3), 168. <https://doi.org/10.1038/nrc.2017.116>
72. Krokan, H. E., Standal, R., & Slupphaug, G. (1997). DNA glycosylases in the base excision repair of DNA. *Biochemical Journal*, 325(1), 1-16. <https://doi.org/10.1042/bj3250001>
73. Wilson, D. M., & Seidman, M. M. (2010). A novel link to base excision repair? *Trends in Biochemical Sciences*, 35(5), 247–252. <https://doi.org/10.1016/j.tibs.2010.01.003>
74. Bergoglio, V., Canitrot, Y., Hogarth, L., Minto, L., Howell, S. B., Cazaux, C., & Hoffmann, J. S. (2001). Enhanced expression and activity of DNA polymerase  $\beta$  in human ovarian tumor cells: Impact on sensitivity towards antitumor agents. *Oncogene*, 20(43), 6181–6187. <https://doi.org/10.1038/sj.onc.1204743>

75. Albertella, M. R., Lau, A., & O'Connor, M. J. (2005). The overexpression of specialized DNA polymerases in cancer. *DNA Repair*, 4(5), 583–593. <https://doi.org/10.1016/j.dnarep.2005.01.005>
76. Wang, D., Xiang, D. B., Yang, X. qin, Chen, L. S., Li, M. X., Zhong, Z. Y., & Zhang, Y. S. (2009). APE1 overexpression is associated with cisplatin resistance in non-small cell lung cancer and targeted inhibition of APE1 enhances the activity of cisplatin in A549 cells. *Lung Cancer*, 66(3), 298–304. <https://doi.org/10.1016/j.lungcan.2009.02.019>
77. Horton, J. K., Srivastava, D. K., Zmudzka, B. Z., & Wilson, S. H. (1995). Strategic down-regulation of DNA polymerase  $\beta$  by antisense RNA sensitizes mammalian cells to specific DNA damaging agents. *Nucleic Acids Research*, 23(19), 3810–3815. <https://doi.org/10.1093/nar/23.19.3810>
78. Kothandapani, A., Dangeti, V. S. M. N., Brown, A. R., Banze, L. A., Wang, X. H., Sobol, R. W., & Patrick, S. M. (2011). Novel role of base excision repair in mediating cisplatin cytotoxicity. *Journal of Biological Chemistry*, 286(16), 14564–14574. <https://doi.org/10.1074/jbc.M111.225375>
79. Caiola, E., Salles, D., Frapolli, R., Lupi, M., Rotella, G., Ronchi, A., ... Marabese, M. (2015). Base excision repair-mediated resistance to cisplatin in KRAS(G12C) mutant NSCLC cells. *Oncotarget*, 6(30), 30072–30087. <https://doi.org/10.18632/oncotarget.5019>
80. Gao, D., Hu, J., Zhang, X., Gao, C., & Hong, J. (2013). Effect of hOGG1 over-expression on cisplatin resistance in esophageal squamous carcinoma cells. *Cancer Biotherapy and Radiopharmaceuticals*, 28(6), 433–440. <https://doi.org/10.1089/cbr.2012.1287>
81. Sawant, A., Floyd, A. M., Dangeti, M., Lei, W., Sobol, R. W., & Patrick, S. M. (2017). Differential role of base excision repair proteins in mediating cisplatin cytotoxicity. *DNA Repair*, 51, 46–59. <https://doi.org/10.1016/j.dnarep.2017.01.002>
82. Arents, G., & Moudrianakis, E. N. (1995). The histone fold: A ubiquitous architectural motif utilized in DNA compaction and protein dimerization. *Proceedings of the National Academy of Sciences of the United States of America*, 92(24), 11170–11174. <https://doi.org/10.1073/pnas.92.24.11170>
83. Hayes, J. J., Clark, D. J., & Wolffe, A. P. (1991). Histone contributions to the structure of DNA in the nucleosome. *Proceedings of the National Academy of Sciences of the United States of America*, 88(15), 6829–6833. <https://doi.org/10.1073/pnas.88.15.6829>

- □ □
84. Farrell, A. W., Halliday, G. M., & Lyons, J. G. (2011). Chromatin structure following UV-induced DNA damage—repair or death?. *International journal of molecular sciences*, *12*(11), 8063-8085. <https://doi.org/10.3390/ijms12118063>
  85. Yu, S., Teng, Y., Waters, R., & Reed, S. H. (2011). How chromatin is remodelled during DNA repair of UV-Induced DNA damage in *saccharomyces cerevisiae*. *PLoS Genetics*, *7*(6). <https://doi.org/10.1371/journal.pgen.1002124>
  86. Smerdon, M. J., & Thoma, F. (1990). Site-specific DNA repair at the nucleosome level in a yeast minichromosome. *Cell*, *61*(4), 675–684. [https://doi.org/10.1016/0092-8674\(90\)90479-X](https://doi.org/10.1016/0092-8674(90)90479-X)
  87. Wellinger, R. E., & Thoma, F. (1997). Nucleosome structure and positioning modulate nucleotide excision repair in the non-transcribed strand of an active gene. *EMBO Journal*, *16*(16), 5046–5056. <https://doi.org/10.1093/emboj/16.16.5046>
  88. Thoma, F. (1999). Light and dark in chromatin repair: repair of UV-induced DNA lesions by photolyase and nucleotide excision repair. *The EMBO Journal*, *18*(23), 6585–6598. <https://doi.org/10.1093/emboj/18.23.6585>
  89. Peterson, C. L., & Côté, J. (2004). Cellular machineries for chromosomal DNA repair. *Genes & development*, *18*(6), 602-616. <https://doi.org/10.1101/gad.1182704>
  90. Godar D. E. (2005). UV doses worldwide. *Photochemistry and photobiology*, *81*(4), 736–749. <https://doi.org/10.1562/2004-09-07-ir-308r.1>
  91. Berger, S. L. (2007). The complex language of chromatin regulation during transcription. *Nature*, *447*(7143), 407-412. <https://doi.org/10.1038/nature05915>
  92. Margueron, R., & Reinberg, D. (2010). Chromatin structure and the inheritance of epigenetic information. *Nature Reviews Genetics*, *11*(4), 285-296. <https://doi.org/10.1038/nrg2752>
  93. Kevin, S. (1998). Histone acetylation and transcriptional regulatory mechanisms. *Genes Dev*, *12*, 599-606. <https://doi.org/10.1101/gad.12.5.599>

94. Bernstein, B. E., Mikkelsen, T. S., Xie, X., Kamal, M., Huebert, D. J., Cuff, J., ... Lander, E. S. (2006). A Bivalent Chromatin Structure Marks Key Developmental Genes in Embryonic Stem Cells. *Cell*, *125*(2), 315–326. <https://doi.org/10.1016/j.cell.2006.02.041>
95. Collas P. (2009). The state-of-the-art of chromatin immunoprecipitation. *Methods in molecular biology (Clifton, N.J.)*, *567*, 1–25. [https://doi.org/10.1007/978-1-60327-414-2\\_1](https://doi.org/10.1007/978-1-60327-414-2_1)
96. Osley, M. A., Tsukuda, T., & Nickoloff, J. A. (2007). ATP-dependent chromatin remodeling factors and DNA damage repair. *Mutation Research - Fundamental and Molecular Mechanisms of Mutagenesis*, *618*(1–2), 65–80. <https://doi.org/10.1016/j.mrfmmm.2006.07.011>
97. Falbo, K. B., & Shen, X. (2006). Chromatin remodeling in DNA replication. *Journal of Cellular Biochemistry*, *97*(4), 684–689. <https://doi.org/10.1002/jcb.20752>
98. Clapier, C. R., & Cairns, B. R. (2009). The biology of chromatin remodeling complexes. *Annual review of biochemistry*, *78*, 273-304. <https://doi.org/10.1146/annurev.biochem.77.062706.153223>
99. Dinant, C., Houtsmuller, A. B., & Vermeulen, W. (2008). Chromatin structure and DNA damage repair. *Epigenetics & Chromatin*, *1*(1), 9. <https://doi.org/10.1186/1756-8935-1-9>
100. Hargreaves, D. C., & Crabtree, G. R. (2011). ATP-dependent chromatin remodeling: Genetics, genomics and mechanisms. *Cell Research*, *21*(3), 396–420. <https://doi.org/10.1038/cr.2011.32>
101. Luijsterburg, M. S., & van Attikum, H. (2011). Chromatin and the DNA damage response: the cancer connection. *Molecular oncology*, *5*(4), 349-367. <https://doi.org/10.1016/j.molonc.2011.06.001>
102. Yu, Y., Teng, Y., Liu, H., Reed, S. H., & Waters, R. (2005). UV irradiation stimulates histone acetylation and chromatin remodeling at a repressed yeast locus. *Proceedings of the National Academy of Sciences of the United States of America*, *102*(24), 8650–8655. <https://doi.org/10.1073/pnas.0501458102>
103. Lans, H., Marteijn, J. A., & Vermeulen, W. (2012). ATP-dependent chromatin remodeling in the DNA-damage response. *Epigenetics & chromatin*, *5*(1), 4. <https://doi.org/10.1186/1756-8935-5-4>

- □ □
104. Kothandapani, A., Gopalakrishnan, K., Kahali, B., Reisman, D., & Patrick, S. M. (2012). Downregulation of SWI/SNF chromatin remodeling factor subunits modulates cisplatin cytotoxicity. *Experimental Cell Research*, 318(16), 1973–1986. <https://doi.org/10.1016/j.yexcr.2012.06.011>
  105. Wang, D., & Lippard, S. J. (2004). Cisplatin-induced post-translational modification of histones H3 and H4. *Journal of Biological Chemistry*, 279(20), 20622–20625. <https://doi.org/10.1074/jbc.M402547200>
  106. Drottar, M., Liberman, M. C., Ratan, R. R., & Roberson, D. W. (2006). The histone deacetylase inhibitor sodium butyrate protects against cisplatin-induced hearing loss in guinea pigs. *Laryngoscope*, 116(2), 292–296. <https://doi.org/10.1097/01.mlg.0000197630.85208.36>
  107. Ho, L., & Crabtree, G. R. (2010). Chromatin remodelling during development. *Nature*, 463(7280), 474–484. <https://doi.org/10.1038/nature08911>
  108. Turner, B. M. (2000). Histone acetylation and an epigenetic code. *BioEssays*, 22(9), 836–845. [https://doi.org/10.1002/1521-1878\(200009\)22:9<836::AID-BIES9>3.0.CO;2-X](https://doi.org/10.1002/1521-1878(200009)22:9<836::AID-BIES9>3.0.CO;2-X)
  109. Lafon-Hughes, L., Di Tomaso, M. V., Mendez-Acuna, L., & Martínez-López, W. (2008). Chromatin-remodelling mechanisms in cancer. *Mutation Research/Reviews in Mutation Research*, 658(3), 191–214. <https://doi.org/10.1016/j.mrrev.2008.01.008>
  110. Kornberg, R. D., & Lorch, Y. (1999). Twenty-five years of the nucleosome, fundamental particle of the eukaryote chromosome. *Cell*, 98(3), 285–294. [https://doi.org/10.1016/s0092-8674\(00\)81958-3](https://doi.org/10.1016/s0092-8674(00)81958-3)
  111. Margueron, R., Trojer, P., & Reinberg, D. (2005). The key to development: interpreting the histone code?. *Current opinion in genetics & development*, 15(2), 163–176. <https://doi.org/10.1016/j.gde.2005.01.005>
  112. Jeppesen, P. (1997). Histone acetylation: a possible mechanism for the inheritance of cell memory at mitosis. *Bioessays*, 19(1), 67–74. <https://doi.org/10.1002/bies.950190111>
  113. Hassa, P. O., & Hottiger, M. O. (2005). An epigenetic code for DNA damage repair pathways?. *Biochemistry and cell biology*, 83(3), 270–285. <https://doi.org/10.1139/o05-034>

- □ □
114. Williams, R. R. E., Azuara, V., Perry, P., Sauer, S., Dvorkina, M., Jørgensen, H., ... Fisher, A. G. (2006). Neural induction promotes large-scale chromatin reorganisation of the Mash1 locus. *Journal of Cell Science*, *119*(1), 132–140. <https://doi.org/10.1242/jcs.02727>
  115. Gibbons, R. J. (2005). Histone modifying and chromatin remodelling enzymes in cancer and dysplastic syndromes. *Human molecular genetics*, *14*(suppl\_1), R85-R92. <https://doi.org/10.1093/hmg/ddi106>
  116. Fog, C. K., Jensen, K. T., & Lund, A. H. (2007). Chromatin-modifying proteins in cancer. *Apmis*, *115*(10), 1060-1089. [https://doi.org/10.1111/j.1600-0463.2007.apm\\_776.xml.x](https://doi.org/10.1111/j.1600-0463.2007.apm_776.xml.x)
  117. Grønbaek, K., Hother, C., & Jones, P. A. (2007). Epigenetic changes in cancer. *APMIS : acta pathologica, microbiologica, et immunologica Scandinavica*, *115*(10), 1039–1059. [https://doi.org/10.1111/j.1600-0463.2007.apm\\_636.xml.x](https://doi.org/10.1111/j.1600-0463.2007.apm_636.xml.x)
  118. De Ruijter, A. J., van Gennip, A. H., Caron, H. N., Kemp, S., & van Kuilenburg, A. B. (2003). Histone deacetylases (HDACs): characterization of the classical HDAC family. *The Biochemical journal*, *370*(Pt 3), 737–749. <https://doi.org/10.1042/BJ20021321>
  119. Acharya, M. R., Sparreboom, A., Venitz, J., & Figg, W. D. (2005). Rational development of histone deacetylase inhibitors as anticancer agents: a review. *Molecular pharmacology*, *68*(4), 917–932. <https://doi.org/10.1124/mol.105.014167>
  120. Santos-Rosa, H., & Caldas, C. (2005). Chromatin modifier enzymes, the histone code and cancer. *European Journal of Cancer*, *41*(16), 2381–2402. <https://doi.org/10.1016/j.ejca.2005.08.010>
  121. Vannini, A., Volpari, C., Filocamo, G., Casavola, E. C., Brunetti, M., Renzoni, D., ... Di Marco, S. (2004). Crystal structure of a eukaryotic zinc-dependent histone deacetylase, human HDAC8, complexed with a hydroxamic acid inhibitor. *Proceedings of the National Academy of Sciences of the United States of America*, *101*(42), 15064–15069. <https://doi.org/10.1073/pnas.0404603101>
  122. Gao, L., Cueto, M. A., Asselbergs, F., & Atadja, P. (2002). Cloning and functional characterization of HDAC11, a novel member of the human histone deacetylase family. *Journal of Biological Chemistry*, *277*(28), 25748–25755. <https://doi.org/10.1074/jbc.M111871200>

- □ □
123. Gui, C. Y., Ngo, L., Xu, W. S., Richon, V. M., & Marks, P. A. (2004). Histone deacetylase (HDAC) inhibitor activation of p21WAF1 involves changes in promoter-associated proteins, including HDAC1. *Proceedings of the National Academy of Sciences of the United States of America*, *101*(5), 1241–1246. <https://doi.org/10.1073/pnas.0307708100>
  124. Mahlknecht, U., & Hoelzer, D. (2000). Histone acetylation modifiers in the pathogenesis of malignant disease. *Molecular Medicine*, *6*(8), 623–644. <https://doi.org/10.1007/bf03402044>
  125. Johnstone, R. W., & Licht, J. D. (2003). Histone deacetylase inhibitors in cancer therapy: is transcription the primary target?. *Cancer cell*, *4*(1), 13–18. [https://doi.org/10.1016/s1535-6108\(03\)00165-x](https://doi.org/10.1016/s1535-6108(03)00165-x)
  126. Kim, M. S., Blake, M., Baek, J. H., Kohlhagen, G., Pommier, Y., & Carrier, F. (2003). Inhibition of Histone Deacetylase Increases Cytotoxicity to Anticancer Drugs Targeting DNA. *Cancer Research*, *63*(21), 7291–7300.
  127. Miyamoto, N., Izumi, H., Noguchi, T., Nakajima, Y., Ohmiya, Y., Shiota, M., ... Kohno, K. (2008). Tip60 is regulated by circadian transcription factor clock and is involved in cisplatin resistance. *Journal of Biological Chemistry*, *283*(26), 18218–18226. <https://doi.org/10.1074/jbc.M802332200>
  128. Zhang, Y., & Reinberg, D. (2001). Transcription regulation by histone methylation: interplay between different covalent modifications of the core histone tails. *Genes & development*, *15*(18), 2343–2360. <https://doi.org/10.1101/gad.927301>
  129. Van Holde, K. E. (2012). *Chromatin*. Springer Science & Business Media
  130. Sawan, C., & Herceg, Z. (2010). Histone modifications and cancer. *Advances in genetics*, *70*, 57–85. <https://doi.org/10.1016/B978-0-12-380866-0.60003-4>
  131. Kouzarides, T. (2002). Histone methylation in transcriptional control. *Current opinion in genetics & development*, *12*(2), 198–209. [https://doi.org/10.1016/s0959-437x\(02\)00287-3](https://doi.org/10.1016/s0959-437x(02)00287-3)
  132. Strahl, B. D., Briggs, S. D., Brame, C. J., Caldwell, J. A., Koh, S. S., Ma, H., ... Allis, C. D. (2001). Methylation of histone H4 at arginine 3 occurs in vivo and is mediated by the nuclear receptor coactivator PRMT1. *Current Biology*, *11*(12), 996–1000. [https://doi.org/10.1016/S0960-9822\(01\)00294-9](https://doi.org/10.1016/S0960-9822(01)00294-9)

- □ □
133. Daujat, S., Bauer, U. M., Shah, V., Turner, B., Berger, S., & Kouzarides, T. (2002). Crosstalk between CARM1 methylation and CBP acetylation on histone H3. *Current Biology*, 12(24), 2090–2097. [https://doi.org/10.1016/S0960-9822\(02\)01387-8](https://doi.org/10.1016/S0960-9822(02)01387-8)
  134. Abbosh, P. H., Montgomery, J. S., Starkey, J. A., Novotny, M., Zuhowski, E. G., Egorin, M. J., ... Nephew, K. P. (2006). Dominant-negative histone H3 lysine 27 mutant derepresses silenced tumor suppressor genes and reverses the drug-resistant phenotype in cancer cells. *Cancer Research*, 66(11), 5582–5591. <https://doi.org/10.1158/0008-5472.CAN-05-3575>
  135. Qiu, Y. Y., Mirkin, B. L., & Dwivedi, R. S. (2005). Inhibition of DNA methyltransferase reverses cisplatin induced drug resistance in murine neuroblastoma cells. *Cancer Detection and Prevention*, 29(5), 456–463. <https://doi.org/10.1016/j.cdp.2005.05.004>
  136. Ahluwalia, A., Yan, P., Hurteau, J. A., Bigsby, R. M., Jung, S. H., Huang, T. M., & Nephew, K. P. (2001). Dna methylation and ovarian cancer: I. Analysis of CpG island hypermethylation in human ovarian cancer using differential methylation hybridization. *Gynecologic Oncology*, 82(2), 261–268. <https://doi.org/10.1006/gyno.2001.6291>
  137. Ehrlich, M., Woods, C. B., Yu, M. C., Dubeau, L., Yang, F., Campan, M., ... Laird, P. W. (2006). Quantitative analysis of associations between DNA hypermethylation, hypomethylation, and DNMT RNA levels in ovarian tumors. *Oncogene*, 25(18), 2636–2645. <https://doi.org/10.1038/sj.onc.1209145>
  138. Tam, K. F., Liu, V. W. S., Liu, S. S., Tsang, P. C. K., Cheung, A. N. Y., Yip, A. M. W., & Ngan, H. Y. S. (2007). Methylation profile in benign, borderline and malignant ovarian tumors. *Journal of Cancer Research and Clinical Oncology*, 133(5), 331–341. <https://doi.org/10.1007/s00432-006-0178-5>
  139. Balch, C., Fang, F., Matei, D. E., Huang, T. H. M., & Nephew, K. P. (2009). Minireview: epigenetic changes in ovarian cancer. *Endocrinology*, 150(9), 4003–4011. <https://doi.org/10.1210/en.2009-0404>
  140. Tomar, T., Alkema, N. G., Schreuder, L., Meersma, G. J., de Meyer, T., van Criekinge, W., ... Wisman, G. B. A. (2017). Methylome analysis of extreme chemoresponsive patients identifies novel markers of platinum sensitivity in high-grade serous ovarian cancer. *BMC Medicine*, 15(1). <https://doi.org/10.1186/s12916-017-0870-0>

- □ □
141. Hua, K. T., Wang, M. Y., Chen, M. W., Wei, L. H., Chen, C. K., Ko, C. H., ... Yen, M. L. (2014). The H3K9 methyltransferase G9a is a marker of aggressive ovarian cancer that promotes peritoneal metastasis. *Molecular Cancer*, *13*(1). <https://doi.org/10.1186/1476-4598-13-189>
  142. Smith, H. J., Straughn, J. M., Buchsbaum, D. J., & Arend, R. C. (2017). Epigenetic therapy for the treatment of epithelial ovarian cancer: A clinical review. *Gynecologic oncology reports*, *20*, 81-86. <https://doi.org/10.1016/j.gore.2017.03.007>
  143. Li, Y., Hu, W., Shen, D. Y., Kavanagh, J. J., & Fu, S. (2009). Azacitidine enhances sensitivity of platinum-resistant ovarian cancer cells to carboplatin through induction of apoptosis. *American Journal of Obstetrics and Gynecology*, *200*(2), 177.e1-177.e9. <https://doi.org/10.1016/j.ajog.2008.08.030>
  144. Cadet, J., & Richard Wagner, J. (2013). DNA base damage by reactive oxygen species, oxidizing agents, and UV radiation. *Cold Spring Harbor Perspectives in Biology*, *5*(2). <https://doi.org/10.1101/cshperspect.a012559>
  145. Li, Z., Pearlman, A. H., & Hsieh, P. (2016). DNA mismatch repair and the DNA damage response. *DNA repair*, *38*, 94-101. <https://doi.org/10.1016/j.dnarep.2015.11.019>
  146. Altaf, M., Saksouk, N., & Côté, J. (2007). Histone modifications in response to DNA damage. *Mutation Research - Fundamental and Molecular Mechanisms of Mutagenesis*, *618*(1-2), 81-90. <https://doi.org/10.1016/j.mrfmmm.2006.09.009>
  147. Lord, C. J., & Ashworth, A. (2012). The DNA damage response and cancer therapy. *Nature*, *481*(7381), 287-294. <https://doi.org/10.1038/nature10760>
  148. Cao, L. L., Shen, C., & Zhu, W. G. (2016). Histone modifications in DNA damage response. *Science China Life Sciences*, *59*(3), 257-270. <https://doi.org/10.1007/s11427-016-5011-z>
  149. Osborne, D. J. (1997). Technologies for detection of DNA damage and mutations. *Endeavour*, *21*(4), 178-179. [https://doi.org/10.1016/s0160-9327\(97\)85666-9](https://doi.org/10.1016/s0160-9327(97)85666-9)
  150. Karbaschi, M., Macip, S., Mistry, V., Abbas, H. H. K., Delinassios, G. J., Evans, M. D., ... Cooke, M. S. (2015). Rescue of cells from apoptosis increases DNA repair in UVB exposed cells: Implications for the DNA damage response. *Toxicology Research*, *4*(3), 725-738. <https://doi.org/10.1039/c4tx00197d>

151. McKelvey-Martin, V. J., Ho, E. T. S., McKeown, S. R., Johnston, S. R., McCarthy, P. J., Rajab, N. F., & Downes, C. S. (1998). Emerging applications of the single cell gel electrophoresis (Comet) assay. I. Management of invasive transitional cell human bladder carcinoma. II. Fluorescent in situ hybridization Comets for the identification of damaged and repaired DNA sequences in i. *Mutagenesis*, *13*(1), 1–8. <https://doi.org/10.1093/mutage/13.1.1>
152. McKelvey-Martin, V. J., & McKenna, D. J. (2009). Development and Applications of the Comet-FISH Assay for the Study of DNA Damage and Repair. *The Comet Assay in Toxicology*, 129-150. <https://doi.org/10.1039/9781847559746-00129>
153. Bruggeman, L. A., Dikman, S., Meng, C., Quaggin, S. E., Coffman, T. M., & Klotman, P. E. (1997). Nephropathy in human immunodeficiency virus-1 transgenic mice is due to renal transgene expression. *Journal of Clinical Investigation*, *100*(1), 84–92. <https://doi.org/10.1172/JCI119525>
154. Gavrieli, Y., Sherman, Y., & Ben-Sasson, S. A. (1992). Identification of programmed cell death in situ via specific labeling of nuclear DNA fragmentation. *Journal of Cell Biology*, *119*(3), 493–501. <https://doi.org/10.1083/jcb.119.3.493>
155. McGahon, A., Bissonnette, R., Schmitt, M., Cotter, K. M., Green, D. R., & Cotter, T. G. (1994). BCR-ABL maintains resistance of chronic myelogenous leukemia cells to apoptotic cell death. *Blood*, *83*(5), 1179–1187. <https://doi.org/10.1182/blood.v83.5.1179.bloodjournal8351179>
156. Engvall, E., & Perlmann, P. (1972). Enzyme-linked immunosorbent assay, Elisa. 3. Quantitation of specific antibodies by enzyme-labeled anti-immunoglobulin in antigen-coated tubes. *Journal of Immunology (Baltimore, Md. : 1950)*, *109*(1), 129–135. Retrieved from <http://www.ncbi.nlm.nih.gov/pubmed/4113792>
157. Santella, R. M. (1999). Immunological methods for detection of carcinogen-DNA damage in humans. *Cancer Epidemiology and Prevention Biomarkers*, *8*(9), 733-739.
158. Perdiz, D., Gróf, P., Mezzina, M., Nikaido, O., Moustacchi, E., & Sage, E. (2000). Distribution and repair of bipyrimidine photoproducts in solar UV-irradiated mammalian cells: Possible role of dewar photoproducts in solar mutagenesis. *Journal of Biological Chemistry*, *275*(35), 26732–26742. <https://doi.org/10.1074/jbc.M001450200>

- □ □
159. Wolf, S. M., & Vouros, P. (1994). Application of Capillary Liquid Chromatography Coupled with Tandem Mass Spectrometric Methods to the Rapid Screening of Adducts Formed by the Reaction of N-Acetoxy-N-acetyl-2-aminofluorene with Calf Thymus DNA. *Chemical Research in Toxicology*, 7(1), 82–88. <https://doi.org/10.1021/tx00037a013>
  160. Rindgen, D., Turesky, R. J., & Vouros, P. (1995). Determination of in Vitro Formed DNA Adducts of 2-Amino-1-methyl-6-phenylimidazo[4,5-6]pyridine Using Capillary Liquid Chromatography/Electrospray Ionization/Tandem Mass Spectrometry. *Chemical Research in Toxicology*, 8(8), 1005–1013. <https://doi.org/10.1021/tx00050a003>
  161. Ravanat, J. L., Turesky, R. J., Gremaud, E., Trudel, L. J., & Stadler, R. H. (1995). Determination of 8-Oxoguanine in DNA by Gas Chromatography—Mass Spectrometry and HPLC—Electrochemical Detection: Overestimation of the Background Level of the Oxidized Base by the Gas Chromatography—Mass Spectrometry Assay. *Chemical Research in Toxicology*, 8(8), 1039–1045. <https://doi.org/10.1021/tx00050a00>
  162. Figueroa-González, G., & Pérez-Plasencia, C. (2017). Strategies for the evaluation of DNA damage and repair mechanisms in cancer. *Oncology letters*, 13(6), 3982-3988. <https://doi.org/10.3892/ol.2017.6002>
  163. Ozols, R. F., Masuda, H., Grotzinger, K. R., Whang-Peng, J., Louie, K. G., Knutsen, T., ... Young, R. C. (1987). Characterization of a cis-Diamminedichloroplatinum(II)-resistant Human Ovarian Cancer Cell Line and its use in Evaluation of Platinum Analogues. *Cancer Research*, 47(2), 414–418.
  164. Ince, T. A., Sousa, A. D., Jones, M. A., Harrell, J. C., Agoston, E. S., Krohn, M., ... Mills, G. B. (2015). Characterization of twenty-five ovarian tumour cell lines that phenocopy primary tumours. *Nature Communications*, 6. <https://doi.org/10.1038/ncomms8419>
  165. Wong, V. W. C., Szeto, Y. T., Collins, A. R., & Benzie, I. F. F. (2005). The COMET assay: A biomonitoring tool for nutraceutical research. *Current Topics in Nutraceutical Research*, 3, 1–14.
  166. Singh, N. P., McCoy, M. T., Tice, R. R., & Schneider, E. L. (1988). A simple technique for quantitation of low levels of DNA damage in individual cells. *Experimental Cell Research*, 175(1), 184–191. [https://doi.org/10.1016/0014-4827\(88\)90265-0](https://doi.org/10.1016/0014-4827(88)90265-0)
  167. Karbaschi, M., & Cooke, M. S. (2014). Novel method for the high-throughput processing of slides for the comet assay. *Scientific Reports*, 4. <https://doi.org/10.1038/srep07200>

- □ □
168. Karbaschi, M., Ji, Y., Abdulwahed, A. M. S., Alohal, A., Bedoya, J. F., Burke, S. L., ... Cooke, M. S. (2019). Evaluation of the major steps in the conventional protocol for the Alkaline comet assay. *International Journal of Molecular Sciences*, 20(23). <https://doi.org/10.3390/ijms20236072>
169. Tice, R. R., Agurell, E., Anderson, D., Burlinson, B., Hartmann, A., Kobayashi, H., ... Sasaki, Y. F. (2000). Single cell gel/comet assay: Guidelines for in vitro and in vivo genetic toxicology testing. *Environmental and Molecular Mutagenesis*, 35(3), 206–221. [https://doi.org/10.1002/\(SICI\)1098-2280\(2000\)35:3<206::AID-EM8>3.0.CO;2-J](https://doi.org/10.1002/(SICI)1098-2280(2000)35:3<206::AID-EM8>3.0.CO;2-J)
170. Cooke, M. S., Duarte, T. L., Cooper, D., Chen, J., Nandagopal, S., & Evans, M. D. (2008). Combination of azathioprine and UVA irradiation is a major source of cellular 8-oxo-7,8-dihydro-2'-deoxyguanosine. *DNA Repair*, 7(12), 1982–1989. <https://doi.org/10.1016/j.dnarep.2008.08.007>
171. Duarte, T. L., Almeida, G. M., & Jones, G. D. D. (2007). Investigation of the role of extracellular H<sub>2</sub>O<sub>2</sub> and transition metal ions in the genotoxic action of ascorbic acid in cell culture models. *Toxicology Letters*, 170(1), 57–65. <https://doi.org/10.1016/j.toxlet.2007.02.005>
172. Almeida, G. M., Duarte, T. L., Steward, W. P., & Jones, G. D. D. (2006). Detection of oxaliplatin-induced DNA crosslinks in vitro and in cancer patients using the alkaline comet assay. *DNA Repair*, 5(2), 219–225. <https://doi.org/10.1016/j.dnarep.2005.09.010>
173. Moneef, M. A. L., Sherwood, B. T., Bowman, K. J., Kockelbergh, R. C., Symonds, R. P., Steward, W. P., ... Jones, G. D. D. (2003). Measurements using the alkaline comet assay predict bladder cancer cell radiosensitivity. *British Journal of Cancer*, 89(12), 2271–2276. <https://doi.org/10.1038/sj.bjc.6601333>
174. Bowman, K. J., Al-Moneef, M. M., Sherwood, B. T., Colquhoun, A. J., Goddard, J. C., Griffiths, T. R. L., ... Jones, G. D. D. (2014). Comet assay measures of DNA damage are predictive of bladder cancer cell treatment sensitivity in vitro and outcome in vivo. *International Journal of Cancer*, 134(5), 1102–1111. <https://doi.org/10.1002/ijc.28437>
175. Komeda, S., Lutz, M., Spek, A. L., Yamanaka, Y., Sato, T., Chikuma, M., & Reedijk, J. (2002). A novel isomerization on interaction of antitumor-active azole-bridged dinuclear platinum(II) complexes with 9-ethylguanine. Platinum(II) atom migration from N<sub>2</sub> to N<sub>3</sub> on 1,2,3-triazole. *Journal of the American Chemical Society*, 124(17), 4738–4746. <https://doi.org/10.1021/ja0168559>

- □ □
176. Komeda, S., Lutz, M., Spek, A. L., Chikuma, M., & Reedijk, J. (2000). New antitumor-active azole-bridged dinuclear platinum(II) complexes: Synthesis, characterization, crystal structures, and cytotoxic studies. *Inorganic Chemistry*, 39(19), 4230–4236. <https://doi.org/10.1021/ic000273v>
177. Wen, Z., Tuttle, P. R., Howlader, A. H., Vasilyeva, A., Gonzalez, L., Tangar, A., ... Wnuk, S. F. (2019). Fluorescent 5-Pyrimidine and 8-Purine Nucleosides Modified with an N-Unsubstituted 1,2,3-Triazol-4-yl Moiety. *Journal of Organic Chemistry*, 84(6), 3624–3631. <https://doi.org/10.1021/acs.joc.8b03135>
178. Meaburn, K. J. (2016). Spatial genome organization and its emerging role as a potential diagnosis tool. *Frontiers in genetics*, 7, 134. <https://doi.org/10.3389/fgene.2016.00134>
179. Meaburn, K. J., Gudla, P. R., Khan, S., Lockett, S. J., & Misteli, T. (2009). Disease-specific gene repositioning in breast cancer. *Journal of Cell Biology*, 187(6), 801–812. <https://doi.org/10.1083/jcb.200909127>
180. Ioannou, D., Kandukuri, L., Simpson, J. L., & Tempest, H. G. (2015). Chromosome territory repositioning induced by PHA-activation of lymphocytes: A 2D and 3D appraisal. *Molecular Cytogenetics*, 8(1). <https://doi.org/10.1186/s13039-015-0146-3>
181. Meaburn, K. J., & Misteli, T. (2007). Cell biology: Chromosome territories. *Nature*, 445(7126), 379–781. <https://doi.org/10.1038/445379a>
182. Meaburn, K. J., Agunloye, O., Devine, M., Leshner, M., Roloff, G. W., True, L. D., & Misteli, T. (2016). Tissue-of-origin-specific gene repositioning in breast and prostate cancer. *Histochemistry and Cell Biology*, 145(4), 433–446. <https://doi.org/10.1007/s00418-015-1401-8>
183. Foster, H. A., & Bridger, J. M. (2005). The genome and the nucleus: a marriage made by evolution. *Chromosoma*, 114(4), 212–229. <https://doi.org/10.1007/s00412-005-0016-6>
184. Ioannou, D., Kandukuri, L., Quadri, A., Becerra, V., Simpson, J. L., & Tempest, H. G. (2015). Spatial positioning of all 24 chromosomes in the lymphocytes of six subjects: Evidence of reproducible positioning and spatial repositioning following DNA damage with hydrogen peroxide and ultraviolet B. *PLoS ONE*, 10(3). <https://doi.org/10.1371/journal.pone.0118886>

- □ □
185. Millan, N. M., Lau, P., Hann, M., Ioannou, D., Hoffman, D., Barrionuevo, M., ... Tempest, H. G. (2012). Hierarchical radial and polar organisation of chromosomes in human sperm. *Chromosome Research*, 20(7), 875–887. <https://doi.org/10.1007/s10577-012-9323-y>
  186. Kallioniemi, O. -P, Koivula, T., Punnonen, R., Mattila, J., & Lehtinen, M. (1988). Prognostic significance of dna index, multiploidy, and S-phase fraction in ovarian cancer. *Cancer*, 61(2), 334–339. [https://doi.org/10.1002/1097-0142\(19880115\)61:2<334::AID-CNCR2820610224>3.0.CO;2-M](https://doi.org/10.1002/1097-0142(19880115)61:2<334::AID-CNCR2820610224>3.0.CO;2-M)
  187. Coward, J., & Harding, A. (2014). Size Does Matter: Why Polyploid Tumor Cells are Critical Drug Targets in the War on Cancer. *Frontiers in oncology*, 4, 123. <https://doi.org/10.3389/fonc.2014.00123>
  188. Rajagopalan, H., & Lengauer, C. (2004). Aneuploidy and cancer. *Nature*, 432(7015), 338–341. <https://doi.org/10.1038/nature03099>
  189. Friedlander, M. L., Hedley, D. W., Taylor, I. W., Russell, P., Coates, A. S., & Tattersall, M. H. (1984). Influence of cellular DNA content on survival in advanced ovarian cancer. *Cancer Research*, 44(1), 397-400.
  190. Friedlander, M. L., Taylor, I. W., Russell, P., Musgrove, E. A., Hedley, D. H., & Tattersall, M. H. N. (1983). Ploidy as a prognostic factor in ovarian cancer. *International Journal of Gynecological Pathology*, 2(1), 55–63. <https://doi.org/10.1097/00004347-198301000-00005>
  191. Alcaraz, A., Takahashi, S., Brown, J. A., Herath, J. F., Bergstralh, E. J., Larson-Keller, J. J., ... Jenkins, R. B. (1994). Aneuploidy and Aneusomy of Chromosome 7 Detected by Fluorescence in Situ Hybridization Are Markers of Poor Prognosis in Prostate Cancer. *Cancer Research*, 54(15), 3998–4002.
  192. Kops, G. J., & Weaver, B. A. (2005). leveland DW. *On the road to cancer: aneuploidy and the mitotic checkpoint*. *Nat Rev Cancer*, 5, 773-85.

VITA

ABDULHADI MOHAMMED S ABDULWAHED

- 2005-2009                      B.A., Clinical Laboratory Sciences  
King Saud University  
Riyadh, Saudi Arabia
- 2013-2014                      Graduate Assistant  
University of New Haven  
New Haven, Connecticut
- 2013-2014                      M.S., Cellular & Molecular Biology  
University of New Haven  
New Haven, Connecticut
- 2015-present                      Ph.D. Candidate, Public Health  
Department of Environmental and Health Sciences  
Florida International University  
Miami, Florida

PUBLICATIONS AND PRESENTATIONS

Karbaschi, M., Ji, Y., Abdulwahed, A. M. S., Alohal, A., Bedoya, J. F., Burke, S. L., ... & Cooke, M. S. (2019). Evaluation of the Major Steps in the Conventional Protocol for the Alkaline Comet Assay. *International Journal of Molecular Sciences*, 20(23), 6072

Azqueta, A., Langie, A.S., Collins, A., Møller, P., Gajski, G., Cook, M.S., Boutet-Robinet, E., ... & Costa, S (2020). Use of the comet assay to evaluate DNA damage in a variety of specimens: from cells to tissues and from yeast to human. (Presubmission document has been submitted to Nature Protocols)

Abdulwahed, A., Quinete, N., Karbaschi, M., Tempest, H., Cooke, M.S. Examination of the Difference in the DNA Damage Response in Chemoresistant and Chemosensitive Ovarian Cell Lines (Chapter 3). (To be published)

□ □ □  
Abdulwahed, A., Gantiva-Mesa, L., Cobb, J., Millan, N., Tempest, H., Cooke, M.S. Evaluation of Gene Positioning and Copy Number Changes in Chemosensitive And Chemoresistant Ovarian Cancer Cell Lines (Chapter 4). (To be published)

Abdulwahed, A., Quinete, N., Cobb, J., Tempest, H., Cooke, M.S (2019) Altered DNA damage response and gene positioning in chemosensitive and chemoresistant ovarian cancer cell lines. The 15th Annual Workshop on LC/MS/MS Applications in Environmental Analysis and Food Safety, 2019 (Accepted abstract and poster presentation)

Abdulwahed, A., Karbaschi, M., Tempest, H., Cooke, M.S (2019). Investigation of the DNA Damage Response in Chemoresistant versus Chemosensitive Ovarian Cancer Cells. Society of Toxicology (SOT) 58<sup>th</sup> annual meeting. San Antonio, 2018. (Accepted abstract and poster presentation)

Abdulwahed, A., Gantiva-Mesa, L., Karbaschi, M., Tempest, H., Cooke, M.S. (2018). Gene positioning in chemosensitive and chemoresistant ovarian cancer cell lines. Florida Science Training and Research (FSTAR), Herbert Wertheim, College of Medicine at FIU (Accepted abstract and poster presentation; Presented by Laura Gantiva-Mesa)

Abdulwahed, A., Karbaschi, M., Tempest, H., Cooke, M.S. (2018). Differences in the DNA Damage Response in Chemoresistant and Chemosensitive Ovarian Cells. Society of Toxicology (SOT) 57<sup>th</sup> annual meeting. San Antonio, 2018. (Accepted abstract and poster presentation)

Abdulwahed, A., Karbaschi, M., Tempest, H., Cooke, M.S. (2017) Measurement of Cisplatin-induced DNA damage and Repair in Ovarian Cancer Cells Using the Comet Assay. Environmental Mutagenesis & Genomics Society (EMGS). 48th annual meeting, Raleigh, North Carolina and GSAW at FIU. (Accepted abstract and poster presentation)